Optical and Transport Properties of Disordered Materials by Computer Simulation

Dissertation
zur
Erlangung des Doktorgrade
der Naturwissenschaften
(Dr. rer. nat.)

dem
Fachbereich Physik
der Philipps-Universität Marburg
vorgelegt von

Vitalii Valkovskii

aus

Lviv, UdSSR

Marburg, 2018

Vom Fachbereich Physik der Philipps-Universität als Dissertation angenommen am: 20.09.2018

Erstgutachter: Prof. Dr. Sergei Baranoskii

Zweitgutachter: Prof. Dr. Wolfram Heimbrodt

Tag der mündlichen Prüfung: 25.09.2018

Hochschulkennziffer: 1180

Zusammenfassung

Diese Arbeit ist eine Zusammenfassung einer Studie zu optischen und Transporteigenschaften ungeordneter Materialien. Da Unordnung eine wichtige Rolle in verschiedenen optoelektronischen Phnomenen spielt, ist eine geeignete theoretische Beschreibung von Unordnungseffekten von entscheidender Bedeutung fr die Entwicklung von elektronischen Bauelementen, wie Transistoren, Speichern, Leuchtdioden und Solarzellen. Diese Arbeit behandelt einige der Probleme, die mit der Rekombination von Exzitonen in ungeordneten Materialien zusammenhngen. Ferner wird der Mechanismus der Befreiung von Trgern aus Fallen und das Konzept der effektiven Temperatur fr den Hopping-Transport, mit besonderem Schwerpunkt auf der Kinetic Monte Carlo Methode (KMC) betrachtet.

In Kapitel 1 wird eine kurze Beschreibung der theoretischen Kernkonzepte des Ladungstrgertransports in ungeordneten Materialien gegeben.

Kapitel 2 widmet sich den Besonderheiten von Photolumineszenz (PL) in Verbindungshalbleitermaterialien, insbesondere in Ga(NAsP). Hier wird gezeigt, dass der vorhandene theoretische Ansatz nicht in der Lage ist, solche experimentallen Abhngigkeiten zu beschreiben, wie eine PL-Linienverschmlerung bei tiefen Temperaturen mit steigender Pumpleistung und die Temperaturabhngigkeit von der Stokes-Verschiebung verdeutlichen. Dazu wird ein verbesserter theoretischer Ansatz, sowie der Algorithmus der Monte Carlo Methode vorgeschlagen.

In Kapitel 3 wird die Rolle der Hoppingbergange fr die Delokalisierung der Ladungstrger in hochelektrischen Feldern diskutiert. Der Einfluss von Hoppingbergngen wird analysiert und mithilfe des KMC-Algorithmus modelliert. Die Analyse zeigt, dass die Untersttzung der Hoppingbergnge die Auslsungsgeschwindigkeit der Trger deutlich erhhen kann. Diese Hoppingprozesse sind in den Verfahren, von groer Bedeutung, die von der Delokalisierung der Trger abhngen.

Im Schlusskapitel (Kapitel 4) wird die Gltigkeit des Effektivtemperaturkonzepts fr die Beschreibung der Trgerbeweglichkeit im Multiple Trapping (MT) Transport demonstriert. Daraus ergibt sich eine Mglichkeit, die Trgerbeweglichkeit des Multiple Hopping Transports wie eine Funktion der Variable $T_{eff}(T, F)$ zu beschreiben. Die Variable bercksichtigt die Kombinationswirkungen der Temperatur und des elektrischen Feldes. Im Rahmen dieser Arbeit wird ein neues Modell der Excitonen-Rekombination in Verbindungshalbleitermaterialien, wie Ga(NAsP)/GaP, zusammen mit Simulationstechniken eingefhrt. Dabei wird eine theoretische Beschreibung der Freisetzung von Trgern aus Fallen, untersttzt durch Sprungbergnge, gegeben. Es wird sowohl analytisch, als

auch mittels Monte-Carlo-Simulation gezeigt, dass das Hopping die Trgerfreisetzungsrate signifikant erhhen kann. Ein solcher Anstieg kann die optischen- und Transporteigenschaften von ungeordneten Systemen stark beeinflussen. Es wird auch gezeigt, wie das Konzept der effektiven Temperatur fr den Fall des MT-Transportregimes erweitert werden kann. Der Algorithmus zur Simulation der Ladungstrgermobilitt im MT-Regime wird bereitgestellt. Die Arbeit wurde unter der Aufsicht von Professor Dr. Sergei Baranovskii in den Jahren 2015 - 2018 am Fachbereich Physik der Philipps Universitt Marburg angefertigt. Die Hauptergebnisse wurden in Zusammenarbeit mit Dr. Alexey Nenashev, Dr. Kakhaber Jandieri, Dr. Mohammad Khaled Shakfa und Dr. Jan Oliver Oelerich erzielt.

Abstract

This thesis is a summary of a research on optical and transport properties of disordered materials. Since disorder plays and important role in various optoelectronic phenomena, appropriate theoretical description of disorder-related effects is of vital importance for development of electronic devices such as transistors, memories, light-emitting diodes and photovoltaics. This work covers some of the problems related to excitons recombination in disordered materials, to the mechanism of carriers detrapping and to the concept of the effective temperature for hopping transport, with particular emphasis on Kinetic Monte Carlo method as a tool for theoretical description of disorder-induced phenomena. The work was done under supervision of professor Dr. Sergei Baranovskii during years 2015 – 2018 at the Physics department of Marburg University. The main results were obtained in collaboration with Dr. Alexey Nenashev, Dr. Kakhaber Jandieri, Dr. Mohammad Khaled Shakfa and Dr. Jan Oliver Oelerich

Acknowledgements

During my work in the University of Marburg, I had the honour to collaborate with wonderful people to whom I want to say many thanks.

First of all, it was a pleasure to work under the supervision of professor Dr. Sergei Baranovskii, who is a great expert in the field of charge transport in disordered materials and related topics.

The main results of Chapter 2 of this thesis were received in close cooperation with Dr. Khaled Shakfa, who has provided interesting experimental results, and Dr. Kakhaber Jandieri, who has made essential contribution discussing and developing a theoretical approach to describe those results. I highly acknowledge productive collaboration with them.

Many thanks to Dr. Alexey Nenashev and Dr. Jan Oliver Oelerich for intensive cooperation on the research described in Chapters 3 and 4. A lot of core theoretical ideas were proposed by Alexey, while discussions with Jan were helpful for developing simulations.

And of course, my work in Marburg would not be possible without support of the German Science Foundation (DFG). Financial support in frame of Research Trainig Group GRK 1782 "Functionalization of Semiconductors" is gratefully acknowledged.

Contents

Zusammenfassung ii

Abstract iv

Acknowledgements v

Abbreviations viii

Physical Constants ix

Introduction 1

1 Hopping transport model and Kinetic Monte Carlo method 4
- 1.1 Localized states and the concept of sites 4
- 1.2 Distribution of sites 6
- 1.3 Hopping rates 6
- 1.4 General assumptions and parameters of the model 9
- 1.5 Analytical and numerical applications of the model 9
- 1.6 Kinetic Monte Carlo approach 10
- 1.7 General remarks on Monte Carlo method and random numbers generation 12

2 Excitons recombination in disordered materials 14
- 2.1 Generic PL features in disordered materials and the BET model 15
- 2.2 Anomalous linewidth broadening and low-temperature linewidth shrinkage in Ga(NAsP) 19
- 2.3 The concept of complex DOS 22
- 2.4 KMC simulation of PL linewidth shrinkage in Ga(NAsP) 24
  - 2.4.1 KMC simulation algorithm 24
  - 2.4.2 KMC simulation results 26
- 2.5 The model of double-scaled disorder 30
- 2.6 The model with two types of impurity sites 32
- 2.7 KMC simulation of PL with two types of impurity sites 35
  - 2.7.1 KMC simulation algorithm 35
  - 2.7.2 KMC simulation results 36
- 2.8 Conclusions 40

3 Carriers release enhanced by hopping **42**
3.1 Multiple-trapping model 42
3.2 Field-assisted carrier release from an isolated trap 43
3.3 Field-assisted carrier release with single additional trap 45
3.4 Field-assisted carrier release with multiple additional traps 51
3.5 KMC simulation algorithm 54
3.6 KMC simulation results 55
3.6.1 Enhancement of the carriers release rate 55
3.6.2 Carriers release at zero field 57
3.6.3 Carriers release rate versus depth of the trap 60
3.6.4 Carriers release rate versus effective mass 61
3.6.5 Comparison of the analytical approach and the KMC simulation . 62
3.7 Conclusions 64

4 Effective temperature for the multiple-trapping transport **66**
4.1 The concept of effective temperature 67
4.2 Carriers release and MT transport in amorphous semiconductors 68
4.3 Theoretical description of carriers mobility in MT regime via effective temperature 69
4.4 KMC simulation of carriers mobility in MT regime 75
4.4.1 KMC simulation algorithm 75
4.4.2 KMC simulation results 76
4.5 Conclusions 79

Conclusions **81**

Bibliography **83**

Abbreviations

DOS	**D**ensity **O**f **S**tates
FWHM	**F**ull **W**idth at **H**alf **M**aximum
KMC	**K**inetic **M**onte **C**arlo
LS	**L**ocalized **S**tate(s)
MT	**M**ultiple-**t**rapping
MQW(s)	**M**ultiple **Q**uantum **W**ell(s)
PL	**P**hoto**l**uminescence

Physical Constants

Bohr radius	a_B	=	$5.291\ 772\ 1067(12) \times 10^{-11}\ m$
Speed of Light	c	=	$2.997\ 924\ 58 \times 10^8\ \mathrm{ms}^{-\mathrm{S}}$
Elementary electric charge	e	=	$1.602\ 176\ 6208(98) \times 10^{-19}\ \ C$
Boltzmann constant	k	=	$8.617\ 3303(50) \times 10^{-5}\ \ eV \times K^{-1}$
Free electron mass	m_0	=	$9.109\ 383\ 56(11) \times 10^{-11}\ \ kg$
Planck constant	$\hbar$	=	$6.582\ 119\ 514(40) \times 10^{-16}\ eV \times s$

Introduction

Scientists all around the World are actively and productively working on the development of novel semiconductor materials for a new generation of devices with special capabilities, ranging from resonant tunnelling transistors to highly efficient components of solar cells. The transport properties of electrons and holes can be continuously tuned, using the methods of band-gap engineering and modern growth techniques, such as molecular beam epitaxy. For instance, modern semiconductor heterojunctions allow production of efficient semiconductor lasers and multijunction solar cells. However, fabrication of perfect (in terms of crystalline structure) semiconductor alloys is fundamentally impossible, due to lattices mismatch and local fluctuations of atomic concentrations of different materials. Therefore, each time when dealing with semiconductor alloys, we should take into account that there is always a certain amount of disorder, due to imperfections of a crystalline structure of the material and to compositional fluctuations. This leads to the emergence of so-called localized states inside the band gap, which may significantly affect optoelectronic and transport properties of the material. Therefore, physics of disordered materials is being a subject of an extensive study for decades, and still, there are a lot of questions to be answered.

A lot of theoretical works have been done so far in that field. However, there is a plenty of problems, which are not solvable analytically and require numerical approaches, such as Monte Carlo simulations. Pioneering works by Bässler [1, 2] have demonstrated the efficiency of Kinetic Monte Carlo method for solving fundamental problems of hopping transport, such as determination of temperature dependence of carrier mobility. Later Monte Carlo approach was applied by Baranovskii, Eichmann and Thomas [3] to describe photoluminescence spectra of III-V heterojunctions. However, the original approach of

Baranovskii, Eichmann and Thomas fails to describe some of the important photoluminescence features in modern materials such as Ga(NAsP)/GaP and Ga(AsBi)/GaAs. Development of the model to resolve this issue became a part of my research.

Growing computational power of modern computers makes Kinetic Monte Carlo approach a powerful tool to study transport and optical properties of disordered materials. The major advantage of Kinetic Monte Carlo simulation method is its flexibility. One can easily introduce some complex properties of the system, such as non-monotonous density of states, correlations between coordinates and energies of states, complex dependencies of carriers lifetimes at different states and a lot of other features. Such a flexibility allows us to test almost any qualitative considerations and to see how various parameters of the system influence its properties and to verify or even improve results obtained with other methods.

Present work summarizes my research dedicated to optical and transport properties of disordered materials using the Kinetic Monte Carlo method. It starts with a brief review of the key concepts of the hopping transport model and Monte Carlo approach in Chapter 1.

In Chapter 2, some peculiarities of the photoluminescence in disordered systems are discussed. In particular, the main emphasis is put on the photoluminescence features of Ga(NAsP)/GaP, which is a promising material for the fabrication of long wavelength lasers and LEDs in the range of $1.3 - 1.5$ μm. Studies, made in collaboration with Dr. Kakhaber Jandieri, extends Baranovskii-Eichmann-Thomas model, to explain unusual low-temperature excitation dependence of the linewidth of Ga(NAsP)/GaP photoluminescence spectrum discovered experimentally by Dr. Khaled Shakfa, and also by other authors in InGaN/GaN [4] and Ga(AsBi)/GaAs [5] heterostructures. Results of this research are published in Ref. [6]. My contribution to this paper, was the core hypothesis of the complex non-monotonous shape of the density of states and Kinetic Monte Carlo simulations to prove the validity of such an approach.

Next in the same chapter the so-called model of double-scaled disorder [7], is being revised. We have found that it is impossible to describe the whole set of experimentally observed features of photoluminescence in Ga(NAsP)/GaP heterojunctions in the frame of that model. I have come up with an alternative approach, assuming two types of localized states, with strongly different non-radiative recombination rates, and applied

Monte Carlo method to validate this model. Results of this research were published in Ref. [8].

Another important issue of hopping transport is the role of hopping transitions in carriers detraping. So-called multiple trapping model, describes carriers transport as successive captures and release of carriers from traps alternating with the free motion. However, this approach doesn't take into account the influence of the surrounding traps on carriers release rate, which can actually be an important effect. In cooperation with Dr. Alexey Nenashev we have made a research to close this gap. Results of this work are the subject of Chapter 3 of this thesis. Dr. Nenashev has suggested a simple analytical model to describe the problem for the case of 2 traps. However, it the problem is not solvable analytically for the general case of many traps. While we can not solve it analytically Kinetic Monte Carlo approach fits perfectly to solve it numerically. Development of the simulation algorithm and analysis of the results of simulation became my main contribution to this research.

The final chapter (Chapter 4) is dedicated to the concept of effective temperature. It was shown in the 1970s that the combined effect of the electric field and temperature for hopping transport can be expressed by a single parameter $T_{eff}\ (F, T)$. Although this concept has been well developed for the case of hopping transport, the applicability of the effective temperature for the case of multiple-trapping transport is still the subject of research. Chapter 4 is based on the recent results of our research [9]. As, one of the coauthors of this paper, I have contributed to the discussion of a theretical part and verification of the validity of effective temperature in multiple trapping transports using Kinetic Monte Carlo approach.

Chapter 1

Hopping transport model and Kinetic Monte Carlo method

In this chapter we will briefly discuss the general concepts of hopping transport, which allows describing the movement of carriers in disordered materials in frames of a simple model. Here we cover only the basic concepts of carrier transport in disordered material. The detailed review of the theory of transport in disordered systems one can find in review papers [10, 11]. A lot of useful results and application of the hopping transport model has been derived purely analytically, however for many problems of hopping transport there are no analytical solutions. Nevertheless, one can implement the hopping transport concepts through numerical approaches such as Kinetic Monte Carlo (KMC) simulation. KMC simulation is a powerful method, which allows to directly simulate tunnelling transitions of the carrier between disorder induced localized states. Collecting statistics over a large number of KMC realizations, one can find out a lot of useful information about electron transport and excitons recombination in disordered systems.

1.1 Localized states and the concept of sites

The defining property for the disordered materials is that, due to impurities and perturbation of the crystal structure, there are localized states (LS) for electrons and holes. In frame of hopping transport model, LS in which carriers can exist are often called "sites" or "traps".

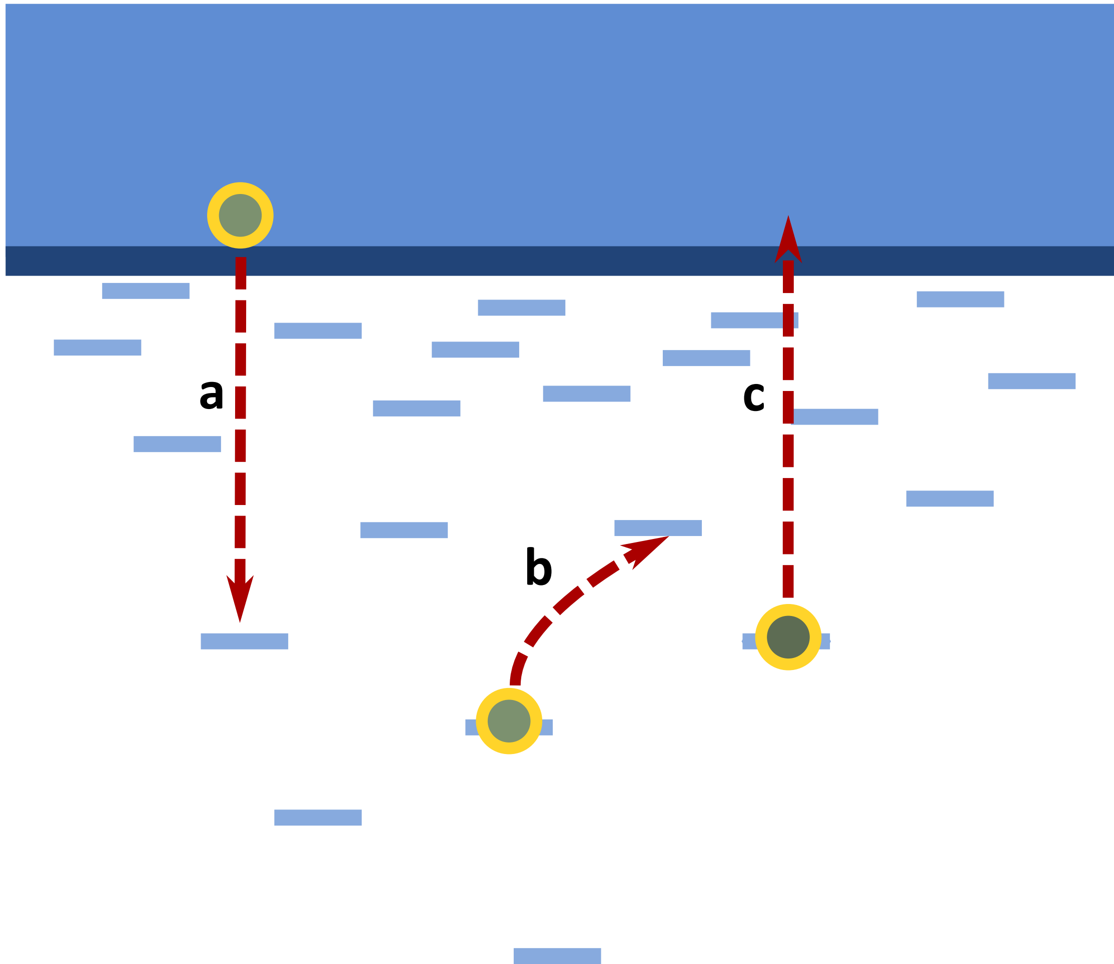

FIGURE 1.1: A sketch to sites and hopping transition concepts. The following processes are depicted: localization of the electron to the trap (a), hopping transition of the electron between two traps (b), thermal activation of the electron to the conduction band (c).

Existence of such traps, induced by disorder, may dramatically affect transport and optical properties of the material. For instance, an electron might be captured on a trap, as it depicted on Fig. 1.1 In this situation there are two kinds of possible processes – thermal activation and tunneling (or "hopping") transition to another site. If the depth of the trap compared to kT is large (or in other words, temperature of the system is low enough), than the probability of thermal activation is low compared to probabilities of possible hopping transitions. Otherwise, electron has high chances to absorb the phonon, that will bring him back to the conduction band. Thus, probabilities of processes defining carriers transport in disordered materials depends on such parameters as concentration and energy distribution of sites, as well as on the temperature and the applied electric field.

1.2 Distribution of sites

In general to solve the problem one must know exact coordinates and energies of all sites. However, on practice to specify disordered system we only need to know some statistical parameters, such as the density of states (DOS) $g(\varepsilon)$ and sites concentration N. Traps are often assumed to be randomly distributed in space with concentration dependent on a degree of imperfection of the sample. Energies of the traps are different, due to difference in there environment, and distributed accordingly to the DOS. The value $g(\varepsilon)d\varepsilon dr$ gives average quantity of LS with energies in range $[\varepsilon, \varepsilon + d\varepsilon]$, per volume dr. The DOS must be chosen according to the material. There are two most popular assumptions for energy distribution of sites – Gaussian and exponential DOS.

In case of organic materials the Gaussian DOS, given by

$$g(\varepsilon) = \frac{N}{\sigma\sqrt{2\pi}} \exp(-\frac{\varepsilon^2}{2\sigma^2}) \tag{1.1}$$

is normally assumed. Here σ is the standard deviation of the sites energy distribution. This assumption is supported by experimental measurements of the absorption bands of organic semiconductor materials and by agreement between experimental results and hopping model predictions.

For inorganic semiconductor materials it is widely assumed that the DOS is given by

$$g(\varepsilon) = \frac{N}{\varepsilon} \exp(-\frac{\varepsilon}{\varepsilon_0}) \tag{1.2}$$

Here ε_0 is energy scale of sites distribution. The assumption of exponential DOS is mainly based on observation of the shape of optical absorption spectrum (also known as Urbach tails [12]) and on agreement between experiments and simulations using hopping transport model, on the other hand [3].

1.3 Hopping rates

Transport and optical properties of disordered materials are in many cases determined by the following events:

- Carriers localization on traps;
- Carriers detrapping (thermal activation);
- Hopping transitions between traps.

In frame of the hopping transport model, it is assumed that the energy difference between initial and final state in detrapping or hopping transition process is gained by absorption or emission of phonons of corresponding energy. Thus, in general, different hopping events are strongly dependent on temperature of the system. The rate of hopping transition between site i with energy ε_i and site j with energy ε_j , assuming $|\mathbf{r}_{ij}|$ is the distance between sites, is often determined by Miller-Abrahams phonon-assisted tunne1ing equation [13]

$$\nu_{ij} = \nu_0 \exp\left(-\frac{2|\mathbf{r}_{ij}|}{a}\right)\gamma(\varepsilon_j - \varepsilon_i) \tag{1.3}$$

with

$$\gamma(\Delta\varepsilon) = \begin{cases} \exp(-\Delta\varepsilon/kT), & \text{if } \Delta\varepsilon > 0, \\ 1, & \text{otherwise.} \end{cases} \tag{1.4}$$

Here T is the temperature of the system, k is the Boltzmann constant, ν_0 is the attempt-to-escape frequency and a is carrier localization radius (or localization length). The value a characterizes spatial size of carriers wave function. As one can see, hopping rate from site i to site j exponentially depends on both – ratio between distance $\mathbf{r}_{ij}$ and localization length a and ratio between energy difference $\Delta\varepsilon$ and the value of kT. Term $\gamma(\Delta\varepsilon)$ describes the probability of absorbing phonon of corresponding energy for the case of hopping to higher energy ($\Delta\varepsilon > 0$). The case of hopping to lower energies involves the emission of phonon, which can be done easily. One can also see that, assuming $|\mathbf{r}_{ij}| = 0$ and $\Delta\varepsilon = |\varepsilon_i|$ for activation process Eq. (1.3) takes the form of simple Boltzman exponent

$$\nu_{ij} = \nu_0 \exp\left(-\frac{\varepsilon_i}{kT}\right) \tag{1.5}$$

To introduce electric field implied in the system, we have to take into account how does the field change the energy differences between sites.

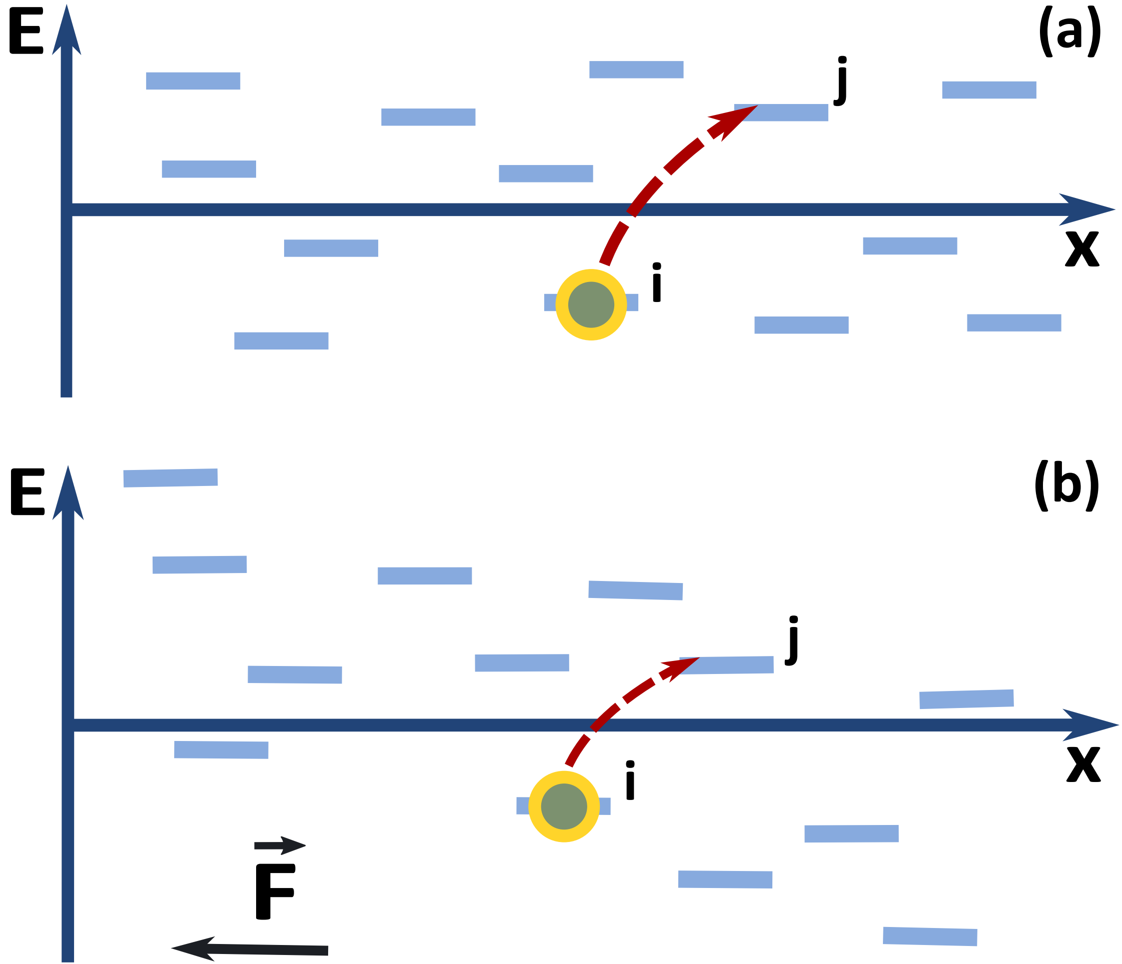

FIGURE 1.2: Distribution of sites in energy and space: (a) without electric field, (b) with electric field

The electric field **F** creates a slope in energy landscape, as schematically depicted in Fig. 1.2. To take **F** into account we should rewrite energy difference $\Delta\varepsilon$ and γ-factor in Eqs. (1.3 - 1.4) as follows

$$\gamma(\Delta\varepsilon) = \gamma(\varepsilon_j - \varepsilon_i + e\mathbf{F} \cdot \mathbf{r}_{ij}) \tag{1.6}$$

Here e is electric charge of the carrier. In such a situation carrier will favor hops to lower sites and on average will move along the field.

Thus, taking into account temperature and electric field, one can write the equation for hopping event rate in the following way:

$$\nu_{ij} = \nu_0 \exp\left(-\frac{2|\mathbf{r}_{ij}|}{a}\right) \gamma(\varepsilon_j - \varepsilon_i + e\mathbf{F} \cdot \mathbf{r}_{ij}) \tag{1.7}$$

with

$$\gamma(\Delta\varepsilon) = \begin{cases} \exp(-\Delta\varepsilon/kT), & \text{if } \Delta\varepsilon > 0, \\ 1, & \text{otherwise.} \end{cases} \tag{1.8}$$

1.4 General assumptions and parameters of the model

When using the hopping transport model, typically a number of assumptions are made. It is assumed that sites has no structure, meaning that hopping rates depends only on the distance and energy difference between initial and final sites. Another approximation is replacing quantum-mechanical tunneling process by s classical random walk, which is justified when the typical tunneling distance is large compared to localization length, i.e. carrier is not "simultaneously spread" over several LS. It is also assumed that sites distributed randomly in space without any spatial-energy correlations. This assumptions will be made throughout this work. Any additional assumptions will be mentioned in details for every specific case. In frame, of this assumptions, properties of the disordered system in hopping transport model depends on the following physical quantities:

- Energy parameters of disorder ε_0, σ, *etc*;
- oncentration of traps N;
- Localization length a;
- Temperature T;
- Electric field $\mathbf{F}$;
- Carrier charge e;

For simplicity and generalization we will in many cases use the set of dimensionless parameters to describe the system: $\frac{\varepsilon_0}{kT}$, $\frac{eFa}{\varepsilon_0}$ and Na^d, where d is dimension of the system.

1.5 Analytical and numerical applications of the model

Analytical treatments for a number of the hopping transport questions are well known. For instance, the case of sites with equal energies in low electric field can be treated in

frame of percolation theory [14]. Another example is Mott variable-range hopping model describing the temperature dependence of conductivity in strongly disordered systems at low-temperature limits [15]. For the opposite case of high temperature and short localization length (in comparison to sites concentration) transport can be described in frame of nearest-neighbor hopping model [15]. The temperature dependence of the mobility has been also analyzed using the concept of transport energy and analytical expression for electron mobility in low-field was derived recently [16]. However, the general, analytical solutions to the hopping transport problem and to the problem of excitons recombination in disordered systems has not been obtained so far. While it is unlikely to solve these problems completely analytically, they are perfectly suited for numerical approaches. One popular technique is solving so-called balance equations – system of linear equations, relating the probabilities of sites to be occupied and the flow of carriers between them. Another numerical method is the Kinetic Monte Carlo (KMC) simulation – direct simulation of hopping processes using random numbers generation. Through this work we will apply the KMC method to study hopping transport and recombination of excitons in disordered materials.

1.6 Kinetic Monte Carlo approach

Simplest Monte Carlo approach to study transport or optical properties of disordered systems is to simulate a single particle hopping. This corresponds to low carriers density, when interaction between carriers could be ignored. The carrier performs a random walk in the system of sites. We are interested in the statistics of this random events. In the Monte Carlo method the transport parameters optical spectrum are determined by actually performing, with a computer program, such a random walk in a randomly generated system of sites. For each hop that the carrier makes in the simulation, the destination site is chosen randomly, but weighted by the hopping rates, to each possible destination site. The time the carrier spends on each site is also chosen randomly, and depends on the total rate of hopping out of that site. In addition, one can extend the KMC approach for the case of many particles, by introducing additional step of choosing carrier to perform next hopping event. Carrier is chose based on cumulative hopping rates of all carriers (sums of the rates of all possible hopping events for the carriers). However, many-particle simulations may be extremely slow in terms of performance.

For simplicity, let us assume a case of single electron. KMC approach to simulate hopping process will look as follows:

1. Generate a system of sites with random energies distributed according to the DOS and random coordinates corresponding to the given concentration;
2. Set up the electron to some initial site;
3. Calculate cumulative rate of all hopping events from the current site;
4. Using random number, determine time spent by electron on current site;
5. Using another random number, chose a hopping event (i.e. determine the new site to which electron will jump) to perform;
6. Move electron to the new site;
7. Return to step 3.

At step 2 of the algorithm we have located the electron at some site i. Hopping rate from site i to some other site j is given by Miller-Abrahams Eq. (1.7). The cumulative rate is the result of the summation of all hopping rates from site i to other sites:

$$\Gamma_i = \sum_j \nu_{ij} \tag{1.9}$$

The probability that the next electron hop will take it from sit i to site j is given by:

$$p_{ij} = \frac{\nu_{ij}}{\Gamma_i} \tag{1.10}$$

And the time spent on site i is determined as:

$$\tau_i = -\frac{\log(x)}{\Gamma_i}, \tag{1.11}$$

where x is random number in range $[0, 1]$. Thus, τ_i has an exponential distribution, with the expected value Γ_i^{-1}. Using this simple algorithm we can directly simulate hopping transitions of the carrier in the disordered system. As one can see, the KMC

method is relatively simple to implement, especially in the case of a single particle. Yet the method can be very effective in terms of performance in comparison to balance equations approach. In this part we have only briefly covered the general ideas of hopping transport model and KMC simulation. In the next chapters we will expand in much greater details the topic of implementing KMC approach to study optical and transport properties of disordered systems.

1.7 General remarks on Monte Carlo method and random numbers generation

To understand the computational complexity of the Monte Carlo approach and important consequences for simulations let us take a look at the general scheme of Monte Carlo method. Let us assume, that we want to determine some unknown value x. And assume we also can generate a set of n random numbers $r_1, r_2...r_n$ with the expected value and dispersion given by:

$$\mathbf{E}r_i = x, \tag{1.12}$$

$$\mathbf{D}r_i = \sigma_0^2. \tag{1.13}$$

According to the Central Limit Theorem, for high enough value of n, probability distribution of the sum $\rho_n = r_1 + r_2 + ... + r_n$ approaches normal distribution with parameters:

$$\mu = nx, \tag{1.14}$$

$$\sigma^2 = n\sigma_0^2 \tag{1.15}$$

Using the so-called three-sigma rule (random value from the normal distribution with dispersion σ will fall into the range $[-3\sigma, 3\sigma]$ with probability better than 0.997) we receive the following formula:

$$P\left\{x - \frac{3\sigma_0}{\sqrt{n}} < \frac{\rho_n}{n} < x + \frac{3\sigma_0}{\sqrt{n}}\right\} \approx 0.997 \tag{1.16}$$

The formula above could be rewritten as:

$$P\left\{\frac{1}{n}\sum_{i=1}^{n}(r_i - x) < \frac{3\sigma_0}{\sqrt{n}}\right\} \approx 0.997 \tag{1.17}$$

Equation 1.17 is of a high importance for Monte Carlo method. It gives us an approach to calculate the approximate value of x and also evaluation of the error of such an approximation, which is almost surely does not exceeds $\frac{3\sigma_0}{\sqrt{n}}$. The last issue is very important for the simulations because it tells us that the convergence of the Monte Carlo approach is $O(\sqrt{n})$, which basically means that in order to increase accuracy by a factor of 10 one must increase the number of realizations in simulation by a factor of 100. In the simulations described in the present work, random numbers are normally used in two steps - while generating the system of LS and then in choosing the hopping events. To get reliable results, the simulation may require generating of over 10^9 random numbers. Therefore, it is important to use random numbers of a good quality. Any correlations between successive random numbers might influence the result. Thus, one should be very careful, using pseudo-random numbers generators. Linear congruential generators, such as the one of C standard library, normally generates sequences of pseudo-random numbers with the maximum period of 2^s, where s is the bits of the system. For instance, for 32-bit system such a period is less than 10^{10}. In my simulations I have used the Mersenne Twister mt19937 algorithm (with the period of 2^{19937}) from C++ Standard Templates Library. It also contains (since C++ 11) implementations of different distributions (in particular Gaussian and exponential) with a good reputation.

Chapter 2

Excitons recombination in disordered materials

In this chapter we are discussing optical properties of disordered semiconductor materials. In particular, dilute nitride III-V alloys, which are in focus of researchers interest because of their potential for application in optoelectronic devices and their unique physical properties. The anticrossing interaction between localized nitrogen states and the extended states of the semiconductor matrix opens a wide range of possibilities for the fabrication of long wavelength lasers and light-emitting diodes in the range of 1.3 – 1.5 μm and a long wavelength component of multi-junction solar cells. The practical implementation of these devices is conditioned by several requirements such as emission wavelength and intensity, the monochromaticity of the emitted light, and the possibility of integrating the semiconductor alloy into monolithic optoelectronic circuits on Si substrates. One of the best candidates to meet these requirements is the GaAs-based Ga(NAsP) quaternary alloy. It is a direct semiconductor and the desired band gap and the lattice parameter can be adjusted by varying the N and P contents. However, the price to be paid for this goal is an essential amount of disorder due to compositional fluctuations. The disorder gives rise to the band tails composed from localized states having a significant influence on the emission wavelength and the emission line-width. The photoluminescence (PL) spectra have become a standard tool for characterizing the optical properties of compound semiconductors and hence, the quality of corresponding optoelectronic devices. For theoretical interpretation of the experimental PL spectra the model suggested by S.D. Baranovskii, R. Eichmann and P. Thomas [3] (further BET

model) is widely used. BET model can be perfectly applied in the frame of KMC approach to simulate PL spectrum of disordered materials and became one of the efficient tools to study peculiarities of PL in disordered materials theoretically. The suggested approach takes into account the hopping transitions of photo-excited excitons between the localized states and gives the excellent explanation for PL features of different compound quantum well structures [17–20], quantum dots [21–23] and bulk semiconductor alloys [24]. However, not all of the PL features of such promising material as Ga(NAsP) or Ga(AsBi) can be explained in frames of original BET model. In the next few sections I will tell in details what is the original BET model, what kind of PL features it could and could not explain,and finally will suggest possible extensions of the BET model, which allow to explain all of the PL peculiarities of Ga(NAsP) in frame of a single approach.

2.1 Generic PL features in disordered materials and the BET model

Disorder-induced localized states have a crucial influence on the PL characteristics of compound materials. Photo-excited charge carriers are rapidly captured by localized states in the tail of the density of states. The hopping dynamics of captured carriers between localized states leads to a significant red-shift of the PL peak energy E_{peak} with respect to the band edge E_{g} (so-called Stokes shift), as shown schematically in Fig. 2.1(a).

At very low temperatures, only the energy-loss hopping, that is, tunnelling transitions downward in energy, is possible. Upon a small increase in temperature, the upward transitions, as well as the ionization of captured charge carriers from localized into extended states, become possible, too. After an upward transition, the charge carriers have a chance to explore more localized states and to find energetically deeper states for recombination. As a result, the PL peak energy goes deeper into the band tail, the corresponding Stokes shift increases, and the PL spectra become broader as a function of temperature, as shown schematically in Figs. 2.1(b) and (c), respectively.

At high temperatures, the energy distribution of the charge carriers tends to a thermal distribution and the Stokes shift decreases as a function of temperature because the density of localized states is larger at higher energies. Correspondingly, the width of

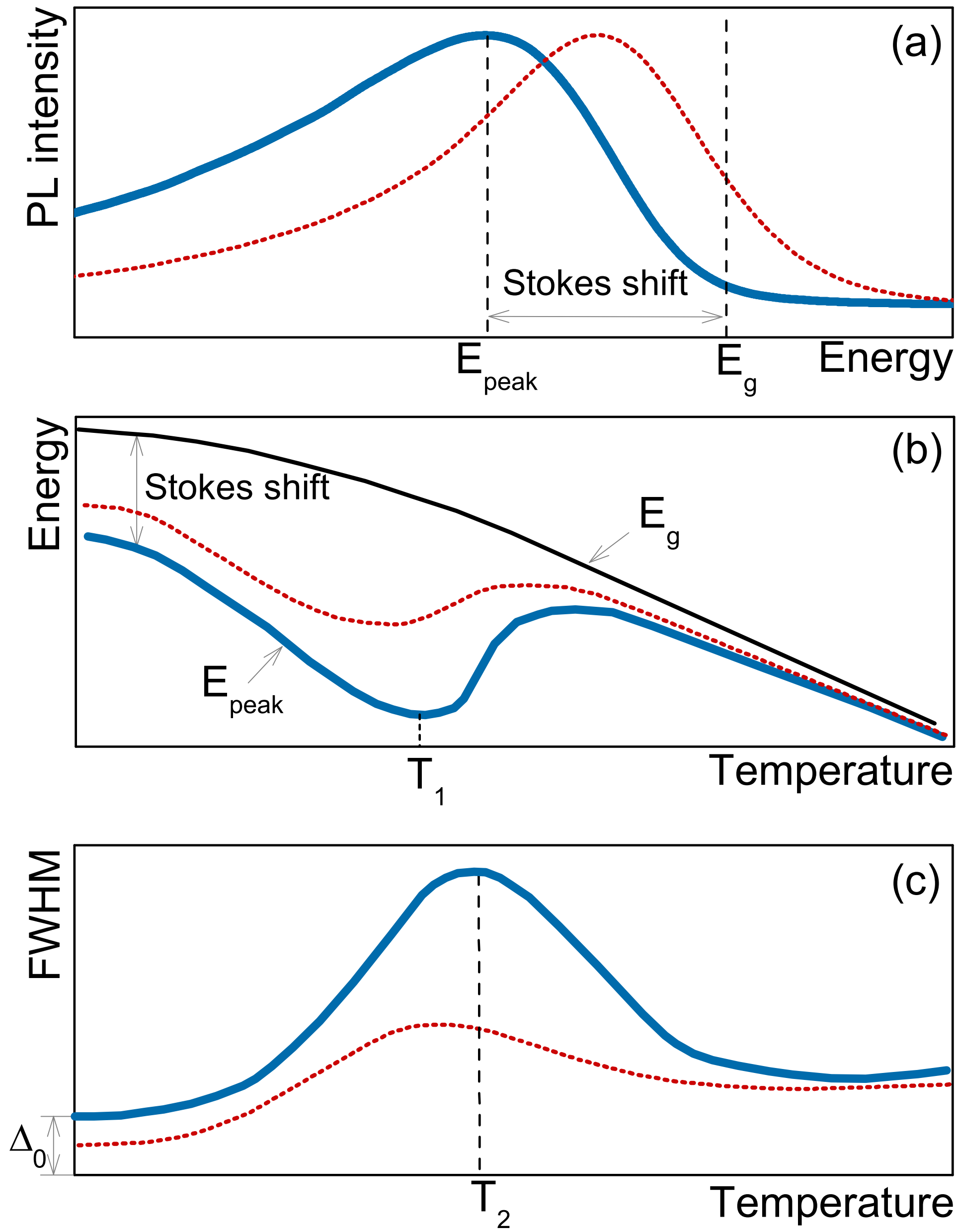

FIGURE 2.1: Schematic PL features: (a) shapes of the PL spectra, (b) temperature-dependent PL peak position, and (c) PL linewidth at low (thick solid line) and high (dotted line) excitation intensities, taking into account hopping transitions of carriers between localized states. In (b), the temperature dependence of the band edge is shown by a thin solid line.

the PL spectra decreases as well. As a result, the charge carrier dynamics leads to non-monotonic temperature dependencies of the Stokes shift and of the PL linewidth with pronounced maxima at temperatures T_1 for the Stokes shift,see Fig. 2.1(b), and at temperature T_2 for the PL line width, see Fig. 2.1(c), respectively.

The PL characteristics of the compound materials are strongly affected by the intensity of the exciting light pulse. An increase of the excitation intensity leads to a larger number of photo-excited carriers, and the energetically deeper part of the band tail becomes 'crowded' by the captured carriers and hence unavailable for the downward hopping transitions from the shallower localized states. As a result, the Stokes shift of the PL peak energy and the PL linewidth decrease with increasing excitation intensity as shown in Fig. 2.1 by the dotted lines. Accordingly, the characteristic temperatures T_1 and T_2 that correspond to the maxima in the temperature-dependence of the Stokes shift and of the PL linewidth decrease.

The crucial material characteristics that determines the general PL features shown in Fig. 2.1 are the shape and the scale of the energy distribution of localized states. These material characteristics can be extracted from the experimental data via a comparison of observed and simulated PL features where the model takes into account the hopping dynamics of photo-excited charge carriers captured in the band tail of localized states.

For a theoretical interpretation of the experimental PL spectra, the BET model is widely used. This model is based on the assumption that electron-hole pairs generated by the optical excitation are captured into localized states induced by the disorder potential. The captured carriers can perform the following processes.

(I) They can recombine radiatively with the rate $\nu_{\mathrm{r}} = 1/\tau_{\mathrm{r}}$, where τ_{r} is the radiative lifetime of the electron-hole pairs;

(II) They can be excited from the localized state i into an extended state with rate

$$\nu_{\mathrm{ion}} = \nu_0 \exp\left(\frac{E_i}{k_{\mathrm{B}}T}\right) , \tag{2.1}$$

where ν_0 is the attempt-to-escape frequency, k_{B} is the Boltzmann constant, T is the temperature, and E_i is the energy of the localized state measured from the mobility edge;

(III) The carriers captured on the localized state i can be transferred to the localized state j. The corresponding hopping probability is governed by the Miller-Abrahams tunneling rate [13]

$$\nu_{ij} = \nu_0 \exp\left(-\frac{2R_{ij}}{\alpha} - \frac{E_j - E_i + |E_j - E_i|}{2k_{\mathrm{B}}T}\right) , \tag{2.2}$$

where E_i and E_j are the energies of the initial (i) and the target (j) sites, respectively, R_{ij} is the distance between the sites and α is the localization length.

The carrier kinetics is carried out under the following assumptions.

(i) The trapping sites are randomly distributed in space;

(ii) The site energies E_i and their spatial positions $\vec{R}_i$ are uncorrelated;

(iii) Electron-hole pairs are strongly correlated into excitons that are localized by the disorder potential that acts on their center of mass [25];

(iv) The exciton density is sufficiently low so that the tail of the density of states can be considered unoccupied.

The crucial input of the BET model is the density of the localized states (DOS). The application of this model to various semiconductor systems [17–24] showed that the PL characteristics of the studied compounds can be described very well by assuming a single-component DOS with exponential energy distribution of the localized states

$$g(E) = \frac{N}{E_0} \exp\left(\frac{E}{E_0}\right) , \tag{2.3}$$

where N is the concentration of the LS and E_0 is the characteristic energy scale. Furthermore, the Monte Carlo simulations for the BET model with the single exponential DOS (2.3) revealed universal relations between the disorder energy scale E_0 and experimentally observed PL features, as collected in the first column of Table 2.1, where T_1 and T_2 denote the characteristic temperatures introduced in the previous section and Δ_0 is the full width at half maximum (FWHM) of the low-temperature PL spectra, see Fig. 2.1(c).

Relation between E_0 and PL features	E_0 (meV) (GaIn)(NAs)[1]	Ga(NAsP)[2]
$k_B T_1 = (0.75 \ldots 0.80)\, E_0$	5.6	10.4
$k_B T_2 = (1.10 \ldots 1.15)\, E_0$	4.6	10.4
$\Delta_0 = (2.5 \ldots 2.7)\, E_0$	6.8	57.0

TABLE 2.1: Universal relations between the disorder energy scale E_0 of the exponential energy density of localized states, see Eq. (2.3), and various PL features (first column) together with the values of E_0 extracted from the PL characteristics for (GaIn)(NAs) (second column) and for Ga(NAsP) (third column).

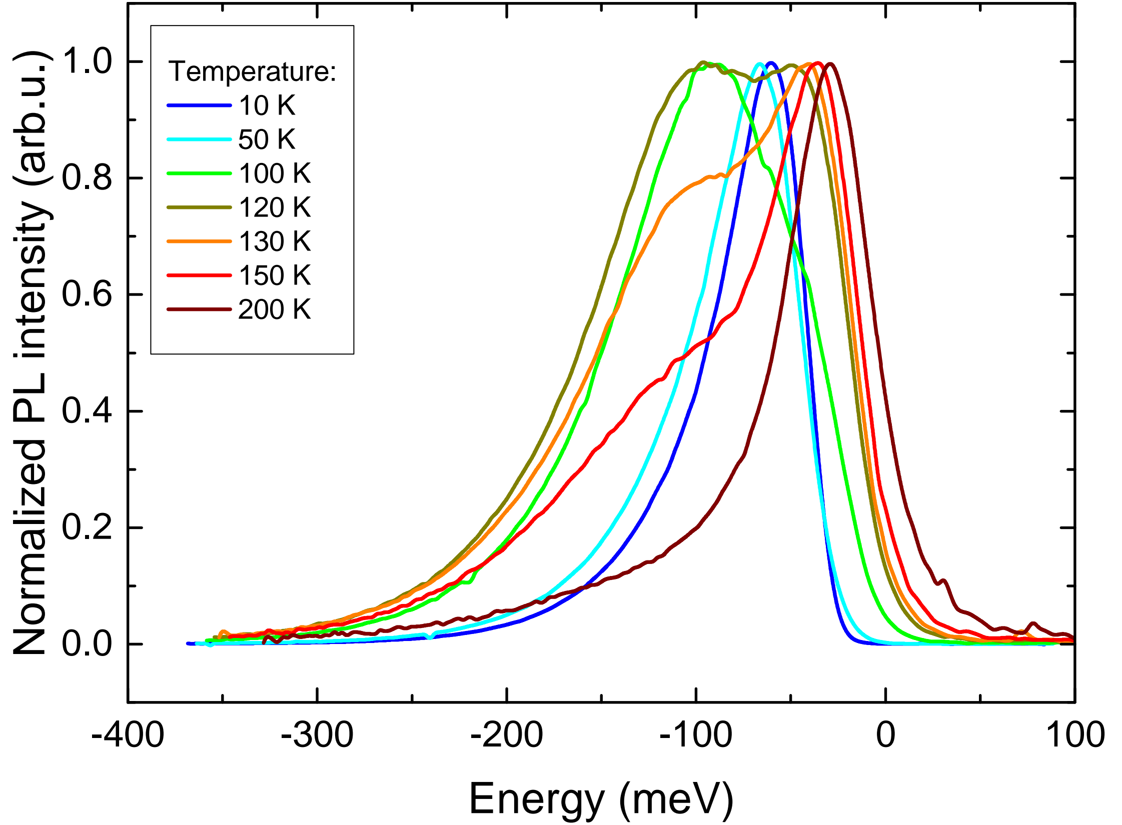

FIGURE 2.2: Experimental PL spectra of the $Ga(N_{0.04}As_{0.91}P_{0.05})/GaP$ compound for various temperatures.

2.2 Anomalous linewidth broadening and low-temperature linewidth shrinkage in Ga(NAsP)

For all compound systems studied in Refs. [17–24], the values for E_0 extracted from the different PL features were in good agreement with each other. For example, the experimental data for T_1, T_2, and Δ_0 obtained for (GaIn)(NAs)/GaAs quantum well structure [18], can be reconciled with $E_0 = (6 \pm 1)$ meV, see the second column of Table 2.1.

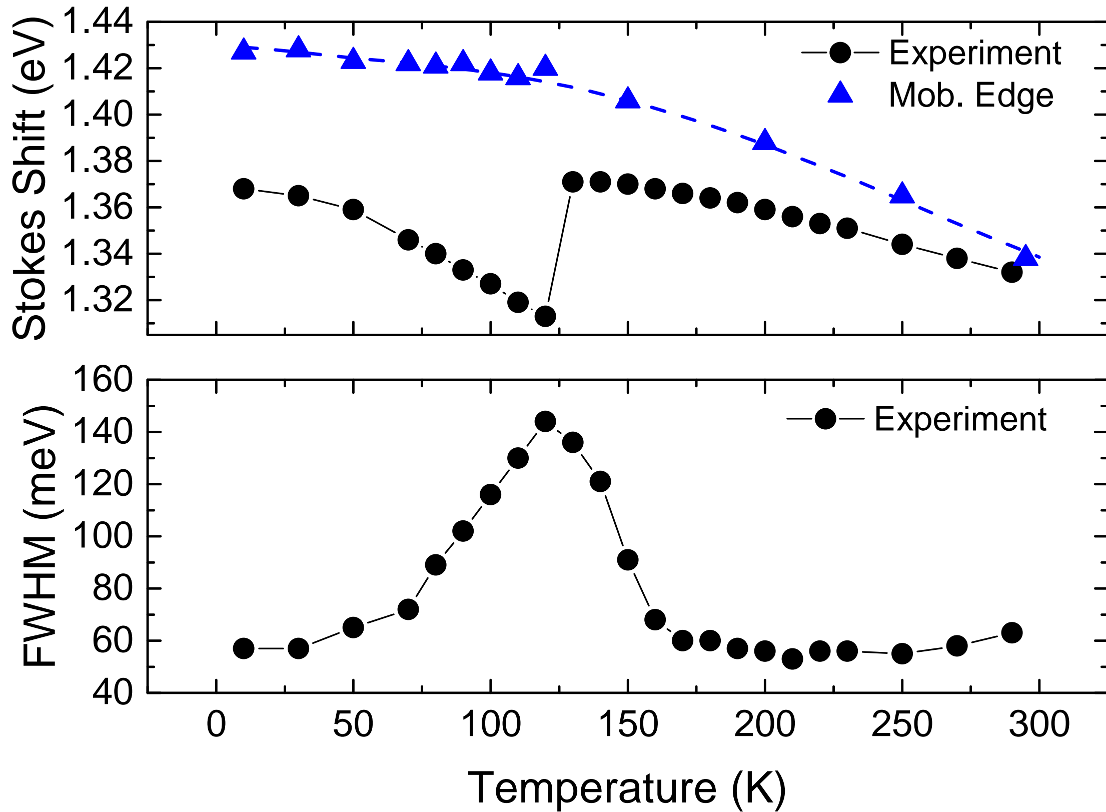

FIGURE 2.3: Experimental Stokes Shift and FWHM of the $Ga(N_{0.04}As_{0.91}P_{0.05})/GaP$ compound.

However, the studies on Ga(NAsP) (as well as Ga(AsBi)) semiconductor compounds revealed that the energy scale of disorder E_0 extracted from the PL linewidth Δ_0 is significantly larger than that estimated from the characteristic temperatures T_1 and T_2. As an example, for a Ga(NAsP)/GaP quantum well structure [7] E_0 as derived from Δ_0 is almost a factor of six larger than E_0 derived from the characteristic temperatures $T_{1,2}$, as shown in the third column of Table 2.1. One can clearly see this by comparing experimentally measured PL spectra (Fig. 2.2) with Stokes Shift and FWHM (Fig. 2.3). Extremes of the PL features in Fig. 2.3 are approximately at 120 K, which, according to the universal relations of the BET model, corresponds to the value of E_0 about 10 meV. At the same time, the value of E_0 extracted from the PL curves(as the slope of a low-energy tale) Fig. 2.2 is greater than 50 meV. The large discrepancy in the extracted values of E_0 necessitates an extension of the conventional BET model to explain the unusual PL behaviour of Ga(NAsP) and Ga(AsBis) compound materials. Thus, one of the problems of the standard BET-model is that some materials, in particular, Ga(NAsP) and Ga(AsBis), demonstrate unexpectedly broad PL linewidth in contradiction to universal relations discussed above.

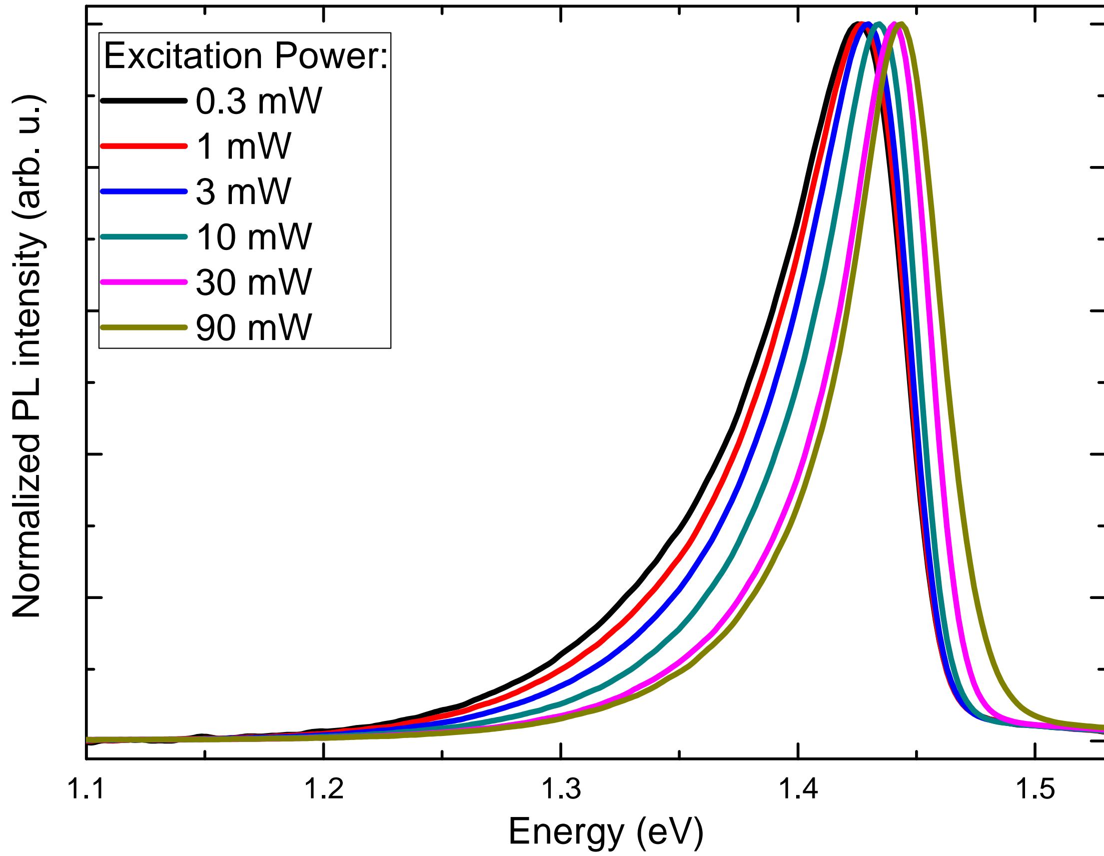

FIGURE 2.4: Excitation dependence of PL spectra of $Ga(N_{0.03}As_{0.92}P_{0.05})/GaP$ MQWs measured at 10 K.

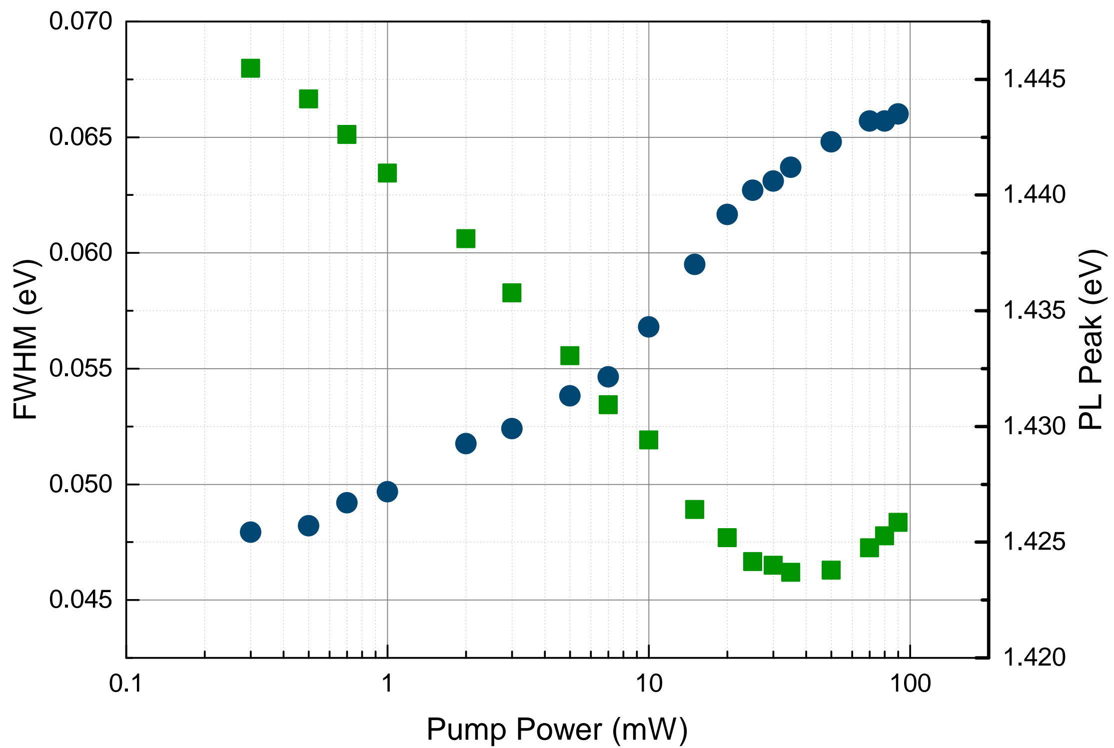

FIGURE 2.5: PL peak (blue circles) energy and FWHM (green rectangles) as functions of the excitation intensity measured in $Ga(N_{0.03}As_{0.92}P_{0.05})/GaP$ MQWs.

Another interesting feature of Ga(NAsP) PL spectrum is low-temperature excitation dependence of the PL linewidth. In Fig. 2.4 depicted experimental measurements of PL spectra in $Ga(N_{0.03}As_{0.92}P_{0.05})/GaP$ multiple quantum wells (MQWs). Measurements were made under different excitation powers in the range from 0.3 to 90 mW at the temperature of 10 K. One can notice, that the width of the PL spectra(FWHM) decreases with the increase of excitation power. Such a behaviour is absolutely contradicting to intuitive expectations. One would rather expect that increasing concentration of excitons in the system should lead to the broadening of the PL spectra, however, the experiment shows opposite dependency. Dependencies of FWHM and PL peak position on excitation intensity is given in Fig. 2.5. One can see that PL FWHM decreases roughly from 70 to 45 meV with the increase of excitation power.

Thus, there are two problems that are not well described in the frame of a conventional BET model:

1. The effect of PL linewidth shrinkage at low temperatures in Ga(NAsP);
2. The anomalously broad PL spectrum of Ga(NAsP), which contradicts to the BET model predictions;

Historically, the first approach to solve the problem of the anomalously broad spectral line of Ga(NAsP)/GaP was developed in 2010 – so-called, BET model with two scales of disorder [7]. However, results of my research on the effect of linewidth shrinkage revealed a number of significant contradictions with that model and eventually led to the alternative model, that allows describing both of the problems. We will start first discussing the problem of PL linewidth shrinkage in Ga(NAsP)/GaP and extension of the BET model, which is necessary to explain this effect.

2.3 The concept of complex DOS

The key input of the conventional BET model is the energy distribution of LS. The application of this model for various quantum wells [18–20], as well as for quantum dots [21–23] and bulk semiconductor alloys [24] reveals the exponential shape of the DOS

$$g(E) = \frac{N_0}{E_0} exp\left(\frac{E}{E_0}\right). \tag{2.4}$$

Also, such a model with the DOS given by (2.4) was successfully applied by M. Barabovskii to describe PL lineshape dependence on excitation in (GaIn)(NAs)/GaAs [26].

However, the experimental results discussed above indicate that the behaviour of the PL linewidth is qualitatively different. As we have already seen, in a wide range of excitation intensities, the PL linewidth decreases drastically, reaching a minimum and beginning to rise at very high excitation intensities. Similar behaviour was also reported by other research groups for InGaN/GaN [4] and GaAsBi/GaAs [5]. KMC simulation is definitely a powerful tool for such type of problems, that allows us to simulate the behavior of the PL line shape assuming different sets of parameters, trying to make a good guess. The key feature that determines the shape of the PL spectra is the shape of the DOS. As I have mentioned above, the standard assumption for conventional BET model is exponential DOS. However, I have tried dozens of KMC simulation with different values of key parameters of the BET model and was not able to achieve at least qualitatively similar behaviour to what we have seen in experiment assuming exponential DOS. Thus, it looks very likely that one should assume none-exponential DOS. Remarkably, the recent studies on thermal quenching of PL in Ga(AsBi)/GaAs quantum well structures [27] revealed that a complex none-monotonous DOS is required to describe the experimentally observed dependence of the PL lineshape on the temperature. Taking into account the fact that the excitation-dependent PL lineshape in Ga(AsBi)/GaAs behaves [6] very similarly to that in Ga(NAsP)/GaP, I have suggested to extend the BET model with a two component DOS to explain the experimentally observed dependencies of the low temperature PL peak energy and the PL lineshape on the excitation intensity in Ga(NAsP)/GaP quantum well structure.

According to our simulation results, the best agreement with experimental data can be achieved assuming the DOS in the following form:

$$g(E) = A_0 exp\left(\frac{E}{E_0}\right) + A_1 exp\left(\frac{(E-E_1)^2}{2\sigma_1}\right), \tag{2.5}$$

composed of exponential and Gaussian distributions with characteristic energies E_0, E_1 and σ_0. A_0 and A_1 are the normalization parameters determined by the relative numbers

N_0/N_1 of the localized states in the exponential and Gaussian components of the DOS, respectively.

2.4 KMC simulation of PL linewidth shrinkage in Ga(NAsP)

2.4.1 KMC simulation algorithm

The simulation was conducted under the following considerations. We assume the system with N LS and N_{ex} excitons. We also assume that excitons behave like a single noninteractive particles in their hopping movement between LS and have typical recombination time τ_0. A step-by-step recipe for the KMC simulation looks as follows:

1. Generate N LS with energy distribution governed by the DOS $g(E)$ and uniform spatial distribution in 2D rectangle;

2. Calculate rates for all possible events for localized and extended states (ES). We assume the following events: hopping transitions between LS with rate ν_{ij},given by 1.3, activation from LS to ES with rate $\nu_i = \nu_0 exp\,(E_i/k_B T)$, capturing excitons from ES to LS with rate ν_0 and recombination with rate $1/\tau_0$;

3. Set N_{ex} excitons to ES (generate initial state of the system);

4. Calculate cumulative event rates for all excitons using expression $\Gamma_i = \sum\limits_{i \neq j} \nu_{ij} + \nu_i + \nu_0 + 1/\tau_0$ and determine the time before next event for each exciton as $\triangle\tau_i = \Gamma_i^{-1} R_i$, where $R_i = ln(x)$ and x is the uniformly distributed random number from the range $(0, 1]$;

5. Select exciton with the shortest time before the next event $\triangle\tau_{min} = min(\triangle\tau_i)$. Use random number $p \in [0, 1]$ to determine which event will occur next with the selected exciton, based on the normalized event rates.

6. Perform the event (update the current state of the system);

7. In case of recombination event save the energy value, otherwise generate new time residual R_0^{new} for the selected exciton. Recalculate time residuals R_i for all other excitons with the expression $R_i^{new} = R_i - \Gamma_i \triangle\tau_0$, to take waiting time into account;

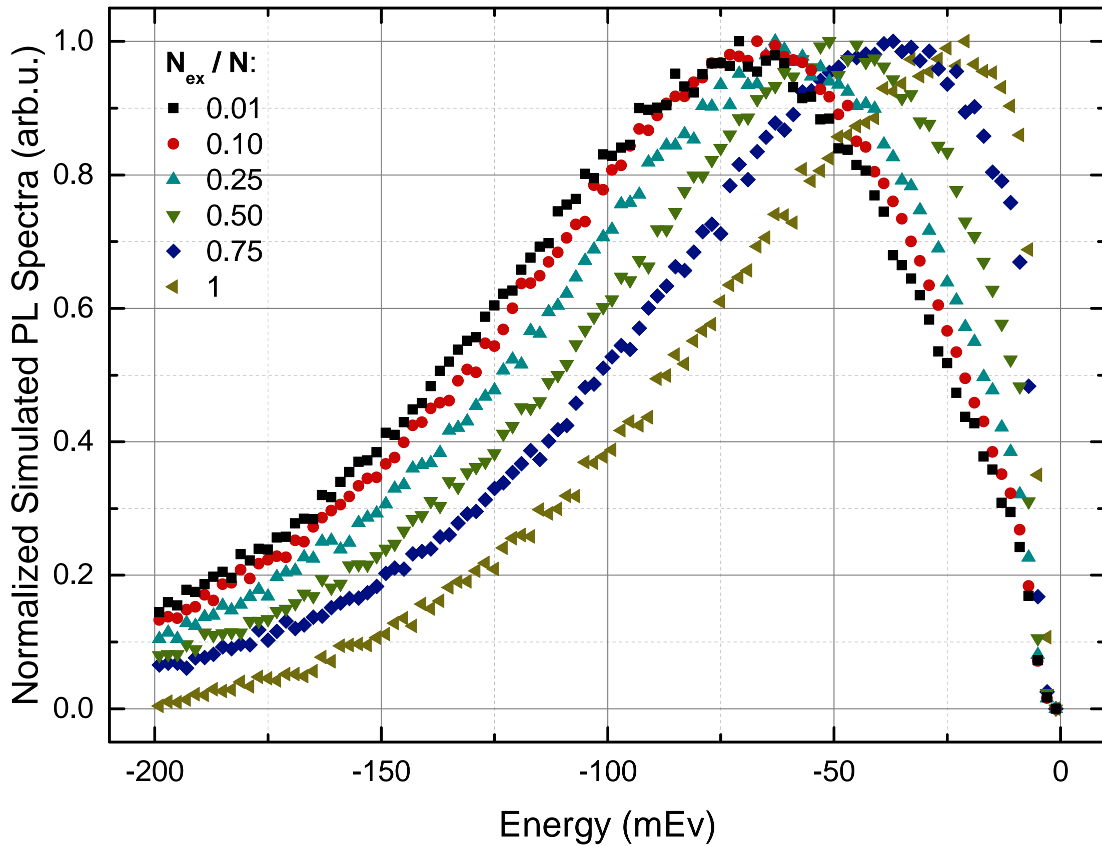

FIGURE 2.6: Simulated PL spectra for exponential DOS, given by Eq. (2.4). N_{ex}/N - filling factor(relation between number of excitons and number of LS).

8. Go to step (v).

As a result of the procedure described above, one receives theoretical PL spectra. In order to get reliable results, the procedure should be repeated a sufficient number of times N_{MC}. In case of my simulations N_{MC} varied from 10^4 to 10^5. Since we are running a many-particles simulation with a large number of excitons, computational complexity increases drastically and it becomes impossible to run the simulation for the large numbers of sites N. In my experience a number of sites for which simulation takes acceptable time is an order of $10^2 - 10^3$. To find if the value of N affects the result I have tested values of N in the range $10^2 - 5 \times 10^2$. Remarkably, already for $N = 10^2$ further increase of the number of sites does not noticeably change the result. Thus the number of LS N in simulation was chosen to be 10^2.

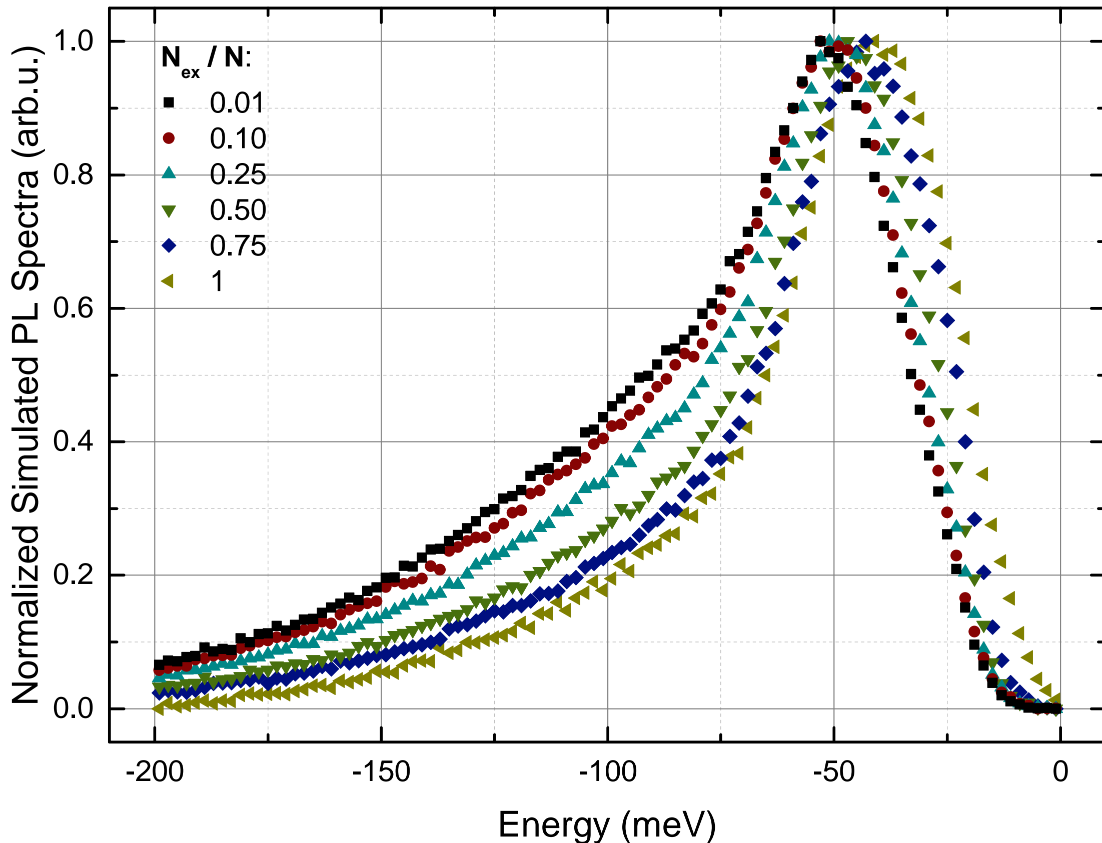

FIGURE 2.7: Simulated PL spectra for composite DOS, given by Eq. (2.5). N_{ex}/N - filling factor(relation between number of excitons and number of LS).

Parameter	Value	Description
N_0/N_1	7/3	Fitting parameter
E_0	46 [meV]	Experimentally determined
E_1	36 [meV]	Fitting parameter
σ_1	16 [meV]	Fitting parameter
$N\alpha^2$	0.06	Fitting parameter
$\nu_0\tau_r$	10^3	Experimentally determined

TABLE 2.2: Simulation parameters for the $Ga(N_{0.03}As_{0.92}P_{0.05})/GaP$ linewidth shrinkage

2.4.2 KMC simulation results

We have applied BET model with different shapes of the DOS to simulate the excitation-dependent PL features in Ga(NAsP) to find out which fits best to describe the effect of PL linewidth shrinkage. In the simulations different excitation intensities W are reproduced by the different numbers of excitons N_{ex} in the system, assuming the linear relation $W \propto N_{ex}$. This is an important assumption, while it allows us to compare simulated dependencies of PL FWHM and energy peak position on excitation power. This assumption looks reasonable due to the linear dependence of the integrated PL

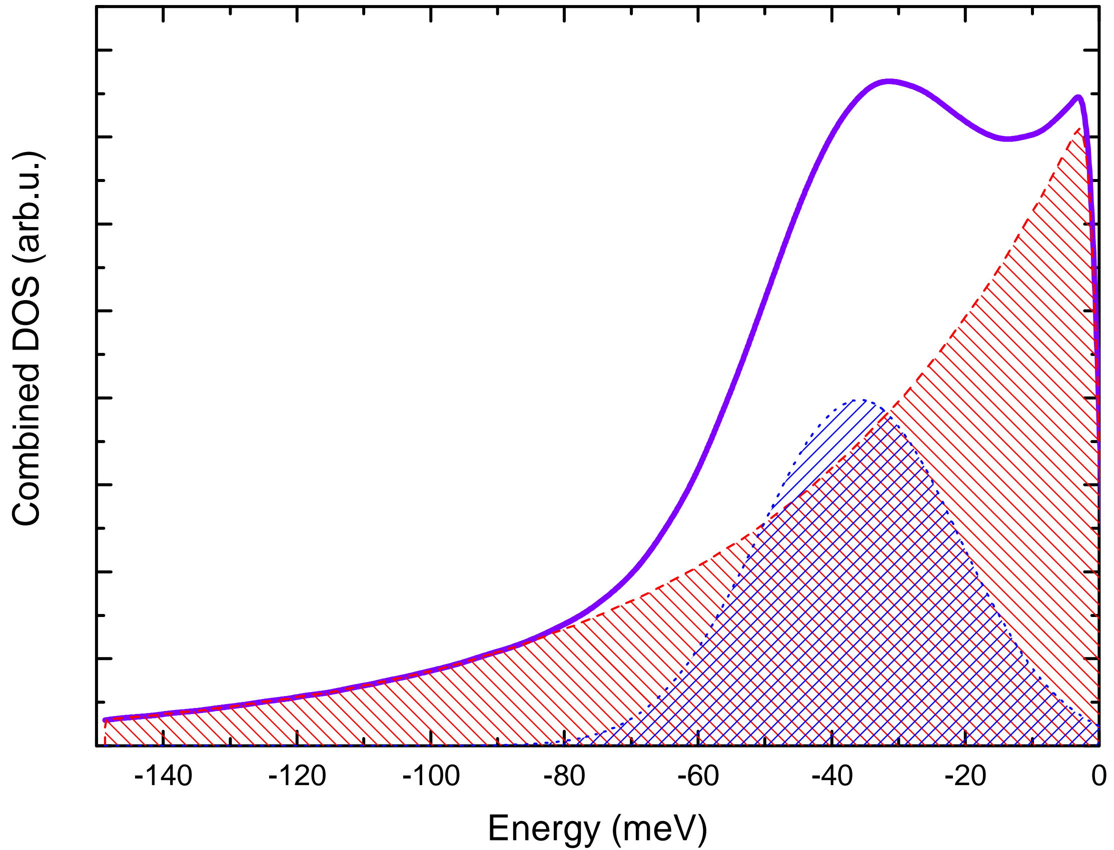

FIGURE 2.8: Combined DOS given by 2.5 with parameters from table 2 (solid line). Exponential and Gaussian components of the DOS are also shown by dashed and dotted lines, respectively.

signal on the excitation intensity observed in experimental studies. One should notice that the dependence of FWHM on excitation is non-monotonous and reaches a minimum at some point. Using this fact, corresponding proportionality factor can be determined by comparing the positions of the minimums in experimentally observed and simulated dependencies of the PL linewidth on the values of W and N_{ex}, respectively. Results of simulation for monotonous shapes of the DOS (such as pure exponential or pure Gaussian) has exposed that it is impossible to achieve such an effect, assuming such DOS. Fig. 2.6 represents typical spectra for various excitations corresponding to exponential DOS. One can clearly see that the width of the PL line does not change much while excitation is being increased. Looking at experimental data (Fig. 2.4) it is easy to see, that this simulation does not reproduce the expected shape of the PL line. Moreover, by testing various other monotonous DOS's, I have came up with the conclusion that PL spectra as given in Fig. 2.4 is a typical picture for all of them. Thus , it is very likely that one should assume some more complex shape of the DOS.

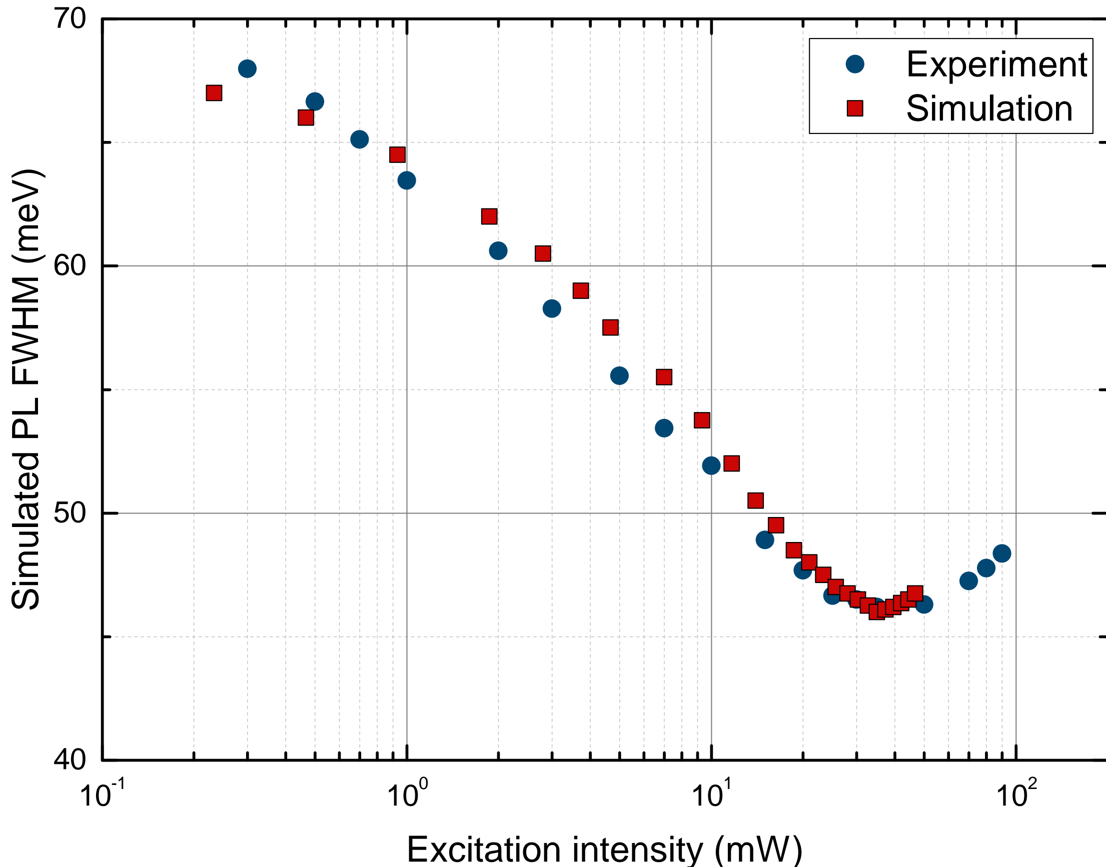

FIGURE 2.9: PL FWHM as functions of the excitation intensity observed experimentally in $Ga(N_{0.03}As_{0.92}P_{0.05})/GaP$ MQWs (circles) and simulated (rectangles) for combined exponential-plus-Gaussian DOS.

As already stated above, the main candidate for this role was combined exponential-plus-Gaussian DOS, given by Eq. (2.5). Such an approach shows very good agreement with experimental results under a certain set of parameters. The complete set of simulation parameters is gathered in table 2, while the shape of the corresponding DOS is depicted in Fig. 2.8.

Simulated PL spectra for this DOS are shown in Fig. 2.7. Simulation results for the excitation dependent PL linewidth and the PL peak energy are shown by rectangles in figures 2.9 and 2.10, respectively. The minimum of the simulated PL linewidth is achieved at $N_{ex} = 75$ excitons per 100 sites, while according to experimental results, the PL linewidth reaches a minimum at the excitation intensity $W = 35$ mW. Therefore, the proportionality factor in the N_{ex} and W relation can be assumed to be 2.14 mW. The further increase of the excitation intensity (and hence, of the number of excitons in the simulation) leads to the broadening of PL spectra. At $W = 45$ mW the manifold of localized states becomes saturated. Therefore, the further blue shift of the PL peak

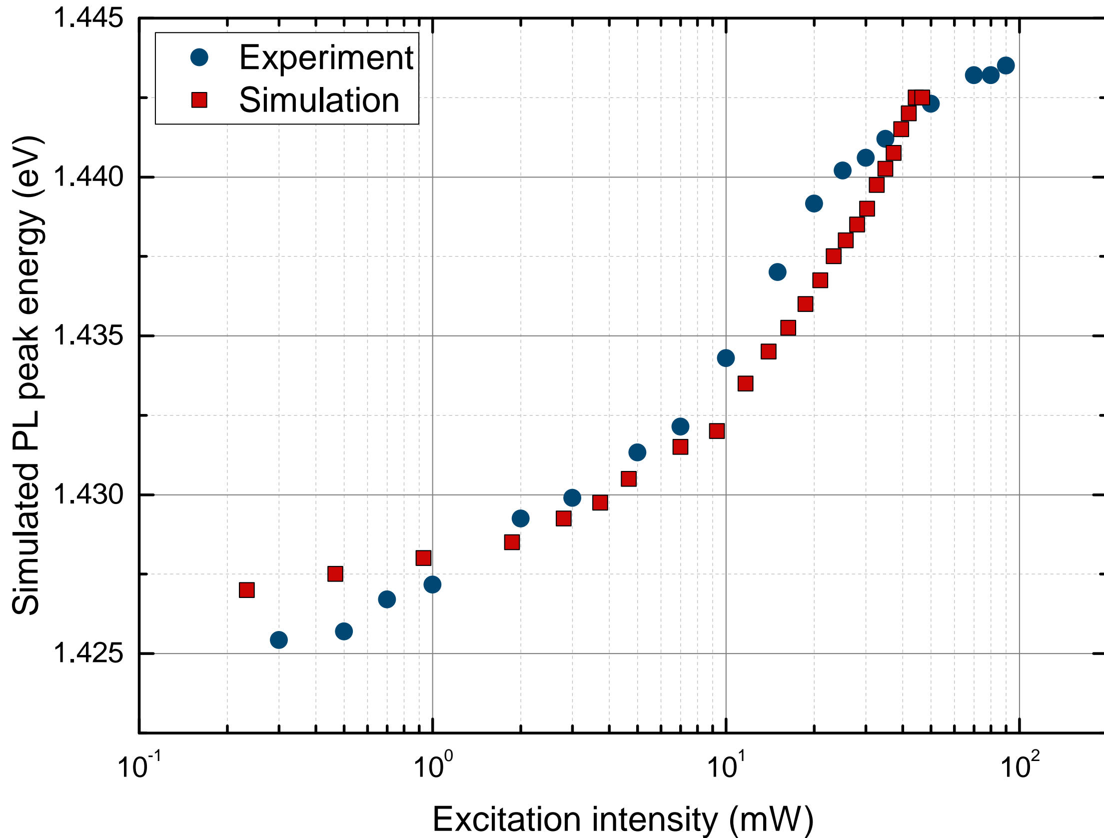

FIGURE 2.10: PL peak position as functions of the excitation intensity observed experimentally in $Ga(N_{0.03}As_{0.92}P_{0.05})/GaP$ MQWs (circles) and simulated (rectangles) for combined exponential-plus-Gaussian DOS.

energy and the increase in the PL linewidth are mainly related to the kinetic processes of free excitons. Furthermore, at fairly high excitation intensities the integrated PL signal tends to deviate from the linear dependence on the excitation intensity indicating the significant nonradiative recombination losses. These features are not included in the proposed theoretical model. Hence, its application is restricted by comparatively small values of the excitation intensity, for which the PL lineshape is mainly conditioned by the hopping relaxation of localized excitons. In order to extend this model to be applicable for higher excitations, one should include the dynamic processes of free excitons with taking into account the flling factor of extended states above the mobility edge. This task, however, stayed beyond the scope of current research.

The main conceptual result of this part is that original BET model should be extended with the assumption of complex exponential-plus-Gaussian DOS in order to explain the effect of PL linewidth shrinkage in Ga(NAsP)/GaP alloy. Moreover, as it was mentioned previously, the very similar behaviour of the PL linewidth has been reported

for the InGaN/GaN [4] and GaAsBi/GaAs [5] semiconductor structures. So, it looks reasonable to assume that the similar approach will be applicable to thous materials as well. The presented result indicates the existence of deep localized states in the bandgap of Ga(NAsP) quaternary alloys. This could be also true in other structures with similar PL behaviour.

2.5 The model of double-scaled disorder

Another problem in a context of the description of the PL in Ga(NAsP)/GaP in the frame of BET approach is the width of PL line. In table 2.1 one can see that the actual linewidth of PL spectra differs significantly from the one predicted by the BET model.

To solve this problem back in 2010 an extended version of the BET model was suggested in Ref. [7] assuming two different spatial scales for the disorder potential.

A brief description of the model looks as follows. Due to geometrical imperfections of the quantum well structure, the model assumes that there is a long-range disorder potential with a spatial scale comparable or larger than the linear size of the area that exciton can explore during its lifetime. Within this area, a short-range disorder at much smaller spatial scale is assumed as a consequence of alloy fluctuations in the compound material. The long-range disorder potential can be represented by a step-like function of the lateral spatial coordinate. The length of the step is determined by the disorder scale. As a result, the whole quantum well layer can be considered as a sequence of the rectangular elements, the so-called ‘cells’. Within each cell, the long-range disorder potential is assumed to be constant which leads to an effective mobility edge for the recombination sites that are generated by the short-range disorder. Optically excited excitons in some given cell are trapped in the recombination sites within the same cell that completely determines the cascade of hopping events during the exciton lifetime. The energy distribution of the long-range disorder potential steps is assumed to be given by

$$g_1(\varepsilon) = A \exp\left(\frac{\varepsilon}{\varepsilon_0}\right) , \tag{2.6}$$

where A is the normalization parameter and ε_0 is the characteristic energy scale for the long-range potential. The energy is measured from some energy level, assuming that all energy states above this level are extended in the whole quantum well structure. Within each cell, the short-range disorder potential generates localized states with energy distribution

$$g_2(E-\varepsilon) = B \exp\left(\frac{E-\varepsilon}{E_0}\right) , \tag{2.7}$$

with normalization parameter B and characteristic energy E_0.

The extended BET model with two spatially different scales of disorder was successfully applied to explain the specific temperature dependencies of the Stokes shift and the spectral linewidth observed in Ga(AsBi) and Ga(NAsP) compounds at low excitation intensities [7, 28, 29].

However, such an approach fails to explain the effect of linewidth shrinkage, discussed in the previous section. Indeed, in the frame of the model of two spatial scales of disorder, the overall PL linewidth is determined by long-range disorder given by exponential dependence 2.6, while, as we have seen previously, the none-monotonous shape of the DOS is required to explain PL line shrinkage. On the other hand, it is also impossible to explain the minimum of Stocks Shift T_1 and maximum of FWHM T_2 at around 120 K, assuming complex exponential-plus-Gaussian DOS instead of two spatial scales of the disorder. After making dozens of simulations with different sets of parameters, I have concluded that, in the frame of the complex DOS approach, one can only expect T_1 and T_2 values to be around 300 K. Moreover, the simulation could not reproduce the exact shape of the PL line from the experiment.

Thus, we came to the point when it was only possible to explain the effect of low-temperature linewidth shrinkage in Ga(NAsP)/GaP in the frame of the complex DOS model. While, on the other hand, it was only possible to explain the contradiction between the values of T_1, T_2 and the actual width of Ga(NAsP)/GaP spectral line by assuming the model of two scales of disorder.

2.6 The model with two types of impurity sites

To solve this problem, we will extend the BET model with complex DOS by introducing site-selective temperature-dependent non-radiative recombination rates [8]. At low temperatures, non-radiative losses can be neglected so that previous results for low-temperature linewidth shrinkage are not altered. At higher temperatures, however, the non-radiative losses strongly influence the temperature dependence of the Stokes shift and of the PL linewidth. The core assumption here is that complex exponential-plus-Gaussian DOS corresponds to two types of impurity sites with strongly different temperature-dependent none-radiative rates.

The importance of the non-radiative recombinations depends on the recombination mechanism. In Ref. [7] the recombination of free carriers from the extended states was assumed to be the dominant loss mechanism [19]. In this case, the non-radiative recombination plays only a minor role for the temperature dependence of the Stokes shift and of the PL linewidth. Therefore, it is not surprising that the BET model with two types of impurity sites failed to reproduce the experimental data.

The alternative approach [26] is to assume that the exciton captured on a localized site can recombine either radiatively or non-radiatively, depending on whether or not the temperature is high enough to overcome the exciton binding energy. Therefore, we can assume that the non-radiative recombination rates are strongly site-selective.

Such assumption is motivated by the two-peak shape of the experimentally observed PL spectra shown in Fig. 2.2. As one can see, the two peaks in the PL spectra have different contributions at different temperatures. At low temperatures, only the high-energy peak is visible. With increasing temperature, the second, low-energy peak becomes discernible in the PL spectra. At $T \approx 120\,\mathrm{K}$ both peaks exhibit equal contributions. A further increase in temperature diminishes the high-energy peak and, at $T \gtrsim 200\,\mathrm{K}$, only the low-energy peak remains. We attribute the high-energy peak to type-I localized states that are generated by the alloy disorder and that are distributed according the exponential part of the complex DOS given by Eq. (2.5). The low-energy peak arises from the type-II localized states in the nitrogen clusters whose energy is distributed according the Gaussian term in the combined DOS.

The approach with two types of localized states resolves the apparent discrepancy between the values of the energy scale of disorder, as extracted from the different PL features using the universal relations given in Table 2.1. Indeed, these relations were obtained on the basis of the conventional BET model with a pure exponential DOS and a single energy scale. The conventional BET applies to semiconductor heterostructures where clusters are absent. In semiconductor compounds with clusters, such as Ga(NAsP) or Ga(BiAs), however, the situation is qualitatively different.The alternative approach [26] is to assume that the exciton captured on a localized site can recombine either radiatively or non-radiatively, depending on whether or not the temperature is high enough to overcome the exciton binding energy. Therefore, we can assume that the non-radiative recombination rates are strongly site-selective.

Such assumption is motivated by the two-peak shape of the experimentally observed PL spectra shown in Fig. 2.2. As one can see, the two peaks in the PL spectra have different contributions at different temperatures. At low temperatures, only the high-energy peak is visible. With increasing temperature, the second, low-energy peak becomes discernible in the PL spectra. At $T \approx 120\,\mathrm{K}$ both peaks exhibit equal contributions. A further increase in temperature diminishes the high-energy peak and, at $T \gtrsim 200\,\mathrm{K}$, only the low-energy peak remains. We attribute the high-energy peak to type-I localized states that are generated by the alloy disorder and that are distributed according the exponential part of the complex DOS given by Eq. (2.5). The low-energy peak arises from the type-II localized states in the nitrogen clusters whose energy is distributed according the Gaussian term in the combined DOS.

The approach with two types of localized states resolves the apparent discrepancy between the values of the energy scale of disorder, as extracted from the different PL features using the universal relations given in Table 2.1. Indeed, these relations were obtained on the basis of the conventional BET model with a pure exponential DOS and a single energy scale. The conventional BET applies to semiconductor heterostructures where clusters are absent. In semiconductor compounds with clusters, such as Ga(NAsP) or Ga(BiAs), however, the situation is qualitatively different. As one can see from the experimentally observed temperature dependence of the Stokes shift shown by circles in Fig. 2.3, the Stokes shift almost jumps near its minimum. This sharp increase results from the switch between the different peaks in the PL spectra shown in Fig. 2.2. The corresponding maximum in the experimental temperature dependence of the spectral

linewidth is equally sharp. This temperature dependence of the PL spectra indicates that the extrema in the temperature dependence of the Stokes shift and of the spectral linewidth are caused by the interplay of the PL emission intensities from localized states of different types. In contrast to the standard BET model, the hopping dynamics and the thermal distribution of localized carriers is not the primary source for the observed temperature dependence of the PL spectra. Therefore, the universal relations given in Table 2.1 are not relevant for the PL features of semiconductor compounds where the impurity atoms tend to cluster.

As one can see from the experimentally observed temperature dependence of the Stokes shift shown by circles in Fig. 2.3, the Stokes shift almost jumps near its minimum. This sharp increase results from the switch between the different peaks in the PL spectra shown in Fig. 2.2. The corresponding maximum in the experimental temperature dependence of the spectral linewidth is equally sharp. This temperature dependence of the PL spectra indicates that the extrema in the temperature dependence of the Stokes shift and of the spectral linewidth are caused by the interplay of the PL emission intensities from localized states of different types. In contrast to the standard BET model, the hopping dynamics and the thermal distribution of localized carriers is not the primary source for the observed temperature dependence of the PL spectra. Therefore, the universal relations given in Table 2.1 are not relevant for the PL features of semiconductor compounds where the impurity atoms tend to cluster.

Thus, in order to describe experimental results let us consider the following model:

1. Sites are distributed with complex DOS, according to Eq. (2.5);
2. Two different types of LS are corresponding to exponential (Type-I) and Gaussian (Type-II) components of the DOS;
3. Exciton can recombine radiativelly or non-radiativelly at any site, while probabilities of radiative and non-radiative recombination processes is temperature dependent, and differs for different types of LS;

2.7 KMC simulation of PL with two types of impurity sites

Simulation in this part differs from the previous in several ways. We assume the case of low excitation, and for this reason, we only simulate a system with single exciton. In addition, we assume temperature dependent non-radiative lifetimes at different types of LS. Detailed algorithm description is given in the next section.

2.7.1 KMC simulation algorithm

Assume that the system has N traps and a single exciton that propagates through the system. Furthermore, traps are randomly distributed in space with characteristic parameter Na^2, where a is the localization length. The characteristic times are given by the dimensionless parameters $\nu_0\tau_{\mathrm{r}}$, $\nu_0\tau_{\mathrm{nr},1}$,and $\nu_0\tau_{\mathrm{nr},2}$, where ν_0 is attempt-to-escape frequency, τ_{r} is the exciton radiative lifetime, and $\tau_{\mathrm{nr},1}$ and $\tau_{\mathrm{nr},2}$ are the exciton non-radiative lifetimes for type-I and type-II localized states, respectively. Type-I LS are distributed according to the exponential part of the DOS in Eq. (2.5) with characteristic energy E_0 as determined from the low-energy tail of the experimental PL spectra. Type-II LS are distributed according to the Gaussian part of the DOS with characteristic parameters E_1 and σ_1. The ratio between the two types of LS is N_0/N_1.

The simulation algorithm performs the following steps.

1. Generate a set of N_0 LS distributed exponentially in energy with characteristic energy E_0, and generate N_1 LS with Gaussian energy distribution and characteristic parameters E_1 and σ_1. There are $N = N_0 + N_1$ localized sites. All LS have a uniform spatial distribution in a two-dimensional rectangle area corresponding to the parameter Na^2;

2. Calculate the rates of all possible events for all LS, namely,

   - ionization from a LS into an extended state with rate ν_{ion} given by Eq. (2.1),
   - hopping transitions between LS with rate ν_{ij} given by Eq. (2.2),
   - trapping of an extended state into a LS with rate ν_0,
   - radiative recombination with rate $\nu_{\mathrm{r}} = 1/\tau_{\mathrm{r}}$ and non-radiative recombination at a LS with rate $\nu_{\mathrm{nr},1;2} = 1/\tau_{\mathrm{nr},1;2}$, depending on the type of LS.

3. Put the exciton onto the randomly selected initial position i;

4. Calculate the cumulative event rate for the exciton $\Gamma_i = \nu_0 + \nu_\mathrm{r}$ or $\Gamma_i = \sum\limits_{i \neq j} \nu_{ij} + \nu_\mathrm{ion} + \nu_\mathrm{r} + \nu_{\mathrm{nr},1;2}$, depending on whether the state i is an extended or a LS, and determine the time before the next event as $\Delta\tau_i = \Gamma_i^{-1} R_i$ where $R_i = \ln(x_i)$ with the random number x_i uniformly distributed in the range $[0, 1]$;

5. Generate another random number $p \in [0, 1]$ and, using normalized event rates, determine the event that happens to the exciton next;

6. Perform the event (update the current state of the system);

7. In case of a radiative recombination event, save the energy of the site from which the recombination occurs and go to step 3 (in case of the non-radiative recombination, go to step 3 without saving the energy); otherwise go to step 4.

Described above algorithm was used to simulate the time-integrated PL spectra in Ga(NAsP) compound at different temperatures. The total number of LS is $N = N_0 + N_1 = 10^2$. In order to obtain reliable results, the algorithm is repeated a sufficiently large number of times, $N_\mathrm{MC} = 10^5..10^6$. The simulation results along with the values of simulation parameters are collected in the next section.

2.7.2 KMC simulation results

As one can see, the model with two types of localized states with different non-radiative recombination rates contains a large number of fitting parameters. In fact, only the characteristic energy scale E_0 of the type-I LS (exponential energy distribution) can be estimated from the low-energy part of the experimentally observed PL spectra. Therefore, the estimation of a unique set of parameters from a comparison of simulation results with experimental data is practically impossible, so it is hard to claim that the suggested model can serve as a convenient tool for the extraction of material characteristics from experimental data. However, we can show that the reproduction of the basic PL features of Ga(NAsP) compounds is possible within the framework of such an approach.

We start with the low-temperature PL spectra for which the non-radiative recombination processes are not relevant. The single-peak shape and the monotonic character of the low-temperature PL spectra shown in Fig. 2.2 indicates that the contributions of the

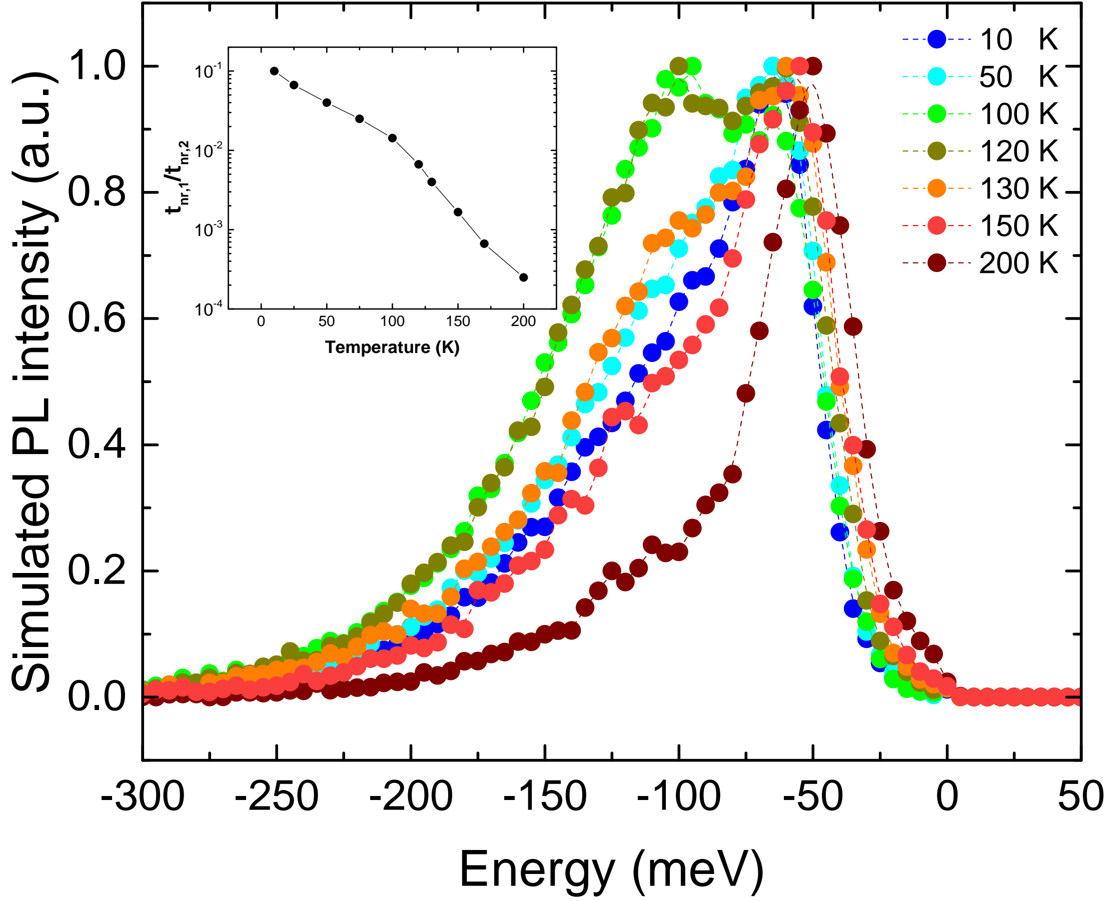

FIGURE 2.11: PL spectra of Ga(AsNP) simulated at various temperatures using the extended BET model with two types of the localized states.

radiative recombination events from the exponential and the Gaussian parts of the localized states lead to PL-peaks that are sufficiently close to each other. These PL features are determined by the interplay between the hopping dynamics and the recombination processes in the exponential and Gaussian domains of the localized states, as well as by the energy characteristics of the DOS. Table 2.2 gives one possible set of simulation parameters that provide a good agreement with experimental data.

Parameter	Value	Description
N_0/N_1	6/4	Fitting parameter
E_0	40 [meV]	Experimentally determined
E_1	38 [meV]	Fitting parameter
σ_1	16 [meV]	Fitting parameter
$N\alpha^2$	0.25	Fitting parameter
$\nu_0\tau_r$	10^3	Experimentally determined

TABLE 2.3: Simulation parameters for the $Ga(N_{0.04}As_{0.91}P_{0.05})/GaP$ PL spectra.

With increasing temperature, the Stokes shifts increases for both types of LS although the LS with an exponential DOS contribute more significantly to the Stokes shift so

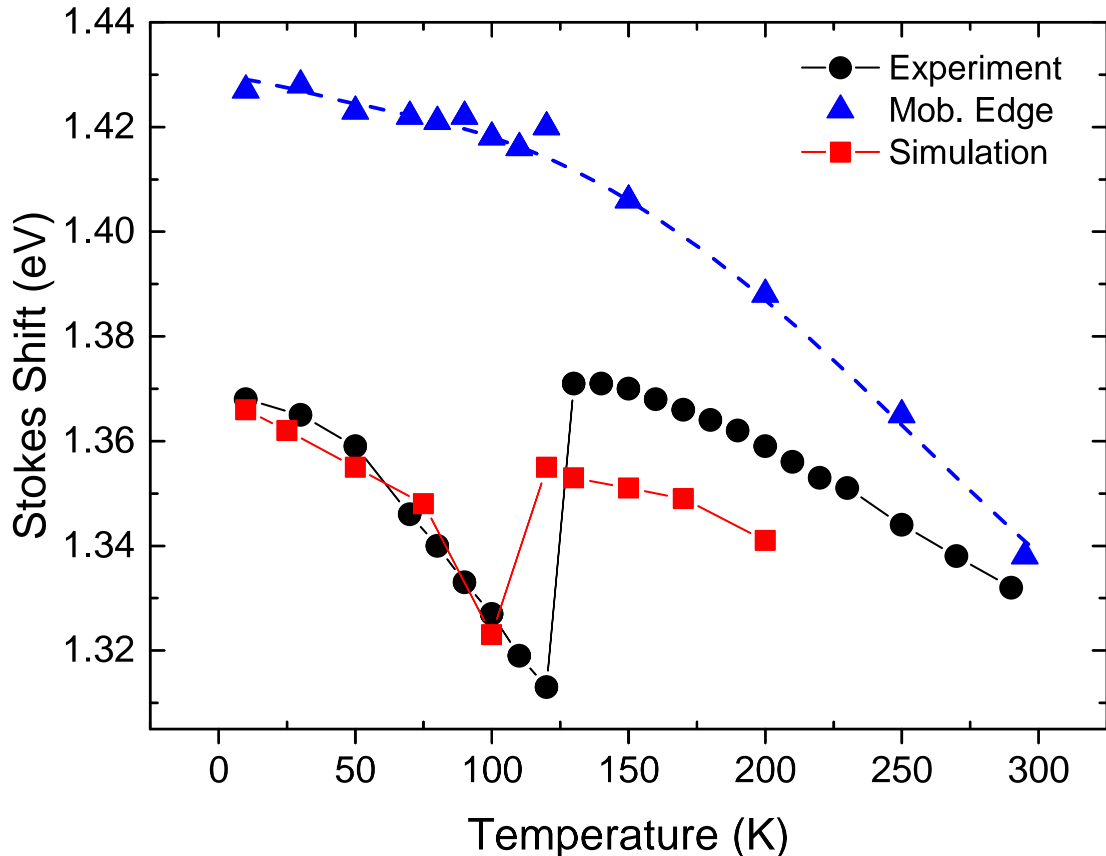

FIGURE 2.12: Experimental and simulated Stokes shift for $Ga(N_{0.04}As_{0.91}P_{0.05})/GaP$.

that the PL spectra display a two-peak structure at elevated temperatures. The low-energy peak can be assigned to the type-I LS (exponential energy distribution) whereas the type-II LS (Gaussian energy distribution) dominate the high-energy peak. With a further increase in temperature, the energy separation between the low-energy and high-energy peaks increases.

The relation $k_B T_{1,2} \approx E_0$, see Table 2.1, and the comparatively large energy scale $E_0 = 40\,\text{meV}$ lead to $T_{1,2} \approx 500\,\text{K}$. Therefore, the two-peak shape of the simulated PL spectra should be seen in the simulations for all temperatures considered experimentally. However, this is in conflict with the experimental observation, as shown in Fig. 2.2, where only the low-energy peak remains discernible at $T \gtrsim 200\,\text{K}$. To reconcile the simulation results and the experimental findings, we assume that the non-radiative recombination rate $\nu_{\text{nr},1}(T)$ of the type-I LS increases significantly with temperature whereas the increase in the non-radiative recombination rate $\nu_{\text{nr},2}(T)$ of the type-II LS is much less pronounced. This assumption readily leads to a reduction of the radiative

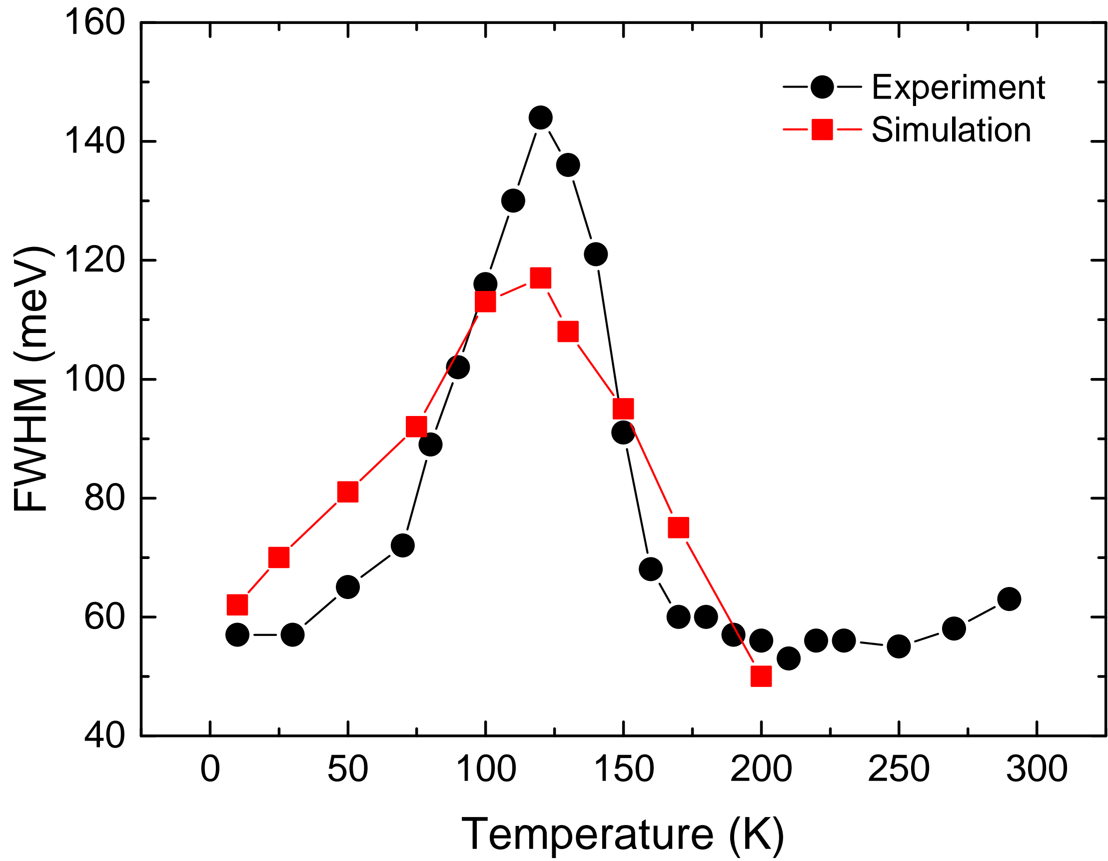

FIGURE 2.13: Experimental and simulated temperature dependencies of FWHM for $Ga(N_{0.04}As_{0.91}P_{0.05})/GaP$.

recombination events of type-I LS and thus to a temperature-induced suppression of the high-energy peak in the simulated PL spectra.

The PL spectra simulated at various temperatures are shown in Fig. 2.11. The corresponding temperature dependencies of the Stokes shift and the PL linewidth are shown by red squares in Fig. 2.12 and Fig. 2.13, respectively. For the simulations we assume a temperature-dependent ratio $\nu_{\text{nr},2}(T)/\nu_{\text{nr},1}(T)$ of the non-radiative recombination rates at the localized states of type-II and type-I as shown in the inset of Fig. 2.11. As seen from the figures, the extended BET model with two types of localized states and temperature-dependent non-radiative recombination rates is able to reproduce the basic temperature-dependent characteristics of the PL spectra observed in Ga(NAsP) compound material.

Note that the sharp rise in the simulated and measured temperature-dependent Stokes shift shown in Fig. 2.3 is caused by the overlay of equally strong high-energy and low-energy PL peaks that originate from the radiative recombinations at the two sorts of

localized states. It is not primarily the interplay between the hopping dynamics of photo-excited carriers and their thermal distribution. This is the key difference between the conventional BET model and the suggested approach.

Thus, we have shown that modification of the original BET model, which assumes 2-types of LS with complex DOS and temperature-dependent non-radiative lifetimes of excitons, allows describing all of the experimentally observed peculiarities of PL in Ga(NAsP).

2.8 Conclusions

In this chapter, we have discussed peculiarities of PL specific for Ga(NAsP) and some other materials, such as Ga(AsBi). One effect is excitation dependent linewidth shrinkage at low temperatures. This behaviour seems very non-intuitive. One would rather assume that the increasing number of excitons in the system should lead to linewidth broadening, instead of shrinkage. However, using KMC approach to simulate low-temperature PL spectra of Ga(NAsP), we have found that, while such an assumption makes sense for monotonous DOS (such as exponential one), the combined exponential-plus-Gaussian DOS (see Fig. 2.8) leads to the linewidth shrinkage just as observed in the experiment. Moreover, recently reported results on temperature quenching of PL line in Ga(NAsP) [27] also revealed non-monotonous DOS with the very similar shape. Thus, we can conclude that it is very likely to be the case, that the DOS in Ga(NAsP) has such a non-monotonous shape and can be described by Eq. (2.5). One possible explanation for such shape of the DOS could be the presence of two types of LS with exponential and Gaussian DOS accordingly.

This assumption became a starting point to resolve the second problem – anomalously broad spectral lines of Ga(NAsP). The first approach to deal with this problem was developed back in 2010 by Karcher, Jandieri *et al* [7], and the key assumption of this approach was, so-called double-scaled disorder described by Eqs. (2.6) and (2.7). However, this model contradicts the concept of complex DOS and is not capable of describing low-temperature linewidth shrinkage effect.

Therefore, we have introduced the alternative self-consistent model [8] capable of describing both of the effects discussed above. The key feature of the new approach is

the assumption of coexistence of two types of the LS. Assuming that type-I sites are distributed in energy exponentially, while energies of type-II sites are distributed according to Gaussian law, we have made an additional conjecture, that the probability of non-radiative recombination of exciton differs for different types of LS and strongly depends on temperature. In the frame of such an approach, at low-temperature limit non-radiative loses assumed to be negligible, thus, results of the previous simulation of linewidth shrinkage remain unaffected. In the same time, we observe a good qualitative agreement between simulation and experimental results for temperature-dependent PL features.

Taking into account, that such features of the PL were reported for materials such as Ga(NAsP) and Ga(AsBi), which tend to form clusters (N-clusters and Bi-clusters correspondingly) [30], it is reasonable to assume that clusters may be the source for the second type of sites. We can suppose that type-I LS are generated by the alloy disorder and distributed according to the exponential part of the combined DOS, while type-II LS are in the nitrogen clusters with energies distributed according to the Gaussian term in the DOS. In the frame of such consideration, PL spectra of materials, which are free from clusters, can be described by means of the conventional BET model, while for materials such as Ga(NAsP) or Ga(AsBi) modified model with 2 types of LS required.

Chapter 3

Carriers release enhanced by hopping

Processes of trapping and release of carriers from traps determines transport and opto-electronic phenomena in disordered semiconductors. In this chapter we will show how hopping transitions between neighbouring traps may essentially enhance carrier release rate, which is of crucial importance for the transport mode known as multiple-trapping (MT). Surprisingly, this question has not been studied so far. Further we will give an analytical approach to the problem along with KMC simulations of the carrier release process.

3.1 Multiple-trapping model

To illustrate the importance of trapping and detrapping processes, let us start with the concept of multiple-trapping mechanism of carriers transport. Illustration of multiple-trapping process is given in Fig. 3.1.

In the multiple-trapping process, a charge carrier moves only via delocalized states with energies above the mobility edge ε_c. This motion is interrupted by trapping of carriers into the localized states with their subsequent activation into the conducting states above the mobility edge. Therefore, carrier transport in such a system is determined by ratio of times carrier spends in conduction band and at localized states bellow ε_c. In

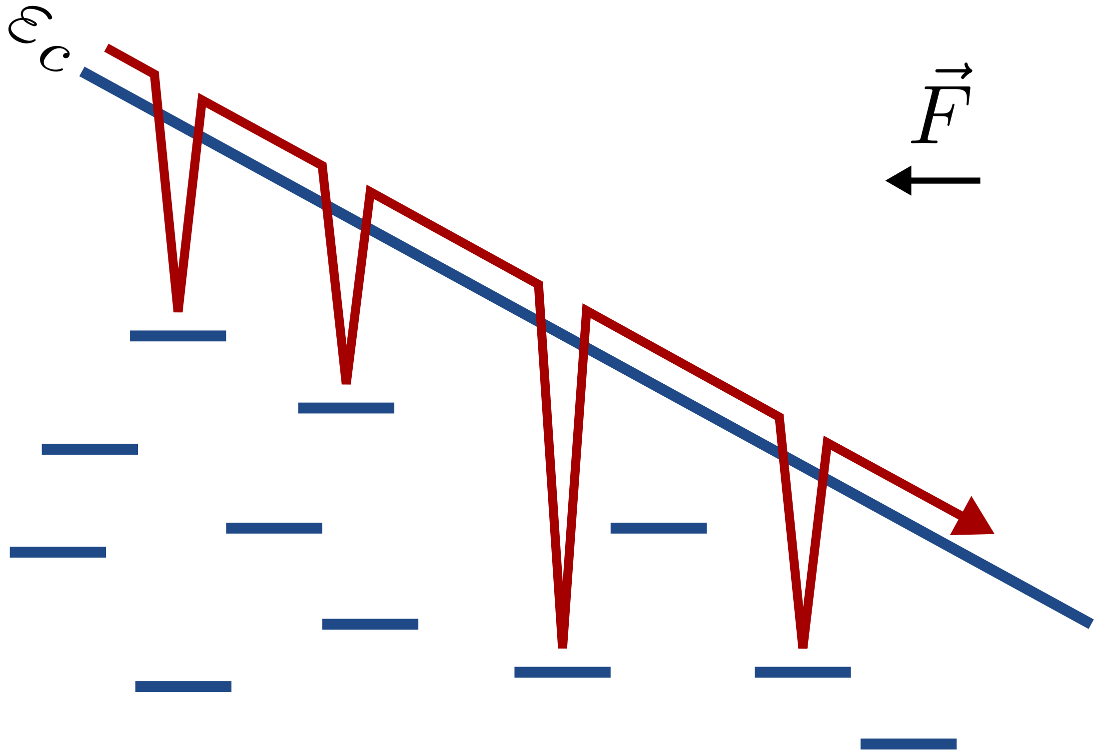

FIGURE 3.1: A sketch to multiple-trapping process.

other words, it is carriers capture and release rates are the parameters responsible for transport properties of the system.

3.2 Field-assisted carrier release from an isolated trap

The simplest model of carriers release looks as follows. Without electric field, the escape rate from a trap into conduction band is assumed equal to

$$\nu_{\text{esc}}(\varepsilon) = \nu_0 \exp\left(-\frac{\varepsilon}{kT}\right), \tag{3.1}$$

If transitions are caused by interaction with phonons, ν_0 is an attempt-to-escape frequency (usually assumed to be of the order of the phonon frequency). However, assuming presence of the external electric field, one should ask himself: how does the electric field affects carriers release rate?

This question has been first studied theoretically by Keldysh [31], who showed that the applied electric field can diminish the activation barrier for the electron escape from a trap, as illustrated schematically in Fig. 3.2.

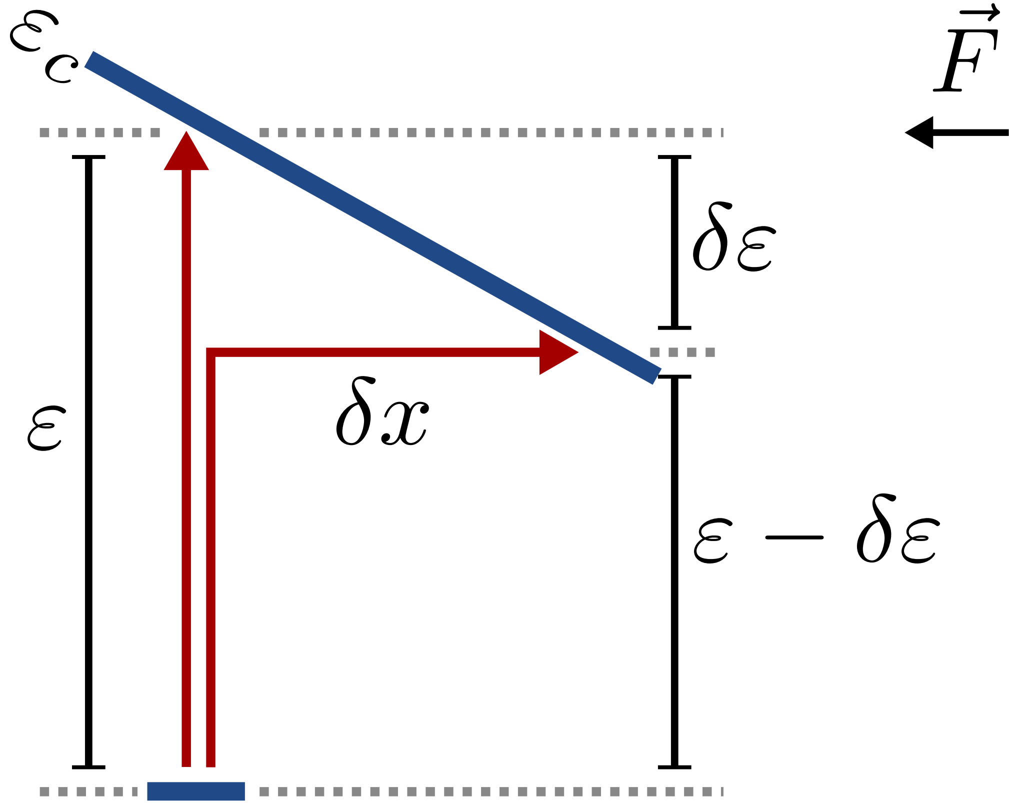

FIGURE 3.2: A sketch to field-assisted detrapping process.

This is a thermal equivalent of the well-known Franz-Keldysh effect. In this scheme, the escape event consists of two processes: activation with the energy deficit $\Delta\varepsilon$, as compared to the trap depth ε, and tunneling over the distance $\Delta x = \Delta\varepsilon/(eF)$ under the triangle energy barrier. Ascribing to the preexponential factor a universal value ν_0, and introducing the variable $z \equiv (\Delta\varepsilon)/kT$. Eventually, Keldysh result is represented by the following expression:

$$\nu_{\text{esc}}(\varepsilon) = \nu_0 \exp\left\{-\frac{\varepsilon}{kT}\right\}\left[1 + \int_0^{\varepsilon/kT} \exp\left\{z - \frac{4\sqrt{2m}(zkT)^{3/2}}{3e\hbar F}\right\} \mathrm{d}z\right], \quad (3.2)$$

where m denotes the effective mass of the charge carrier.

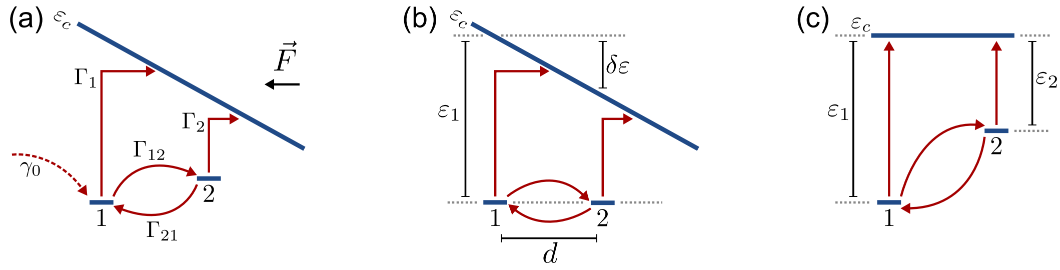

FIGURE 3.3: Two localized states under electric field **F**: (a) space-energy diagram for the general case; (b) specific case of the isoenergetic traps; (c) specific case of $F = 0$.

3.3 Field-assisted carrier release with single additional trap

In eqs. (3.1) and (3.2), it is assumed that the rate of carrier release from a given trap is not affected by the presence of other traps. However, it appears to be the case that the presence of nearby sites may significantly affect the release rate of given carrier, especially when assuming the case of a deep energy level of the trap and strong electric fields.

The simplest model, in which the hopping-assisted detrapping can take place is illustrated in Fig. 3.3. It includes one electron, two sites (trap 1 and trap 2) and the conduction band, which is tilted due to the external electric field. Let us assume that electron is initially captured by trap 1 (with rate γ_0) From the trap 1 electron can escape to the conduction band with rate Γ_1 or jump to the trap 2 with rate Γ_{12}. Similarly, if the electron resides on the trap 2, the possible processes are the escape to the conduction band (with the rate Γ_2) and a hop to the trap 1 (with the rate Γ_{21}). Let us say t is a mean time between the moment when electron arrives on the trap 1 and the moment when it escapes to the conduction band. We are trying to understand if the presence of the additional trap can enhance electron release significantly because of hopping transition to the nearby trap? In other words: can the value of t be considerably smaller than the correspondent time $1/\Gamma_1$ in the absence of the trap 2?

In order to calculate the mean time t exactly, it is convenient to analyse a steady state with a continuous supply of electrons on the trap 1 with a constant rate γ_0 that is infinitely small as compared to to other rates. When an electron reaches the conduction band, it disappears from our consideration. In this setting, the mean escape time t is

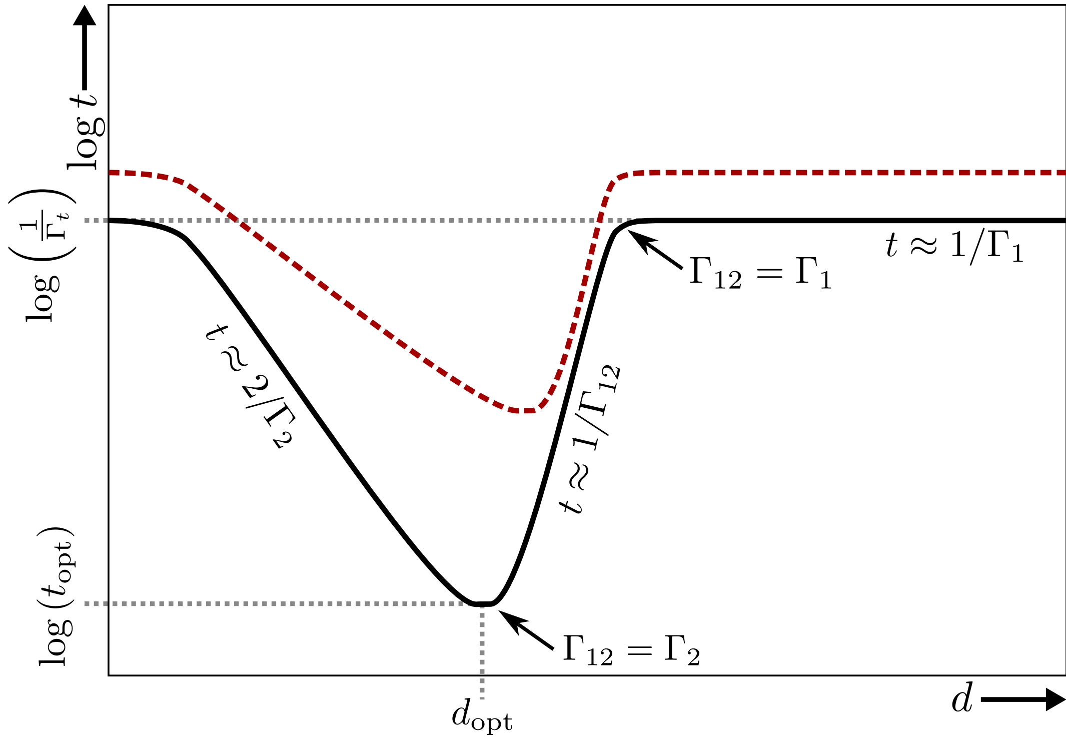

FIGURE 3.4: Escape time t versus distance d between traps in the model of two traps with the same energy, Fig. 3.3b. Red dotted line corresponds to the electric field twice smaller than that for solid blue line.

expressed as

$$t = \frac{p_1 + p_2}{\gamma_0}\,, \tag{3.3}$$

where p_1 and p_2 are the probabilities of finding the electron in the steady state on the trap 1 and trap 2, respectively. These probabilities can be found from a system of balance equations for the two traps,

$$\begin{cases} (\Gamma_1 + \Gamma_{12})\, p_1 = \Gamma_{21}\, p_2 + \gamma_0\,, \\ (\Gamma_2 + \Gamma_{21})\, p_2 = \Gamma_{12}\, p_1\,. \end{cases} \tag{3.4}$$

Equations (3.3) and (3.4) provide the solution in the form:

$$t = \frac{\Gamma_2 + \Gamma_{12} + \Gamma_{21}}{\Gamma_1\Gamma_2 + \Gamma_{12}\Gamma_2 + \Gamma_{21}\Gamma_1}\,. \tag{3.5}$$

Let us consider a particular case of the traps with equal energies. Let the direction from the trap 1 to te trap 2 be against the electric field, so that the trap 2 is more shallow

than the trap 1, as depicted in Fig. 3.3b. Since the traps are isoenergetic, the principle of the detailed balance prescribes that $\Gamma_{12} = \Gamma_{21}$. The dependence of the hopping rates on the distance d between the traps is governed by the localization length a:

$$\Gamma_{12} = \Gamma_{21} = \nu_h \exp\left(-\frac{2d}{a}\right), \tag{3.6}$$

where ν_h is the attempt-to-escape frequency. The ratio of the escape rates Γ_2/Γ_1 is defined mainly by the difference $\delta\varepsilon$ between their depths with respect to the mobility edge:

$$\frac{\Gamma_2}{\Gamma_1} \simeq \exp\left(\frac{\delta\varepsilon}{kT}\right) = \exp\left(\frac{eFd}{kT}\right). \tag{3.7}$$

Substituting $\Gamma_{21} = \Gamma_{12}$ into Eq. (3.5) and neglecting the last term in the denominator (since $\Gamma_1 \ll \Gamma_2$), one obtains

$$t \approx \frac{1}{\Gamma_2} \frac{\Gamma_2 + 2\Gamma_{12}}{\Gamma_1 + \Gamma_{12}}. \tag{3.8}$$

In Fig 3.4, we plot schematically the dependence $t(d)$, for a given depth of the trap 1. When the distance d is sufficiently small,Γ_{12} is much larger than the other rates present in Eq. (3.8). Neglecting Γ_1 and Γ_2 in the last factor, one can conclude that

$$t(d) \approx \frac{2}{\Gamma_2(d)} \simeq \frac{2}{\Gamma_1} \exp\left(-\frac{eFd}{kT}\right), \tag{3.9}$$

where we have expressed Γ_2 via Γ_1 using Eq. (3.7). In this regime (a decreasing part of the dependence $t(d)$ in Fig. 3.4), electron typically hops between the traps 1 and 2 back and forth many times, and only afterwards it escapes from the shallow trap 2. Hence, the process of the electron escape is controlled in this regime by the rate Γ_2.

With increasing distance d, the hopping rate Γ_{12} decreases according to Eq. (3.6), and the escape rate Γ_2 increases because the trap 2 becomes shallower with increasing d. At some "optimal" distance $d_{\rm opt}$ the two rates become equal to each other:

$$\Gamma_{12}(d_{\rm opt}) = \Gamma_2(d_{\rm opt}). \tag{3.10}$$

Neglecting Γ_1 in Eq. (3.8), one obtains the corresponding "optimal" mean escape time $t_{\rm opt} = t(d_{\rm opt})$:

$$t_{\rm opt} \approx \frac{3}{\Gamma_2(d_{\rm opt})}\,. \tag{3.11}$$

At larger distances d, the hopping rate Γ_{12} is small as compared to Γ_2, though still large as compared to Γ_1. According to Eqs. (3.8) and (3.6), this yields:

$$t(d) \approx \frac{1}{\Gamma_{12}(d)} = \nu_h^{-1} \exp\left(\frac{2d}{a}\right). \tag{3.12}$$

The corresponding regime is depicted by the increasing part of the dependence $t(d)$ in Fig. 3.4 In this regime, the electron typically resides on the trap 1 until it hops to the trap 2, which is followed by a fast escape from the trap 2 into the conduction band. The dynamics of this process is mainly governed by the hopping rate Γ_{12}.

Finally, at sufficiently large distances d, the hopping rate Γ_{12} becomes smaller than both Γ_1 and Γ_2, and it therefore can be neglected in Eq. (3.8). In this regime, the escape time does not depend on d anymore:

$$t(d) \approx \frac{1}{\Gamma_1} \tag{3.13}$$

(a horizontal section of the dependence $t(d)$ in Fig. 3.4). Indeed, if $\Gamma_{12} \ll \Gamma_1$ then the most probable scenario is that the electron escapes to the conduction band directly from the trap 1, instead of visiting the additional trap 2 because the trap 2 becomes too remote from the trap 1 to be involved into the escape process.

The overall dependence $t(d)$ (the solid line in Fig. 3.4) consists, therefore, of the three regions corresponding to Eqs. (3.9), (3.12) and (3.13). If the strength of the electric field is halved, the dependence $t(d)$ is represented in Fig. 3.4) by the dotted line. One can see that the additional trap enhances the process of the electron release most effectively

when such a trap is located at a distance $d_{\rm opt}$, which can be found via Eqs. (3.6), (3.7) and (3.10):

$$d_{\rm opt} = \left(\frac{2}{a} + \frac{eF}{kT}\right)^{-1} \ln \frac{\nu_h}{\Gamma_1} \, . \tag{3.14}$$

The corresponding mean escape time $t_{\rm opt}$, according to Eqs. (3.7), (3.11) and (3.14), is equal to

$$t_{\rm opt} \approx \frac{3}{\Gamma_1} \left(\frac{\Gamma_1}{\nu_h}\right)^{1/(1+2kT/eFa)} \, . \tag{3.15}$$

In a moderate electric field, when $eFa \ll kT$, one can simplify this expression, by representing the exponent $1/(1+2kT/eFa)$ as $\approx eFa/2kT$, and by neglecting all contributions to the ratio Γ_1/ν_h but the Boltzmann's factor,

$$\frac{\Gamma_1}{\nu_h} \simeq \exp\left(-\frac{\varepsilon_1}{kT}\right) , \tag{3.16}$$

ε_1 being the depth of the trap 1. Herewith one obtains the following rough estimate:

$$t_{\rm opt} \simeq \Gamma_1^{-1} \exp\left(-\frac{\varepsilon_1 eFa}{2(kT)^2}\right) . \tag{3.17}$$

Aiming to reveal, how effectively may an additional trap enhance the release of the electron to the conduction band, it is convenient to consider the enhancement factor $\mathcal{F}$ defined as a ratio between the mean escape time of a single trap 1, Γ_1^{-1}, and the escape time $t_{\rm opt}$ in the two-trap system with the optimal position of the second trap:

$$\mathcal{F} = \frac{\Gamma_1^{-1}}{t_{\rm opt}} \, . \tag{3.18}$$

With $t_{\rm opt}$ estimated by Eq. (3.17), the enhancement factor is

$$\mathcal{F} \simeq \exp\left(\frac{\varepsilon_1 eFa}{2(kT)^2}\right) . \tag{3.19}$$

The factor $\mathcal{F}$ increases with the applied electric field, and it reaches exponentially large values if the trap is sufficiently deep, ($\varepsilon_1 \gg kT$).

This enhancement of the detrapping efficiency has been derived so far for a specific case of the additional trap having the same energy as the trap 1. In a more general case, the enhancement can be even more pronounced. It is worth emphasising that the effect appears in the presence of an external electric field. In contrast, the increase of the release rate due to the presence of an additional trap without electric field cannot exceed the factor of two. In the case of $F = 0$ depicted in Fig. 3.3c, the ratio Γ_{21}/Γ_{12} and the ratio Γ_2/Γ_1 are defined by the same Boltzmann's factor $\exp[(\varepsilon_1 - \varepsilon_2)/kT]$:

$$\Gamma_{21} = \Gamma_{12} \exp\left(\frac{\varepsilon_1 - \varepsilon_2}{kT}\right) \tag{3.20}$$

and

$$\Gamma_2 = \Gamma_1 \exp\left(\frac{\varepsilon_1 - \varepsilon_2}{kT}\right). \tag{3.21}$$

Substituting Eqs. (3.20) and (3.21) into Eq. (3.5), one can express the enhancement factor $\mathcal{F}$ in the absence of electric field as

$$\mathcal{F} = \frac{\Gamma_1^{-1}}{t} = \frac{\Gamma_1 + 2\Gamma_{12}}{\Gamma_1 + \left[1 + e^{-(\varepsilon_1 - \varepsilon_2)/kT}\right]\Gamma_{12}}. \tag{3.22}$$

One can see that $\mathcal{F}$ cannot be larger than two, because the numerator of the right-hand side is in any case smaller than the doubled denominator. The largest possible value $\mathcal{F} \approx 2$ can be reached if $\exp[-(\varepsilon_1 - \varepsilon_2)/kT] \ll 1$ (i. e. the additional trap 2 is higher in energy than the trap 1 by at least several kT) and simultaneously $\Gamma_{12} \gg \Gamma_1$, which can be fulfilled if the traps are sufficiently close to each other. In such a case, the additional trap just provides another channel for the electron escape, which is as fast as the direct escape from the trap 1. At the same time, the additional trap provides a channel for electron capture from the conduction band to the trap 1. The capture efficiency and the release efficiency are enhanced in the same proportion, as it should be in the absence of the electric field due to the detailed balance.

Thus, we have shown on the simplest model that the electron release from a trap to the conduction band can be essentially enhanced by the presence of an additional, more shallow trap. Without external electric field, the factor of enhancement of the electron

release $\mathcal{F}$ is not larger than two. On the other hand, with electric field F the factor of enhancement depends on F exponentially according to Eq. (3.19). It can enhance the release rate by orders of magnitude.

3.4 Field-assisted carrier release with multiple additional traps

To generalize the model for the case of many additional traps let us assume the following. Electron is placed initially at trap 1. The initial trap is surrounded with a large number of additional sites with the spatial density corresponding to $N\alpha^3$ and the DOS $g(\varepsilon)$. The following electron dynamics is determined by the rates Γ_{mn} of hopping from a trap m to a trap n, and by the rates Γ_n of activation from the trap n, as illustrated in Fig. 3.5.

In this model with several traps, Eq. (3.4) turns into the following system of balance equations:

$$\begin{cases} \left(\Gamma_1 + \sum_{n\neq 1} \Gamma_{1n}\right) p_1 = \sum_{n\neq 1} \Gamma_{n1}\, p_n + \gamma_0 \,, \\ \left(\Gamma_2 + \sum_{n\neq 2} \Gamma_{2n}\right) p_2 = \sum_{n\neq 2} \Gamma_{n2}\, p_n \,, \\ \dots \\ \left(\Gamma_m + \sum_{n\neq m} \Gamma_{mn}\right) p_m = \sum_{n\neq m} \Gamma_{nm}\, p_n \,, \\ \dots \end{cases} \tag{3.23}$$

where $p_1, p_2, \dots$ are the probabilities of finding an electron at the corresponding traps. The mean time before escaping into the conduction band t is to be found as

$$t = \frac{\sum\limits_{n} p_n}{\gamma_0} \,, \tag{3.24}$$

which is a direct generalization of Eq. (3.3). Such a problem could be solved by means of linear algebra methods. However, we are using KMC approach to simulate directly electron hopping transition for performance reasons and also because such an approach allows us to gather more information about hopping processes. For instance, we can gather the statics on how many jumps carrier performs before release to conduction band, or how much time it spends on average at different sites. Nevertheless, Eq. (3.23)

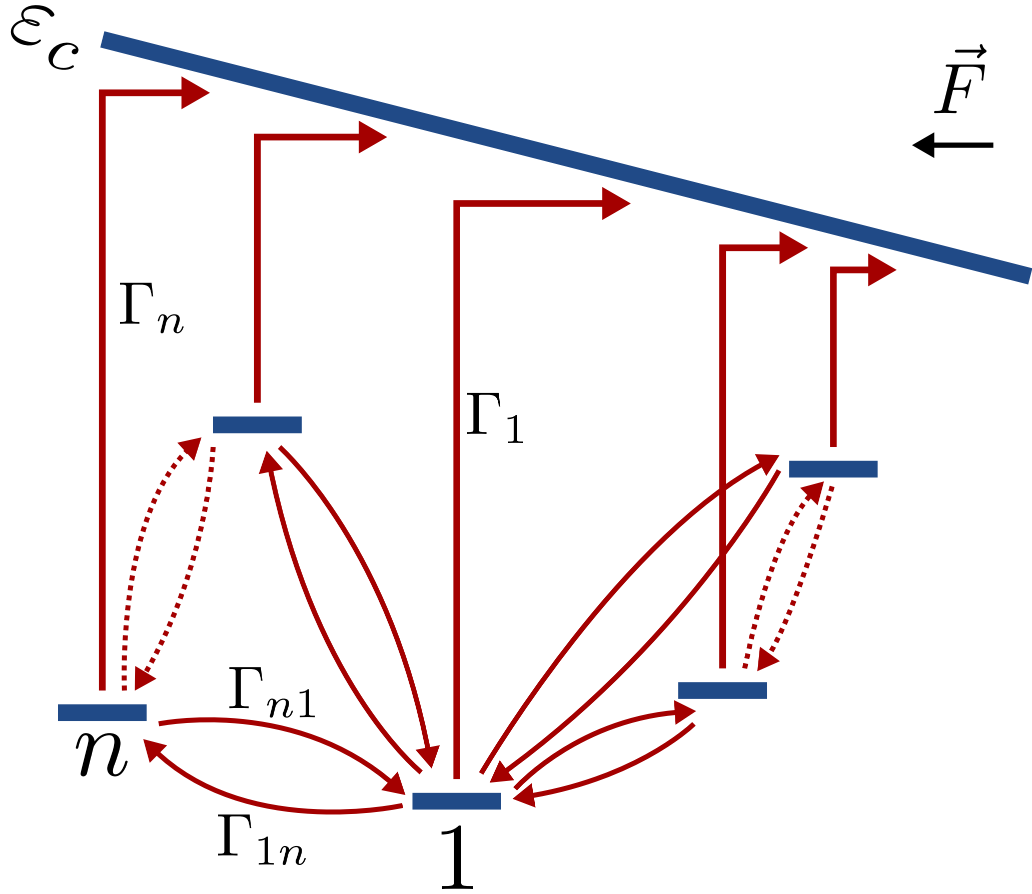

FIGURE 3.5: A sketch to carriers release assisted by hopping in the case of multiple traps. All possible hopping and release processes are depicted by red arrows. Dashed arrows corresponds to the hopping transitions, which are not taken into account in Eq. (3.26).

can be considerably simplified if we assume that one can neglect all the hops between the sites, other than hops from/to the trap 1 (further we will check this assumption by comparison with KMC simulation). Under assumption of "switched off" transitions the system of balance equations (3.4) simplifies to the following form:

$$\begin{cases} \left(\Gamma_1 + \sum_{n\neq 1} \Gamma_{1n}\right) p_1 = \sum_{n\neq 1} \Gamma_{n1}\, p_n + \gamma_0\,, \\ (\Gamma_2 + \Gamma_{21})\, p_2 = \Gamma_{12}\, p_1\,, \\ \quad \dots \\ (\Gamma_m + \Gamma_{m1})\, p_m = \Gamma_{1m}\, p_1\,, \\ \quad \dots \end{cases} \tag{3.25}$$

and they can be conveniently solved by the elimination of p_2 $(p_3, \dots)$ using the second

(third, etc.) equation. As a result, the expression for the mean escape time t acquires a closed form:

$$t = \frac{1 + \sum\limits_{n \neq 1} \dfrac{\Gamma_{1n}}{\Gamma_n + \Gamma_{n1}}}{\Gamma_1 + \sum\limits_{n \neq 1} \dfrac{\Gamma_{1n}\Gamma_n}{\Gamma_n + \Gamma_{n1}}} . \tag{3.26}$$

Such a method, as well as KMC simulation, requires computer generation of the system of sites and calculation of Γ_{mn} and Γ_1 values. However, one can go further to obtain analytical estimation for release time t without dealing with random realizations. It can be done in the following manner. Let us average the numerator and the denominator in Eq. (3.26) independently (angle brackets denote averaging over realizations):

$$\langle t \rangle \simeq \frac{\left\langle 1 + \sum\limits_{n \neq 1} \dfrac{\Gamma_{1n}}{\Gamma_n + \Gamma_{n1}} \right\rangle}{\left\langle \Gamma_1 + \sum\limits_{n \neq 1} \dfrac{\Gamma_{1n}\Gamma_n}{\Gamma_i + \Gamma_{n1}} \right\rangle} . \tag{3.27}$$

This procedure is justified for estimating the averaged t if the denominator does not vary in an exponentially broad range. Summations in the averaging can be replaced by the integrations:

$$\sum_n \quad \rightarrow \quad \int d\mathbf{r}_n \int d\varepsilon_n \; g(\varepsilon_n), \tag{3.28}$$

where $g(\varepsilon)$ is the density of states. Herewith, one obtains an analytical estimate for the averaged escape time:

$$\langle t \rangle \simeq \frac{1 + \int d\mathbf{r}_n \int d\varepsilon_n \; g(\varepsilon_n) \; \dfrac{\Gamma_{1n}(\mathbf{r}_n, \varepsilon_n)}{\Gamma_n(\varepsilon_n) + \Gamma_{n1}(\mathbf{r}_n, \varepsilon_n)}}{\Gamma_1 + \int d\mathbf{r}_n \int d\varepsilon_n \; g(\varepsilon_n) \; \dfrac{\Gamma_{1n}(\mathbf{r}_n, \varepsilon_n) \; \Gamma_n(\varepsilon_n)}{\Gamma_n(\varepsilon_n) + \Gamma_{n1}(\mathbf{r}_n, \varepsilon_n)}} . \tag{3.29}$$

All the rates contributing to Eq. (3.29) should be found taking the external electric field into account. The range of the integration over $d\varepsilon_n$ starts at the energy of the given trap 1 and extends towards the conduction band edge.

3.5 KMC simulation algorithm

As stated above, the generalized problem is not solvable analytically, however KMC method allows to solve it by simulation. The algorithm, which allows to simulate release of carrier from the trap, consists of the following steps:

1. First, a set of N_0 sites, is generated. The sites are distributed exponentially in energy with a characteristic energy E_0 The sites are distributed randomly in space with concentration N determined by a given value of the dimensionless parameter $N\alpha^3$, where a is the localization length of a single trap.

2. A trap with energy E_i is placed at the origin of the coordinate system $(0, 0, 0)$ and the escape of a charge carrier from this trap is simulated. Since the detrapping from the LS with energies in the vicinity of the Fermi level dominate all the transport phenomena, we assume that E_i corresponds to Fermi level. The traps with energies below E_i are, therefore, assumed occupied by carriers, while sites with energies above E_i are assumed empty from charge carriers.

3. The rates of all possible events are calculated. The rate of the straight release of a charge carrier from a trap into the conduction band is described by Eq. (3.2) The hopping rates are assumed to be described by the MillerAbrahams expression [13]. For each pair of sites (i, j), the transition rate ν_{ij} is determined by the separation between sites, $\mathbf{r}_{ij} \equiv \mathbf{r}_j - \mathbf{r}_i$, and the energy difference $\varepsilon_j - \varepsilon_i$,

$$\nu_{ij} = \nu_0 \exp\left(-\frac{2|\mathbf{r}_{ij}|}{a}\right)\gamma(\varepsilon_j - \varepsilon_i + e\mathbf{F}\cdot\mathbf{r}_{ij}) \tag{3.30}$$

   with

$$\gamma(\Delta\varepsilon) = \begin{cases} \exp(-\Delta\varepsilon/kT), & \text{if } \Delta\varepsilon > 0, \\ 1, & \text{otherwise.} \end{cases} \tag{3.31}$$

4. The cumulative event rate $\Gamma_i = \nu_{esc} + \sum_{i\neq j} \nu_{ij}$ is calculated and the time before the next event is determined as $\Delta\tau_i = \Gamma_i^{-1} R_i$ where $R_i = -\ln(x_i)$ includes the random number x_i uniformly distributed in the range $[0, 1]$;

5. In order to determine the particular event that happens with the charge carrier, the rates of all possible events were normalized via the cumulative event rate Γ_i and another random number $p \in [0, 1]$ was used.

6. If the chosen event is a release of the carrier to the conduction band, the simulation with the given charge carrier was finished with updating the cumulative time. If the chosen event is a hopping transition, the carrier is moved, the cumulative time, which the carrier spends on the localized states $\tau = \tau + \Delta\tau_i$ is updated and the algorithm returns to step 3.

In our simulations results were averaged over $10^4 - 10^6$ realizations. The number of traps N_0 in the simulations was varied in the range $10^3 - 10^4$. Test simulations showed that 10^5 realizations at the system with 10^3 LS is enough to get well reproducible and reliable results for a wide range of values of Na^3 and E_i. The characteristic energy of the exponential DOS was set to $E_0 = 5 \times 10^{-2}$ eV. The values of the parameter $N\alpha^3$ were varied from 10^{-3} to 10^{-1} and the strength of the electric field F was varied from 0 to 1 MV/cm. In all of the simulations, a room temperature $T = 300K$ was taken. The effective mass (included in Eq. (3.2)) of the electron is taken to be equal to free electron mass in all simulations, except the subsection dedicated to the influence of the effective mass.

3.6 KMC simulation results

Using the algorithm given above, we have simulated release times for "deep" traps with energies 0.3 eV and 0.5 eV. The corresponding results along with discussion are given further in this section.

3.6.1 Enhancement of the carriers release rate

In Figs. 3.6-3.7 one can see the results of the simulation for trap with energy depth 0.3 eV. Red dotted line in fig 3.6 corresponds to the case of a single trap. At this point let us assume that there are no additional traps around, and release rate depends purely on the depth of the LS, the temperature of the system and the magnitude of the electric field. To describe such a case, we simulate an activation from a single LS with energy $E_i = 0.3$ eV. The escape rate of an electron in such a case is determined just by Keldysh Eq. (3.2). One can see that, due to tunneling assisted activation, the release time of the electron decreases significantly with the growth of the electric field, which is the

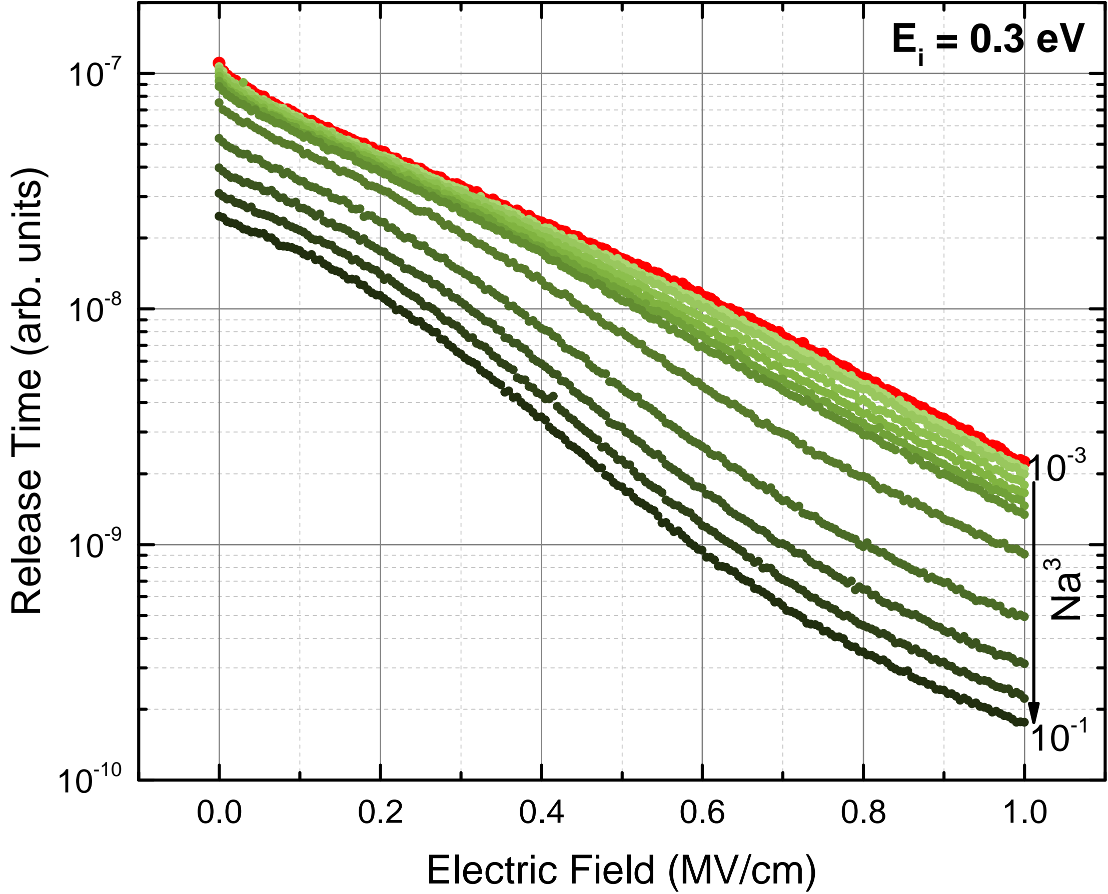

FIGURE 3.6: Escape time t versus field F for the trap with energy $E_i = 0.3$ eV. The red dotted line corresponds to the single trap, green dotted lines correspond to multiple traps cases with different values of Na^3. Na^3 varies from 10^{-3} to 10^{-1}, darker color corresponds to higher value of Na^3.

well-known result so far. For the 1 MV/cm field release time of electron reduces for two orders of magnitude.

Now let us look at the following situation: electron is initially localized at the similar deep trap with the energy $E_i = 0.3$ eV and in addition the initial trap surrounded by other traps, which are randomly distributed in space with a density given by Na^3 and energies distributed according to some given DOS $g(\varepsilon)$. Taking into account neighbouring LS, we can "turn on" hopping transitions between the sites to find out how hopping may affect electrons release. Results of the simulations for such a case are depicted by green dotted-lines in fig 3.6. These simulations were carried for different values of Na^3 in range $10^{-3} - 10^{-1}$, assuming the DOS given by 1.2 with parameter $E_0 = 5 \times 10^{-2}$ eV. It is clearly visible that the assistance of neighbouring traps intensifies the escape rate of the electron significantly (at least for high enough values of Na^3). This becomes even more clear when we look at the relative (with respect to a case of a single trap) escape

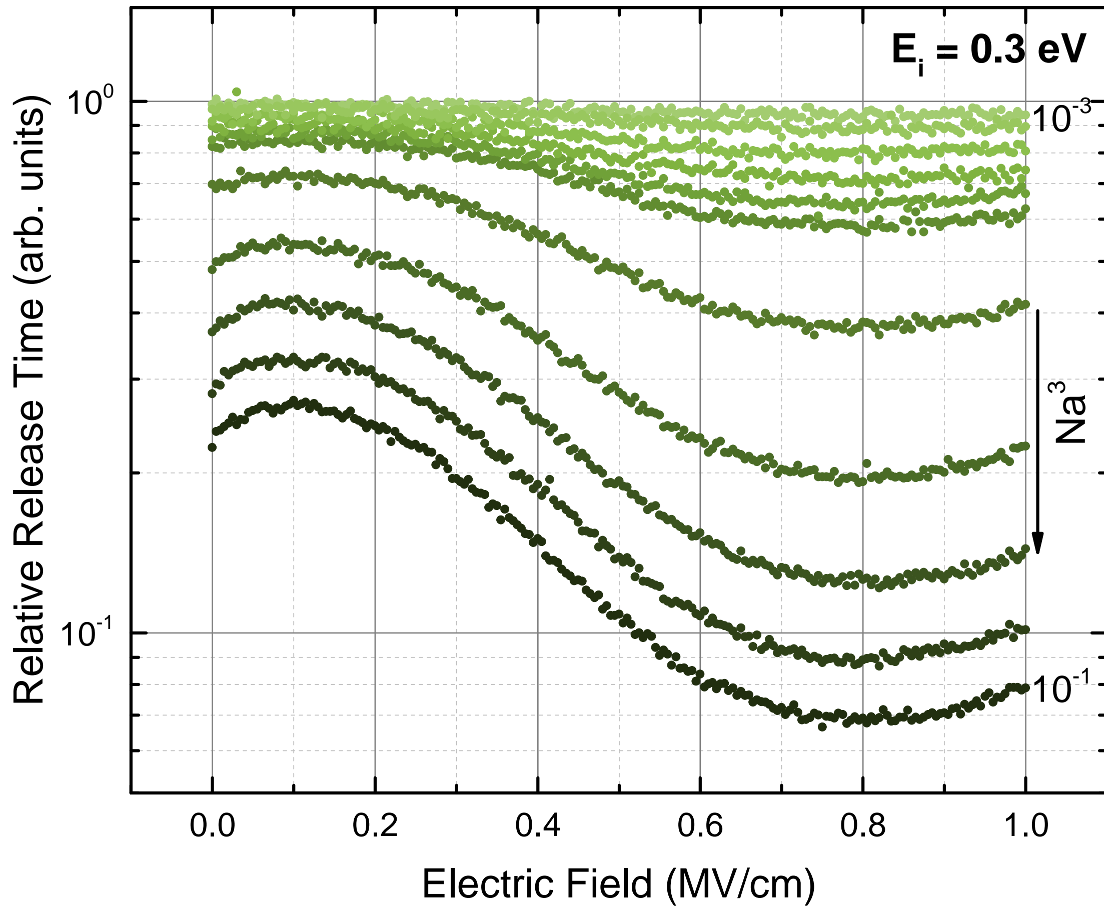

FIGURE 3.7: Relative escape time t_r versus field F for the trap with energy $E_i = 0.3$ eV. Na^3 varies from 10^{-3} to 10^{-1}, darker color corresponds to higher value of Na^3

time, depicted in Fig. 3.7. One can see how the effect depends on the value of Na^3. Electron release rate increases up to an order of magnitude in the strong electric field for the case of $Na^3 = 10^{-1}$, while in case of $Na^3 = 10^{-3}$ the effect almost disappears. The similar simulations for the case of even deeper initial LS with $E_i = 0.5$ eV are shown in Figs. 3.9-3.10. One can see that the enhancement of electron release in high fields is way stronger than in case of $E_i = 0.3$ eV. For $Na^3 = 10^{-1}$ electron release time at high fields is several orders of magnitude lower than in case of a single trap, while in case of $Na^3 = 10^{-3}$ the effect is already insignificant.

3.6.2 Carriers release at zero field

It is also seen that already at $F = 0$, depending on Na^3, the release rate $\nu_{\text{esc}}(\varepsilon)$ from a given trap in the presence of other traps is enhanced as compared to the case of a single trap. This effect is accompanied by the equal enhancement of the trapping rate

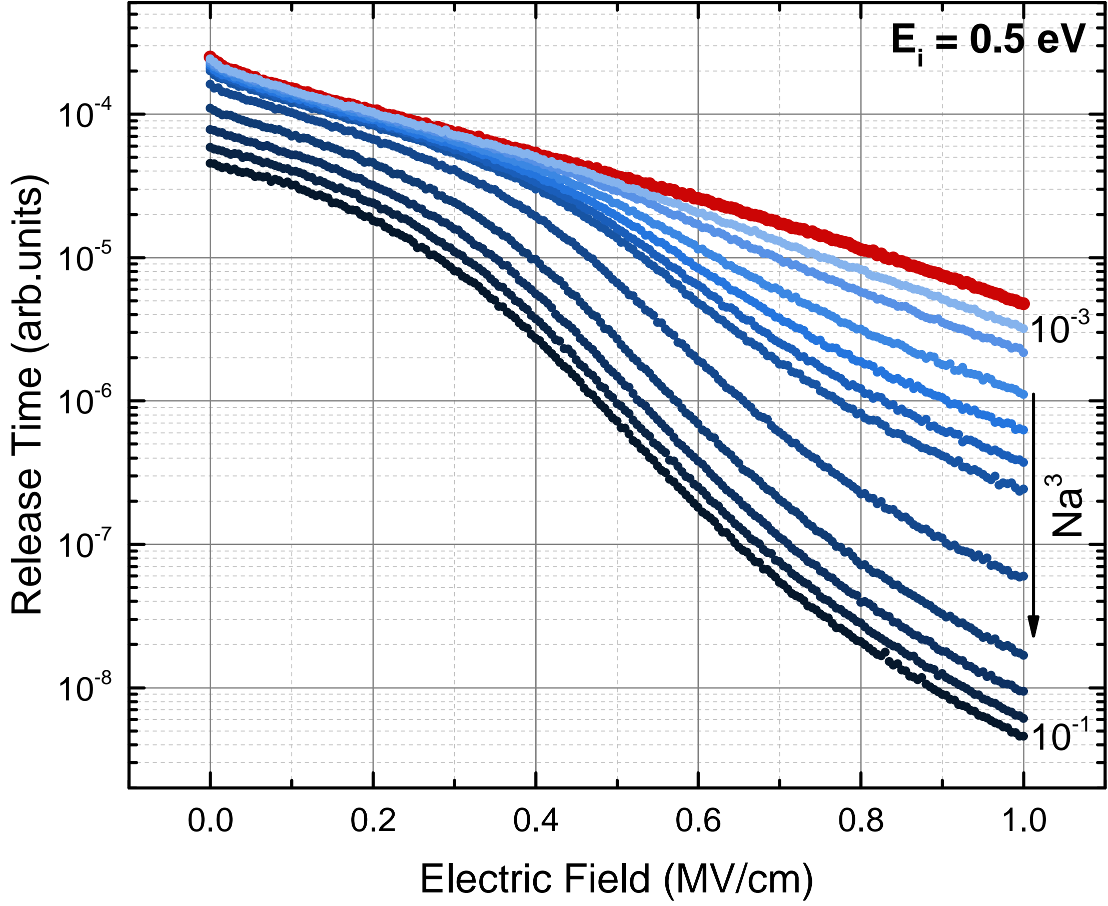

FIGURE 3.8: Escape time t versus field F for the trap with energy $E_i = 0.5$ eV. The red dotted line corresponds to the single trap(ST), blue dotted lines correspond to multiple traps cases with different values of Na^3. Na^3 varies from 10^{-3} to 10^{-1}, darker color corresponds to higher value of Na^3.

$\nu_{\text{trap}}(\varepsilon)$ into a given trap due to the assistance of the surrounding traps. Dependence of such an enhancement on Na^3 is shown in Fig. 3.10. This enhancement of $\nu_{\text{esc}}(\varepsilon)$ does not affect the equilibrium concentration of carriers in the conducting states above the mobility edge because of the validity of the detailed balance

$$\nu_{\text{esc}}(\varepsilon)/\nu_{\text{trap}}(\varepsilon) = \exp\left(-\varepsilon/kT\right). \tag{3.32}$$

Not the escape rate itself, but the ratio between the trapping and the escape rates governs the equilibrium concentration of carriers. Because of the detailed balance at $F = 0$, this ratio depends only on the energy of a given trap and it is not influenced by the presence of other traps. However, as we can see from simulations, the absolute value of escape rate increases with the growth of Na^3. It is easy to understand that higher values of Na^3 correspond to higher capture rates since we have a higher spatial

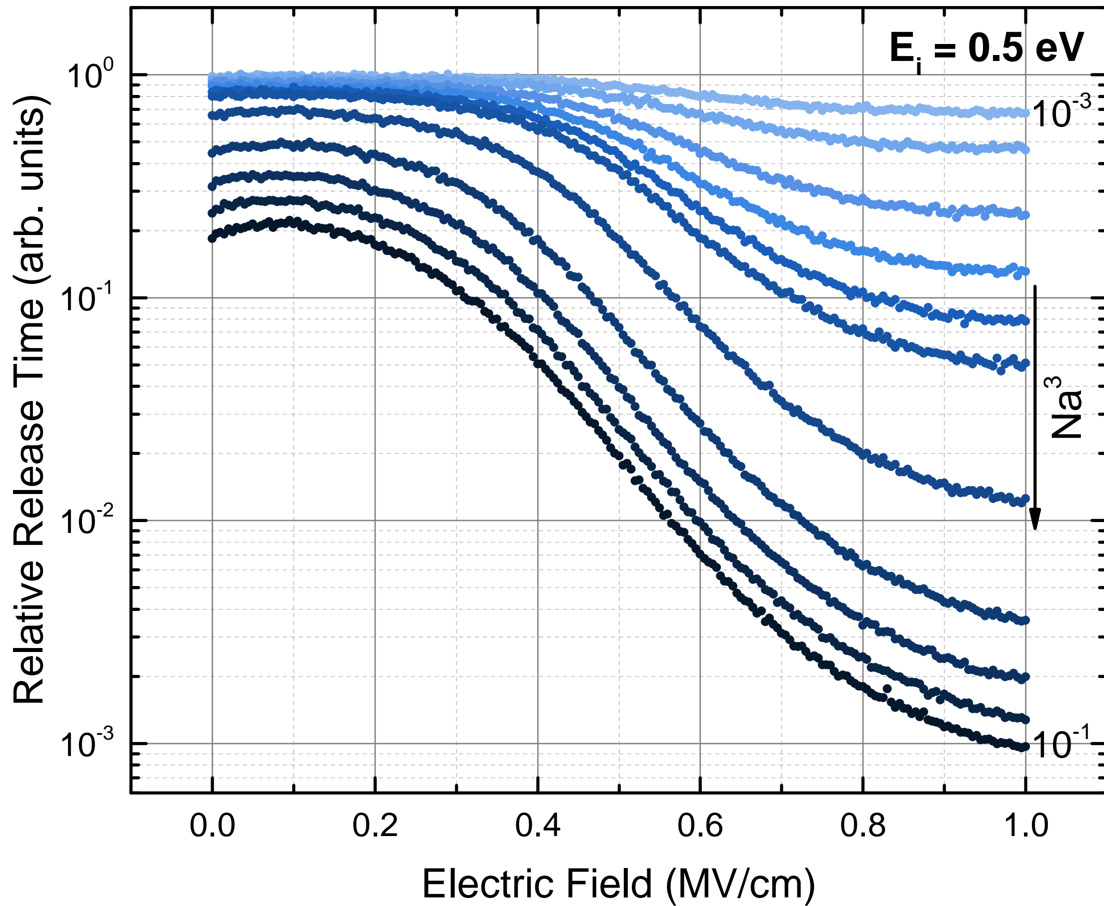

FIGURE 3.9: Relative escape time t_r versus field F for the trap with energy $E_i = 0.5$ eV. Na^3 varies from 10^{-3} to 10^{-1}, darker color corresponds to higher value of Na^3

density of traps. Thus, the release rate should increase by exactly the same factor to keep Eq. (3.32). Therefore, this effect did not influence such a property as, for instance, carriers mobility, since the increase of capture rates are being compensated by the increase of release rates, however, it may strongly affect phenomena, which are determined solely by the escape rate $\nu_{\mathrm{esc}}(\varepsilon)$. For instance, the thermally stimulated luminescence. In contrast to the thermally stimulated conductivity, which is governed by the interplay between the trapping and detrapping processes [32], the thermally stimulated luminescence is often claimed to be determined solely by a single event of the carrier release from a trap into conduction band [33, 34]. Thus, thus the increase of the escape rate due to hopping between traps may be a very important issue.

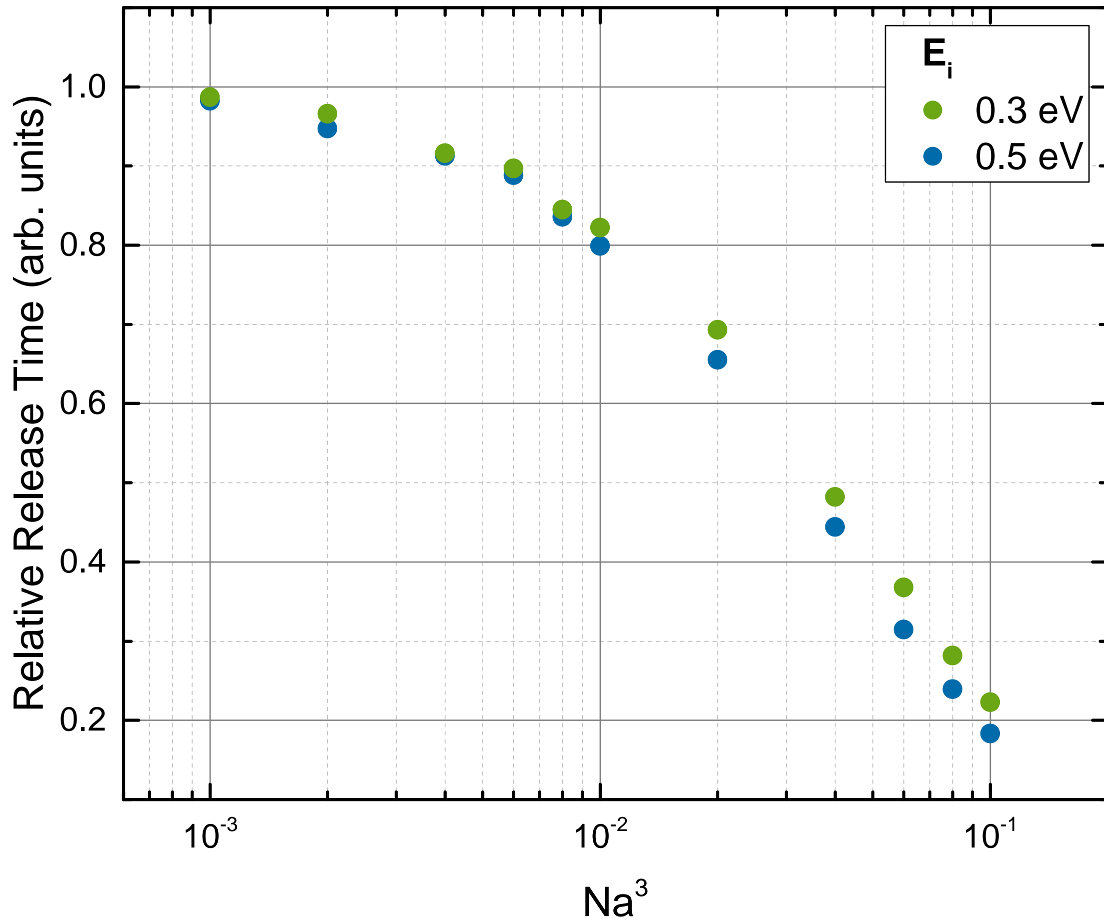

FIGURE 3.10: Relative escape times t_r versus Na^3 at zero field F for the traps with energies 0.3 eV and 0.5 eV.

3.6.3 Carriers release rate versus depth of the trap

Another important issue is how the effect depends on the relation between the depth of the initial trap and the scale of the DOS $\frac{E_i}{E_0}$ To address this question have made the simulation of electron relative release times for different values of $\frac{E_i}{E_0}$, while the value of Na^3 was fixed to be equal to 10^{-1}. Results of the simulation are depicted in Fig. 3.13. It is seen that strongly pronounced effect is only observed in case of deep traps with $\frac{E_i}{E_0} > 4$. Moreover, for shallow traps ($\frac{E_i}{E_0} = 2$), the strong external field does not enhance release speed of the carrier but reduces it. Such a behaviour can be explained by the fact that at the strong enough field vast majority of the nearby traps are deeper in energy than the initial shallow trap and therefore hopping transitions to such neighbours can increase the release time of the carrier. For deep LS, however, the opposite effect takes place. The majority of nearby traps are shallower in energy. Therefore, hopping transitions to such LS results in exponentially higher probabilities of carriers detraping. One should also

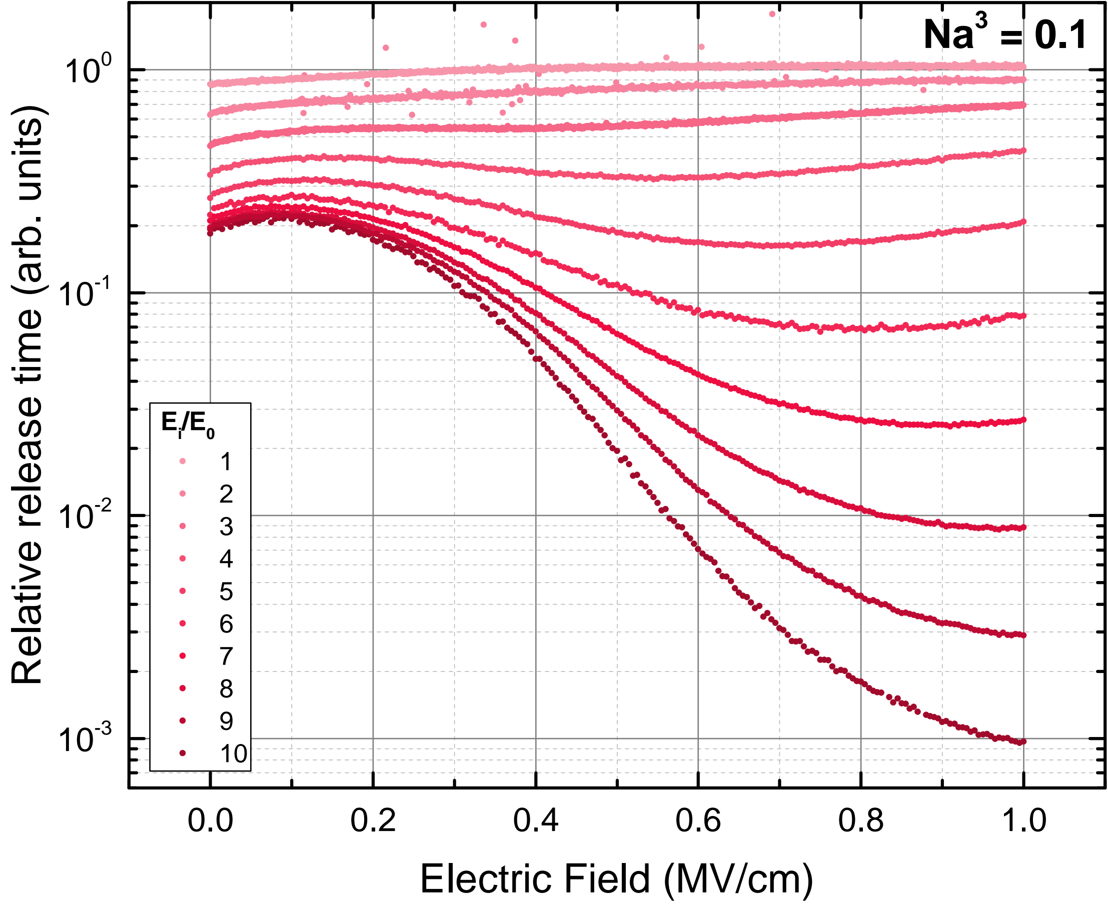

FIGURE 3.11: Dependence of the electron relative release time on the relation between trap depth E_i and the scale of the DOS E_0 ($Na^3 = 0.1$).

have noticed, how the increase of detraping enhancement in zero-field depends on $\frac{E_i}{E_0}$. For deep enough traps ($\frac{E_i}{E_0} > 4$) and $F = 0$ time of the carriers release saturates around $0.2\tau_0$, where τ_0 is the release time from an isolated trap. Thus, for deep enough traps release of carrier at zero-field depends only on the values of Na^3 (see the dependence on Fig. 3.10), however, for traps with the $\frac{E_i}{E_0} < 4$, both of the parameters Na^3 and $\frac{E_i}{E_0}$ are important.

3.6.4 Carriers release rate versus effective mass

One more important issue we have not discussed so far is the fact that Keldysh equation for field-assisted activation(Eq. (3.2)) includes the effective mass of the electron m. In all of the previous simulations value of the effective mass was considered to be equal to the value of free electron mass $m = m_e$. In order to check how the value of the effective mass influences the result we have simulated the process of carriers release from the LS with

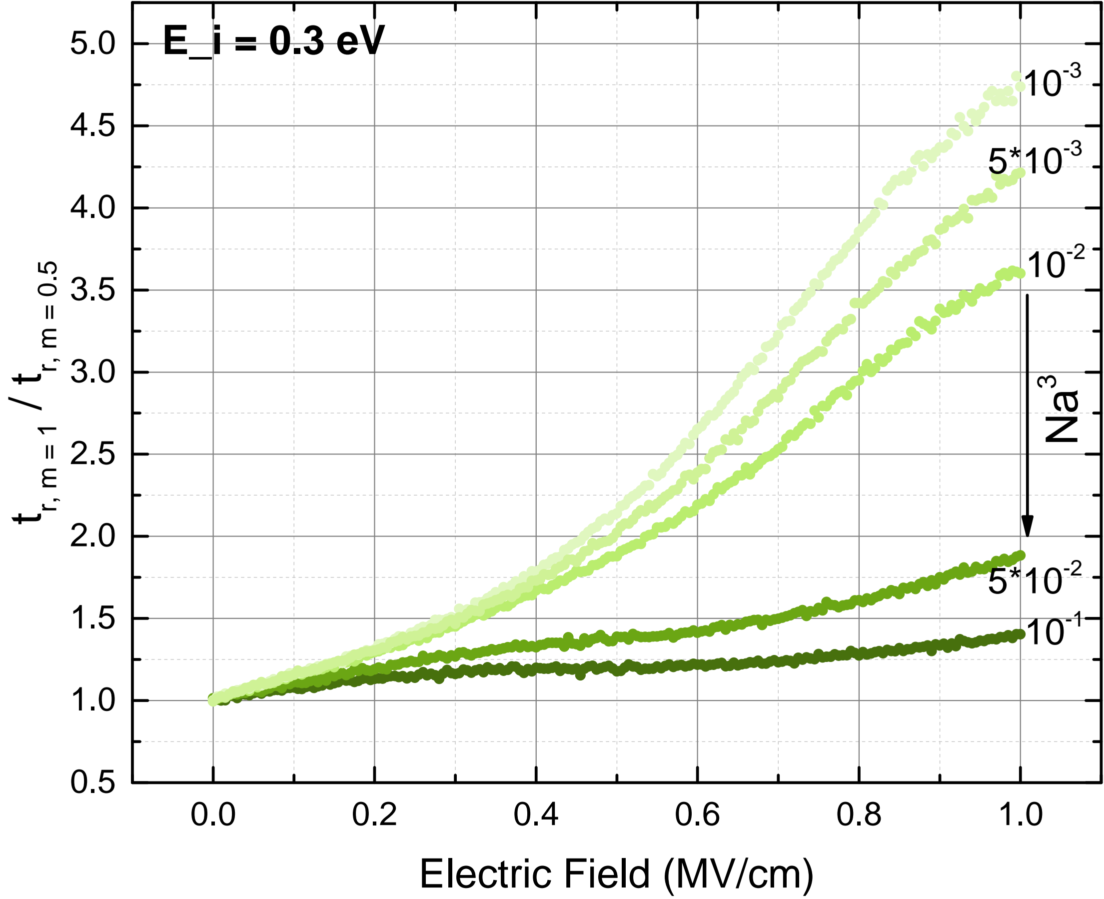

FIGURE 3.12: Relative time of carriers release at different effective masses. $E_i = 0.3$ eV, Na^3 varies from 10^{-3} to 10^{-1}.

$E_i = 0.3$ eV for the cases of $m = m_e$ and $m = 0.5m_e$. Relative escape time is depicted in Fig. 3.12. One can see the following patterns: the relative escape time strongly depends on the magnitude of the electric field (which is expected due to Eq. (3.2)); the effect became less significant for higher concentrations of traps, and almost vanishes at $Na^3 = 10^{-1}$. Thus, we can conclude that for high enough concentrations of traps one can consider $m = m_e$ (cause it does not affect the result significantly), while, at low concentrations, electron release time will also strongly depend on the effective mass. The relative escape time $\frac{\tau_{m=m_e}}{\tau_{m=0.5m_e}}$ at $Na^3 = 10^{-3}$ increases up to 5 times for $F = 1$ Mv/cm.

3.6.5 Comparison of the analytical approach and the KMC simulation

As we can see, simulation by means of KMC technique is an efficient method to study dependencies of the carriers detraping rate on the traps density and the magnitude of electric field. However, we have also derived the carriers release time for the case

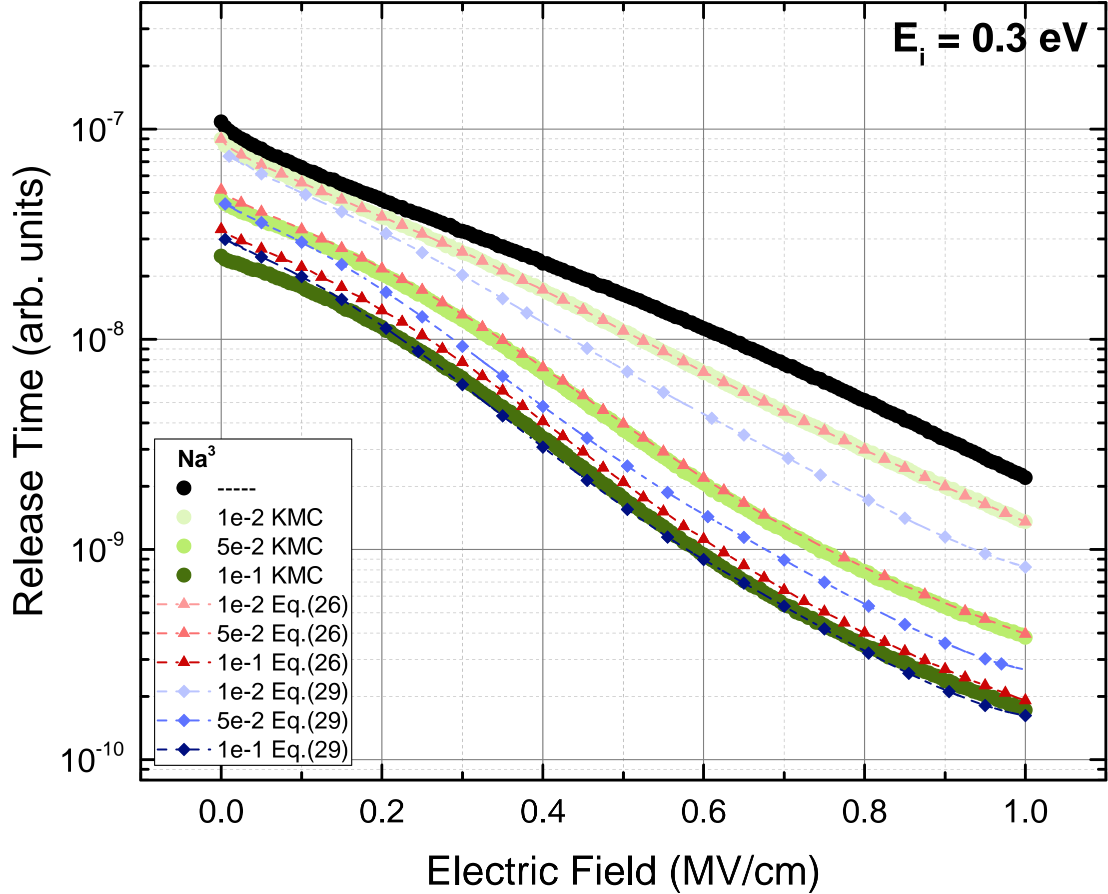

FIGURE 3.13: Comparing KMC simulation with Eq. (3.26)(red solid lines) and Eq. (3.29)

when backward jumps to the initial trap are "switched off" (see Eq. (3.26)). As it was mentioned before, the advantage of KMC approach is that it allows to collect statistics for the number of carriers hops before the activation or even track carriers path, counting how many times it visits certain LS. We have used such an approach to track exactly which hoping transitions are taking place during the release process. Analysis of the results revealed that for deep traps the average number of hops before activation is less than 3 even for the highest assumed values of Na^3, while the backward hopping transitions to the initial LS are extremely unlikely. Based on that, one can conclude that the assumption of "switched off" backward jumps is quite a reasonable (at least for the case of deep traps). Thus, one should expect Eq. (3.26) to provide pretty close results to those obtained by KMC. As noted earlier, such an approach still requires the generation of the system of sites in a similar manner as it is done in KMC approach. However, the computational complexity of calculation of the escape time using Eq. (3.26) may be significantly better compared to the KMC simulation (depends on the number

of sites and number of Monte-Carlo realizations). Moreover, as discussed previously, moving from summation to integration in 3.26, one arrives to an analytical formula Eq. (3.29). This could be easily calculated using standard numerical approaches, such as Simpson method, but the validity of such an approach is not obvious and must be put on test.

In Fig. 3.11 the comparison between KMC simulation(green dotted lines) and results obtained with Eq. (3.26)(red solid lines) and Eq. (3.29)(blue dotted lines) is shown. In order to solve the problem numerically, we apply the same sites generation procedure as described above with averaging the result of Eq. (3.26) over 10^5 realizations. One can see that Eq. (3.26) provides a good approximation to the results of the simulation. Unlike Eq. (3.26), Eq. (3.29)s does not imply averaging over different realizations, this is a purely analytical formula which could be easily solved by means of simple numerical integration methods. However, as one can see at Fig. 3.11 there is a significant discrepancy between the simulation results and the results obtained with Eq. (3.29), especially in case of high fields F and low traps concentrations Na^3. Thus, we can conclude that only Eq. (3.26) provides reliable estimation for the carriers release time dependence on electric field.

3.7 Conclusions

In this chapter we have discussed the model of electron detrapping assisted by hopping transitions to neighbouring sites. Analytical description of the problem has been provided along with the detailed review of the KMC algorithm. Based on the results of these studies we can make important conclusions. For deep LS hopping through the nearby traps in high field may enhance electrons escape rate significantly – up to several orders of magnitude. While for shallow traps these effects are negligible, for deep traps:

i effective capture cross section increases with the increase of traps concentration;

ii the field-assisted release of carrier described by Keldysh, significantly intensified by hopping to the nearby shallower traps;

These two effects together lead to a complex dependence of the escape rate of the carrier on the following parameters: traps concentration and localization radius Na^3,

the relative depth of the LS E_i/E_0, the magnitude of the external electric field F and also the effective mass of the electron m.

In general, such a dependence could be efficiently simulated by means of KMC approach. In addition, one can use the Eq. (3.26) to calculate electrons release time under the assumption, that electron is unlikely to jump back to the initial site.

Chapter 4

Effective temperature for the multiple-trapping transport

Studying charge transport in disordered material, we are interested in finding charge flow in response to an applied electric field. This flow, however, depends not only on the magnitude of electric field F, but also on temperature T. Aiming to simplify the model of hopping transport, Shkovskii [35] has introduced, so-called, effective temperature $T_{eff}(F, T)$. In frame of the effective temperature concept it is assumed that increase of the magnitude of electric field can be approximated by the effect of increasing the temperature. This approach provides a convenient way to express carriers mobility as a function of a single variable T_{eff}. The effective temperature concept is well developed and tested for for hopping conductivity [35–37]. However, for a wide range of amorphous inorganic semiconductor materials (such as a-Se and poly-PbO [38, 39]) it is often assumed that the charge transport is governed by multiple-trapping (MT) process, instead of hopping. Although, it is well known that carriers mobility in these materials strongly depends on electric field, there is still no consistent description of this effect. In this chapter we will show that the concept of effective temperature could be extrapolated on the case of MT transport to describe carriers mobility in amorphous inorganic materials.

4.1 The concept of effective temperature

In the case of pure band transport, when capture of carriers on traps does not play any essential role, the effect of the electric field on the carrier mobility can be described [40] by introducing effective temperature T_{eff}, which depends on the magnitude of the electric field F, $kT_{\text{eff}} \sim eFl/\hbar\omega$, where e is the carrier charge, k is the Boltzmann constant, $\hbar\omega$ is the phonon energy and l is the mean-free-path. This regime is valid in amorphous semiconductors only at very high temperatures, when the thermal energy kT is larger than the energy scale ε_0 and most carriers are in delocalized states above the mobility edge.

The effect of the electric field F on the carrier mobility μ in the hopping regime (which corresponds to the case of low temperatures $kT << \varepsilon_0$) received its theoretical interpretation already in 1970's thanks to Shklovskii [35]. He has recognized that for hopping conduction electric field plays a very similar role to that of temperature, and the combined effect of the electric field F and temperature T can be described by effective temperature T_{eff} (F, T). When performing hopping transition for a given distance x in the direction of electric field electron gains energy $\delta = eFx$ even assuming $T = 0$. The tunneling probability $\nu(x) \propto exp(-2x/a)$ can be than present as $\nu(\delta) \propto exp(-\delta/kT_{eff})$, with $T_{eff} \simeq eFa/2$, as if it was the effect of temperature activation. A very similar result was obtained later by Grünwald and Movaghar in their study of hopping energy relaxation of electrons through band tails at low temperatures and high electric fields [41]. The same idea was used by Shklovskii, who suggested that, at $T = 0$, one can calculate the field dependence of the conductivity in amorphous semiconductors by replacing the laboratory temperature T in formulas for the low-field finite-temperature theory by an effective temperature $T_{eff} \simeq eFa/2$. For the case of non-zero temperature Marianer and Shklovskii [36] suggested the following expression for the effective temperature:

$$T_{eff} = \left[T^2 + \left(\gamma \frac{eFa}{k} \right)^2 \right]^{1/2} , \tag{4.1}$$

where γ is fitting parameter. Values of γ in range $0.5 \leq \ \gamma \leq 0.7$ where reported depending on the considered transport phenomena [36, 42, 43].

However, neither pure band transport nor hopping transport, but rather MT transport is inherent in amorphous semiconductors, such as a-Se and poly-PbO, at temperatures relevant to experimental studies and to applications, when the thermal energy kT is neither much larger, nor much smaller than $\varepsilon_0 \sim 0.1$ eV. A theoretical description of the field-dependent mobility in the MT regime is still missing.

4.2 Carriers release and MT transport in amorphous semiconductors

Aiming to study this effect in amorphous semiconductors such as a-Si:H, a-Se, poly-PbO, we will consider carriers release mechanism as described in Chapter 3. Also we consider electrically neutral traps in the absence of carriers, and charged if carriers are present on the traps. It is widely accepted that localized states forming the band tails in amorphous materials appear not due to the introduction of electrically active donors or acceptors, but rather due to fluctuations of the distances between the atoms and of the angles between the covalent bonds [44–46]. States in the band tails can, for instance, appear on the elongated covalent bonds, in which the energy difference between the bonding and antibonding orbitals are smaller than on average. Therefore, traps are neutral in the absence of carriers. The release of carriers from traps in our study is in contrast to the ionization of traps studied, for instance, by Frenkel [47], who considered traps to be neutral when occupied by electrons, and to be ionized (positively charged) when electrons are released from the traps. First we assume low concentration of traps, when the effect of hopping to nearby sites can be neglected. In case of low traps concentration the carrier mobility in the MT transport regime is proportional to the probability for electrons to be released from the traps into conducting states [44, 45]. As we have seen in previous chapter, external electric field enhances the release rate ν_{esc} and this may strongly affect carrier mobility. However, in the general case of many traps, one should also consider a complex process of hopping enhancement of carriers release and capture rates, as described in Chapter 3. And for this purpose we use KMC approach to simulate carriers mobility.

4.3 Theoretical description of carriers mobility in MT regime via effective temperature

As we have already seen in Chapter 3, electrons escape rate in field is given by Keldysh equation (3.2). One can use the saddle-point method to evaluate the integral in the exponent, which yields the following expression [31, 48]:

$$\nu_{\text{esc}}(\varepsilon) \propto FT^{-3/2} \exp\left(-\frac{\varepsilon}{kT} + \frac{1}{24m}\frac{(e\hbar F)^2}{(kT)^3}\right). \tag{4.2}$$

Apparently, the saddle point exists, and Eq. (4.2) is valid, only in the case $\varepsilon > \frac{(e\hbar F/kT)^2}{8m}$. In the opposite case, it is favorable for carriers to leave the traps via isoenergetic tunneling without thermal activation. The same equations were obtained later by Vincent *et al*. [48]. These results were slightly modified by Karpus and Perel [49], who also predicted a parabolic field dependence in the exponent of the escape probability at low fields and found that only tunneling is responsible for carrier escape from the traps at high fields. Hijazi and Kabir [50] recently addressed Eq. (4.2) and claimed that considering the wide variation of the vibrational energy, the enhancement factor for the carrier release can be written as $\exp[(aF + bF^2)/kT]$, where a is the effective tunneling distance in the direction of the electric field and b is related to a fitting parameter for amorphous materials. However, it has not been explained how this result could be derived.

Aiming to analyze the field dependence of the mobility $\mu(F)$ using Eq. (3.2), let us express μ in terms of the escape rate ν_{esc}. In the case of the exponential density of states, most electrons in the steady state at $kT < \varepsilon_0$ have energies in the vicinity of the Fermi level ε_f. The fraction of the conducting electrons in the states above the mobility edge is proportional to the ratio between the escape rate $\nu_{\text{esc}}(\varepsilon_f)$ from a trap at the Fermi level,and a rate for a capture of an electron to such a trap. The drift mobility is proportional to the fraction of carriers in the conducting states:

$$\mu(T, F) \propto \frac{\nu_{\text{esc}}(\varepsilon_f, T, F)}{\nu_0}. \tag{4.3}$$

Let us show that it is possible to present the results of Eqs. 3.2 and 4.3 in the form

$$\mu(T,F) = \mu_0 \exp\left(-\varepsilon_a/kT_{\text{eff}}\right), \tag{4.4}$$

where T_{eff} is combination of temperature T and electric field F.

The rate of the carrier detrapping given by Eq. (3.2) depends on the carrier effective mass m. The carrier effective masses in amorphous semiconductors are not known with high accuracy yet. Usually, the values range from m_0 to $0.25m_0$, where m_0 is the free electron mass, are used for chalcogenide glasses [51]. The values $m = 0.34m_0$ for a-Si:H, $m = 0.22m_0$ for a-Ge:H and $m = 0.46m_0$ for a-As_2S_3 have been prereported in the literature [52]. To be definite, we use the value $m = 0.3m_0$ in the calculations. This assumption is not crucial for the results. The effective mass m enters Eq. (3.2) in the combination $\sqrt{m}/F$. The results for another choice of m can be obtained from our calculations for $m = 0.3m_0$ by a corresponding rescaling the F-axis.

In Fig. 4.2 and Fig. 4.1, we show the results for the carrier mobility $\mu(T,F)$ obtained via Eqs. (3.2 and 4.3) for $\varepsilon_f = 0.5$ eV and for $\varepsilon_f = 0.3$ eV, respectively. In Figs. 4.2a and 4.1a, the data are plotted as functions of the electric field for a set of temperatures between $T = 200$ K and $T = 300$ K with step size 20 K, while in Figs. 4.2b and 4.1b, the data are plotted as functions of temperature for a set of electric fields between $F = 0.05$ MV/cm and $F = 0.4$ MV/cm with step size 0.05 MV/cm.

We fit in Fig. 4.3 the theoretical data given in Fig. 4.2 and Fig. 4.1 to become straight lines when $\ln \mu(T,F)$ is plotted versus $1/T_{\text{eff}}$, where T_{eff} is given by Eq. (4.1). The only fitting parameter necessary to achieve this goal, i.e., the data to align, is the product γa present in Eq. (4.1).

For the results calculated via Eq. (3.2) with $\varepsilon_f = 0.5$ eV and shown in Fig. 4.2, the data in Fig. 4.3 were fitted with the value $\gamma a = 0.28$ nm, while for the results calculated via Eq. (3.2) with $\varepsilon_f = 0.3$ eV and shown in Fig. 4.1, the data in Fig. 4.3 were fitted with the value $\gamma a = 0.40$ nm.

From the data in Fig. 4.3, one can estimate the values of the activation energies ε_a via the slopes of the straight lines fitted by Eq. (4.4). Apparently, the data calculated via Eqs. (3.2), (4.3) for $\varepsilon_f = 0.5$ eV provide the activation energy $\varepsilon_a = 0.506$ eV, while the data calculated via Eqs. (3.2), (4.3) for $\varepsilon_f = 0.3$ eV point at the activation energy $\varepsilon_a = 0.306$ eV. The values obtained for ε_a are in perfect agreement with the values of

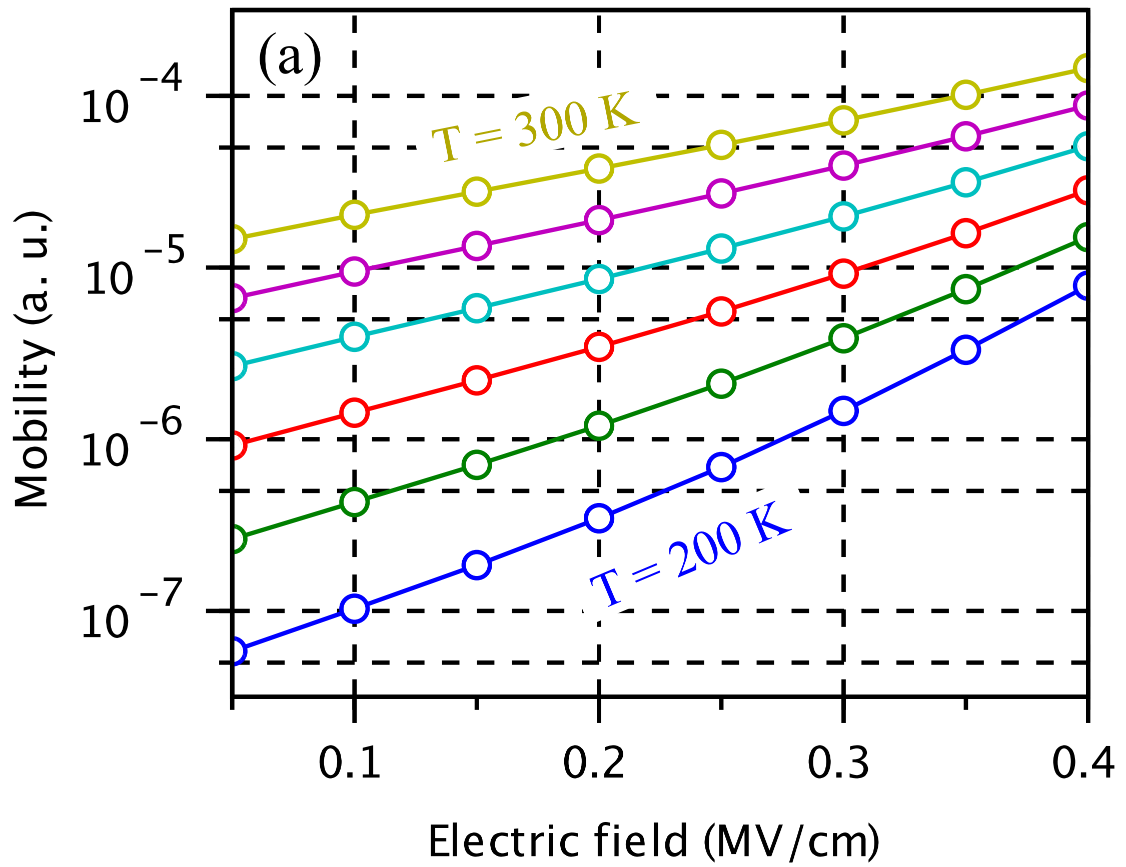

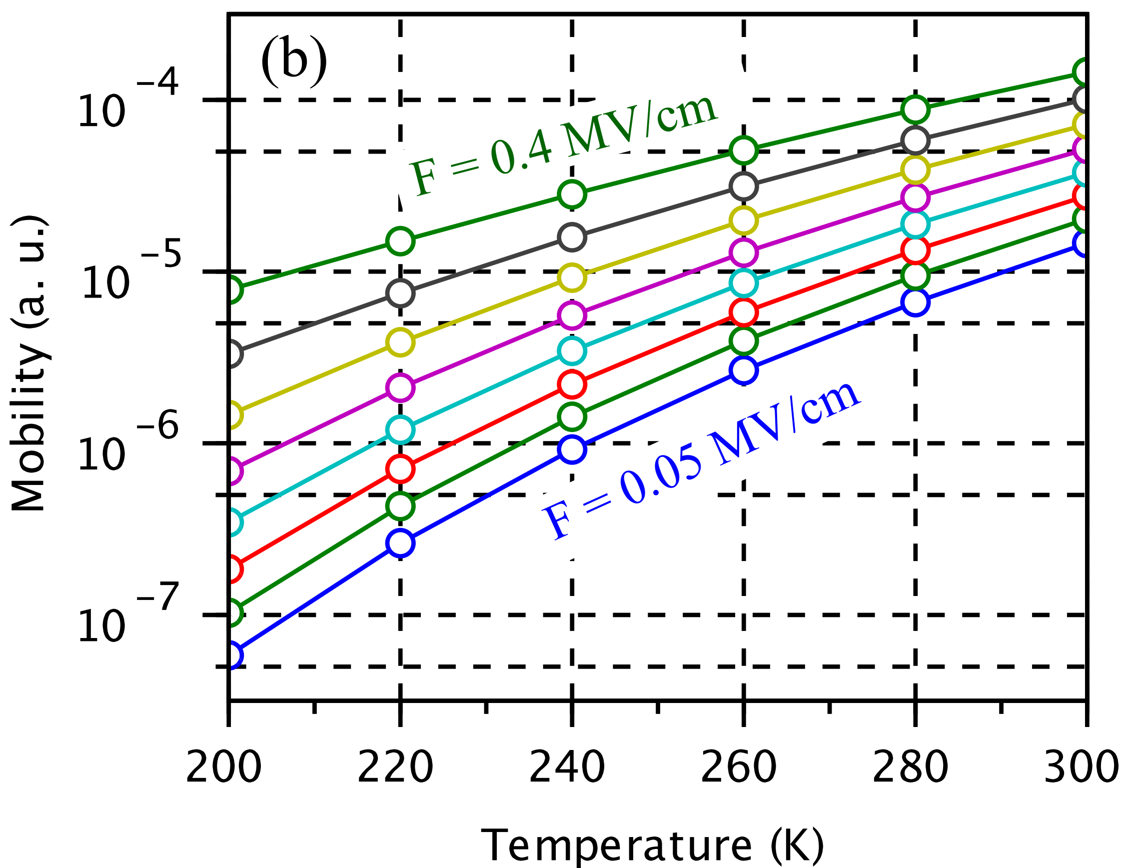

FIGURE 4.1: Results of Eqs. (3.2) and (4.3) for $\varepsilon_f = 0.3$ eV.

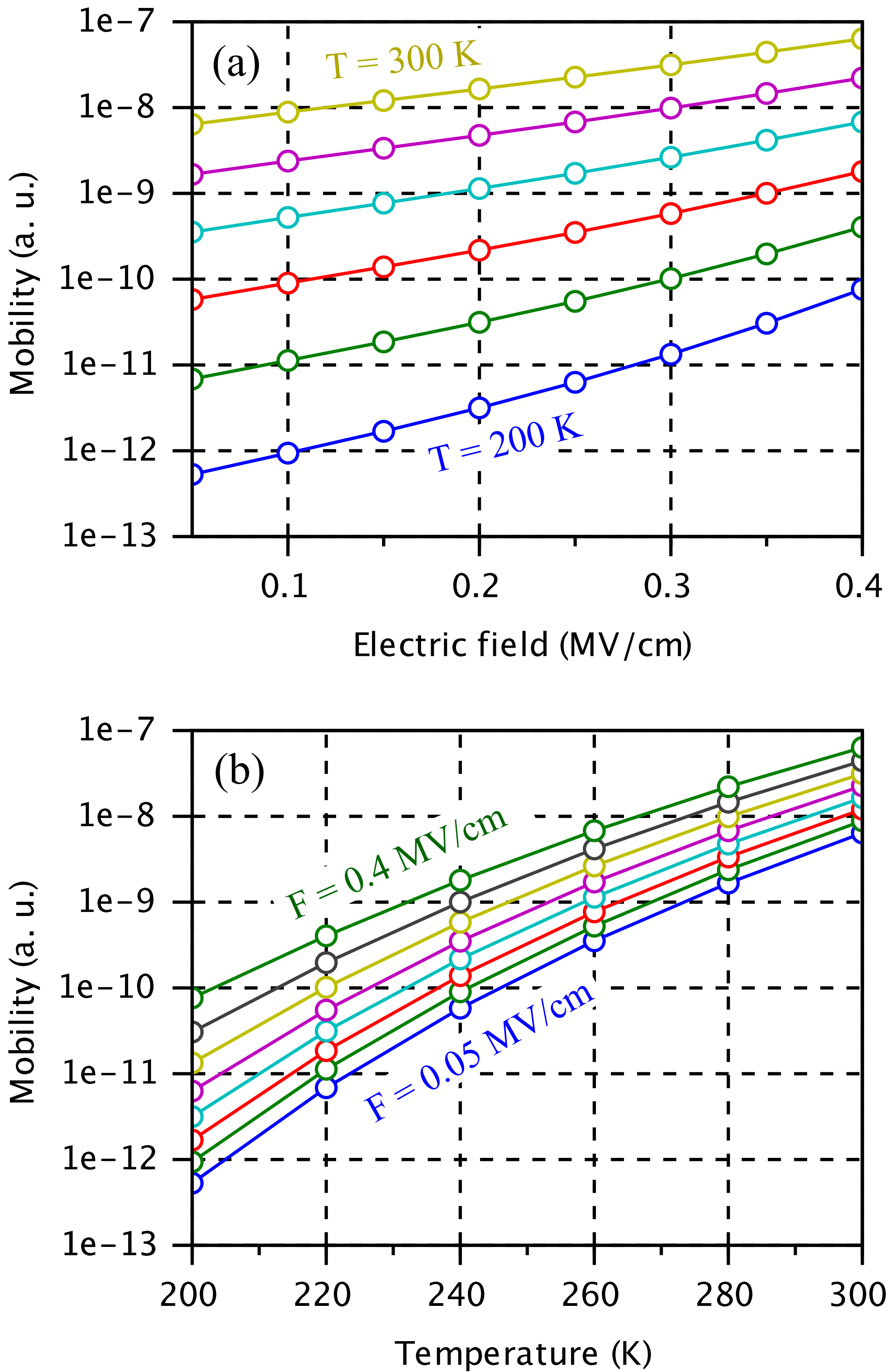

FIGURE 4.2: Results of Eqs. (3.2) and (4.3) for $\varepsilon_f = 0.5$ eV.

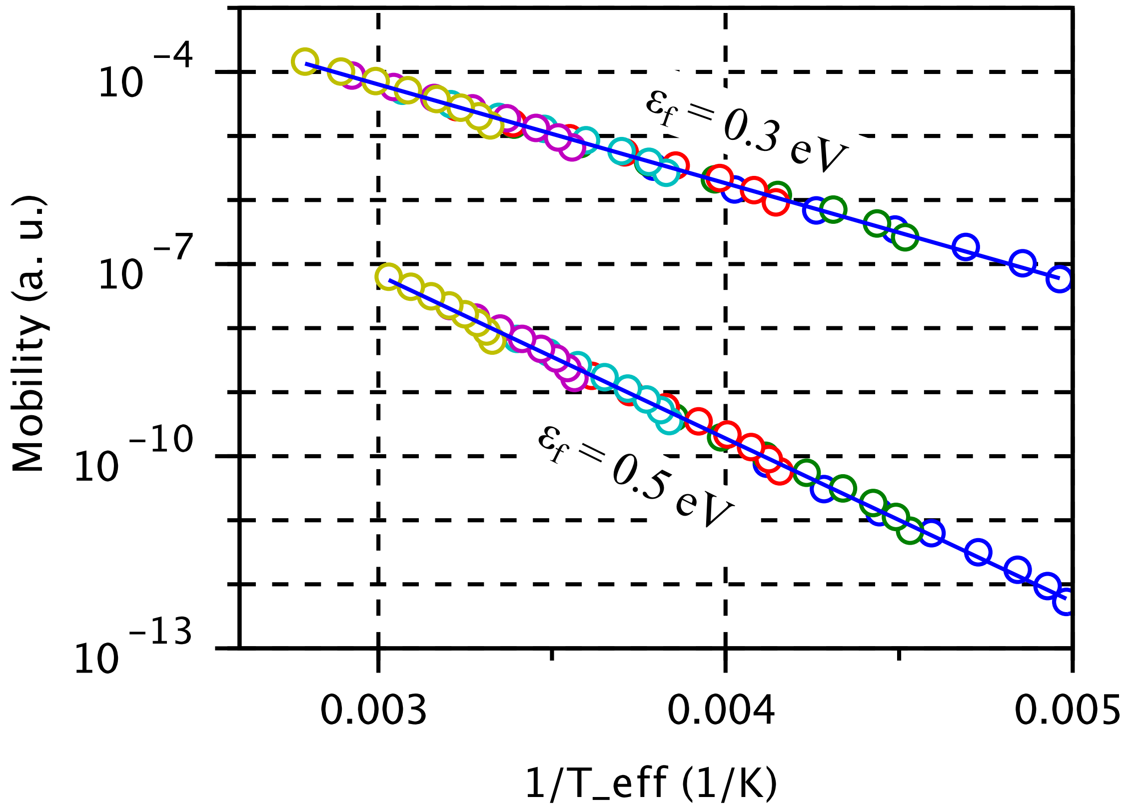

FIGURE 4.3: Arrhenius plot for the dependence of the mobility calculated via Eqs. (3.2) and (4.3) vs the effective temperature given by Eq. (4.1).

$\varepsilon_f = 0.5$ eV and $\varepsilon_f = 0.3$ eV used in our calculations. This result is not trivial. It shows the ability of the approach based on the effective temperature T_{eff} to account for the effect of the electric field F on the release rate.

Fittings of the theoretical data by Eq. (4.4) shown in Fig. 4.3 were achieved using the values $\gamma a = 0.28$ nm and $\gamma a = 0.40$ nm for $\varepsilon_f = 0.5$ eV and $\varepsilon_f = 0.3$ eV in Eq. (4.1), respectively. Taking the value $\gamma = 0.6$ to fit experimental data by the effective temperature T_{eff} given by Eq. (4.1) results in the estimates $a = 0.47$ nm and $a = 0.67$ nm for $\varepsilon_f = 0.5$ eV and $\varepsilon_f = 0.3$ eV, respectively.

The length scale a that appears in Eq. (4.1) must be a combination of the model parameters—namely, of the effective mass m, Fermi energy ε_f, and the Planck constant $\hbar$. There is only one combination of these parameters that has the dimensionality of length. It is the localization length of an electron trapped at the energy level ε_f.

$$a = \frac{\hbar}{\sqrt{2m\varepsilon_f}} \,. \tag{4.5}$$

Inserting in Eq. (4.5) the value $m = 0.3m_0$ used in our calculations, one obtains $a = 0.48$ nm and $a = 0.62$ nm for for $\varepsilon_f = 0.5$ eV and $\varepsilon_f = 0.3$ eV, respectively. These values are similar to the estimates for a obtained from the fitting of Eqs. (3.2, 4.3) with the effective temperature T_{eff} given by Eq. (4.1). It is worth noting that the localization length usually appears in the theory of hopping transport. In above analysis of the MT transport, hopping does not play any role, but, remarkably, the localization length a also becomes an important parameter.

Obtained results shows that this theoretical description can be literally used to account for the field-dependent mobility at high electric fields with just replacing the laboratory temperature T by the field-dependent $T_{\text{eff}}(T, F)$ in all theoretical expressions derived for the case of low fields. This recipe to describe the non-linear effects at high electric fields by just renormalizing the temperature T is not at all trivial. There is no general reason that the effect of a large electric field on the carrier mobility can be reduced to the renormalzation of the temperature $T \to T_{\text{eff}}(T, F)$. In this work, we present a proof for the capability of a single parameter $T_{\text{eff}}(T, F)$ to account for the combined effects of temperature and of the electric field on the carrier mobility in the MT transport regime. This conclusion is supported by the analysis of the experimental data for the dependences of the carrier mobility μ on temperature T and on the applied electric field F obtained previously in a-Se [38] and in poly-PbO [39]. We have shown [9] that these data can be described by a single parameter, the field-dependent effective temperature $T_{\text{eff}}(T, F)$.

Furthermore, the strength of the electric field F can enter the expression for the effective temperature $T_{\text{eff}}(T, F)$ only in the form of the product eLF, where L is some characteristic length. In the case of band transport, there is an apparent characteristic length, the mean free path of charge carriers. Therefore, it is not surprising that it is the mean free path that relates the effective temperature to the electric field for the case of the band transport [40]. In the case of hopping transport, there also is an apparent fundamental length scale, the localization length a responsible for the tunneling of charge carrier between the localized states. Recently, it has been proven [53] that a is the length that relates the effective temperature $T_{\text{eff}}(T, F)$ to the strength of the electric field F in the case of hopping transport. In the MT regime, on the contrary, there is no apparent fundamental length scale that anyhow affects the charge transport at low electric fields. At low fields, charge carriers are released from the traps into conducting

states by thermal activation with the rate dependent solely on the depth of the energy traps ε and on temperature T, as described by Eq. (3.1). Our results show that a characteristic length appears to affect charge transport in the MT regime at high electric fields and that this characteristic length is the localization length of charge carriers a. It is the same fundamental length scale that determines the relation between $T_{\text{eff}}(T, F)$ and F in the hopping transport regime.

4.4 KMC simulation of carriers mobility in MT regime

Strictly speaking, the above analysis is valid only for the case of low traps concentration, when the effect of hopping transitions between nearby sites can be neglected. In the general case, Eq. (4.3) is not quite accurate. For the case of high spatial density of traps hopping transitions to nearby traps may have a strong impact. As we have studied in Chapter 3, hopping transitions to the surrounding traps, on the one hand, may significantly increase the release rate of a carrier, but, on the other hand, the presence of additional traps also increases capture rate. Thus, for the general case, one should also assume non-constant capture rate $\nu_{\text{trap}}(\varepsilon_f, T, F)$, and the mobility given by

$$\mu(T, F) \propto \frac{\nu_{\text{esc}}(\varepsilon_f, T, F)}{\nu_{\text{trap}}(\varepsilon_f, T, F)}, \tag{4.6}$$

instead of Eq. (4.3). Although there is no analytical description that allows calculating proper ratio between escape and capture rates, we can obtain it by means of KMC method, using the below recipe.

4.4.1 KMC simulation algorithm

An algorithm for simulation of the mobility is similar to the one for simulation of carrier release time (see Chapter 3), except the fact, that for mobility we have to take into account not only increase of escape rate due to hopping, but also increase of capture rate. Indeed, in case of a single isolated trap electron has only one path to be captured to this specific trap. However, if we add some extra traps to the system, the electron has a chance to be captured to the chosen site not only directly from the band, but also by hopping via transitional traps. Thus, additional sites create additional paths for the

electron to be captured on a given trap. Of course, this is consistent with the principal of detailed balance. In thermal equilibrium at zero filed both release and capture rates increases equally due to presence of nearby traps.

However, in the electric field the balance is broken and the ratio of release and capture rates changes with increasing field. To simulate this ratio we have to take into account contributions of all possible paths for the electron to be captured and all of the release paths. For that purpose one can modify the algorithm from Chapter 3 in the following manner:

i set electron initially to site i (it could any possible site, not only the "chosen" one) and let it perform hopping transitions until the release to conduction band;

ii accumulate the total amount of time τ_f, that electron spends on the "chosen" site (*at the Fermi energy* ε_f);

iii repeat for all sites $i \in [1..N_0]$.

The above procedure takes into account proper ratio between release and capture rates, and allows to express mobility as:

$$\mu \propto \frac{1}{\langle \tau_f \rangle}, \tag{4.7}$$

where τ_f is averaged over sufficient number of realizations.

The core difference between this algorithm and the one from Chapter 3 is that, instead of setting electron at the "chosen" site initially, we are setting it successively at all possible sites. By doing so, we take into account all possible ways of trapping electron to the "chosen" trap, as well as all possible ways of electron release from the "chosen" trap.

4.4.2 KMC simulation results

Using the above approach, we were able to simulate carriers mobility for MT transport and test the concept of effective temperature for the case of high concentration of traps. Simulations were conducted for the case of $\varepsilon_f = 0.5$ eV and corresponding localization radius $a = 0.48$ nm (given by Eq. (4.5)), assuming the exponential DOS with scale

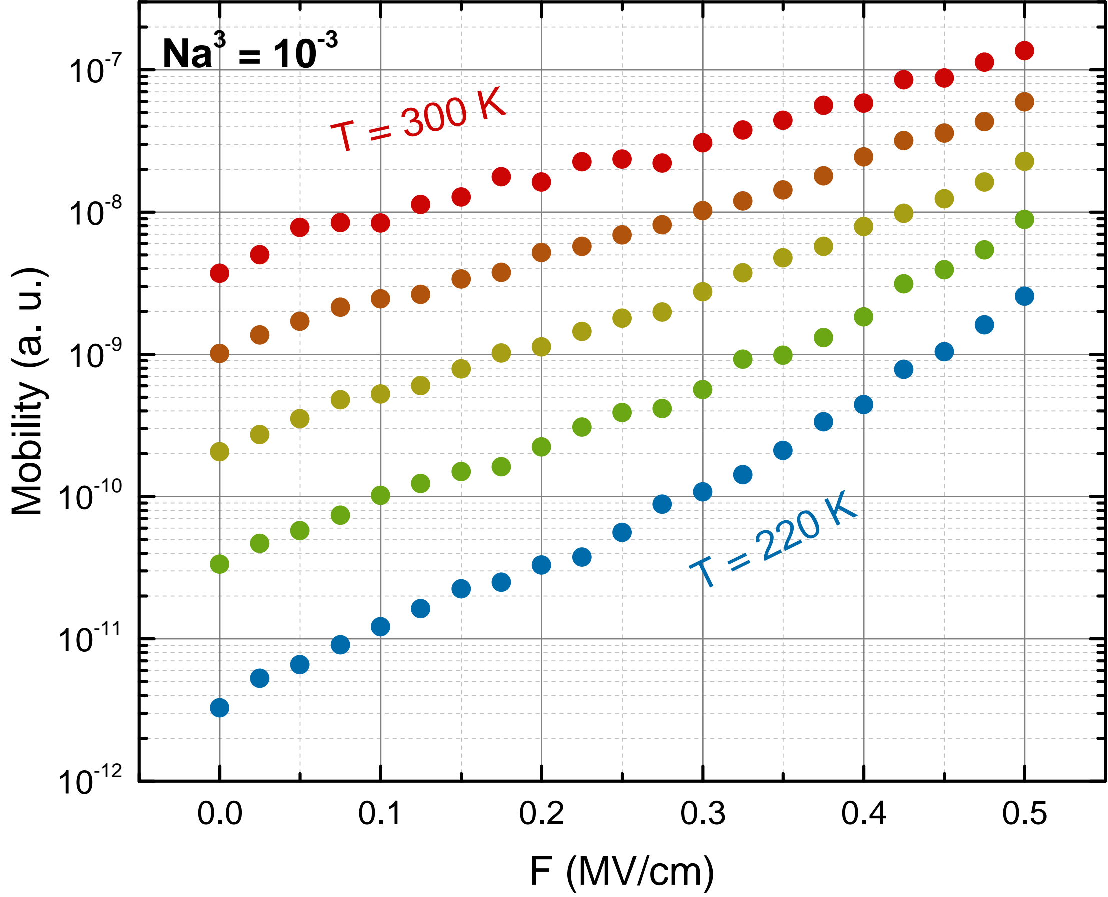

FIGURE 4.4: KMC simulation of mobility for MT transport, $\varepsilon_0 = 0.05$ eV, $\varepsilon_f = 0.5$eV, $Na^3 = 10^{-3}$.

$\varepsilon_0 = 0.05$ eV. Effective mass again was chosen to be $m = 0.3m_0$. Reasonably wide range of traps concentrations was tested varying Na^3 from 10^{-3} to 10^{-1}. Number of sites in the simulation was chosen to be 500, while results were averaged over 10^5 realizations.

Simulations were made for different temperatures in range $220 - 300$ K with step 20 K, while the electric field magnitude varied from 0.1 to 0.5 MV/cm. Results of simulations are ploted in Figs. 4.4 ,4.5. One can clearly see that in case of high concentration of sites ($Na^3 = 10^{-1}$) mobility at high fields changes noticeably stronger compared to the case of $Na^3 = 10^{-3}$, showing an order of magnitude difference in high field. This is an expected behavior, since, as we have seen in Chapter 3 (see Fig. 3.9), carriers release time in high fields differs significantly for different concentrations of traps. Even though capture rate also increases, its increase is not that strong as of the release rate, so the ratio between ν_{esc} and ν_{cap} in Eq. (4.6) still grows at high fields.

The simulated dependences of mobility on the electric field are well fitted by the effective

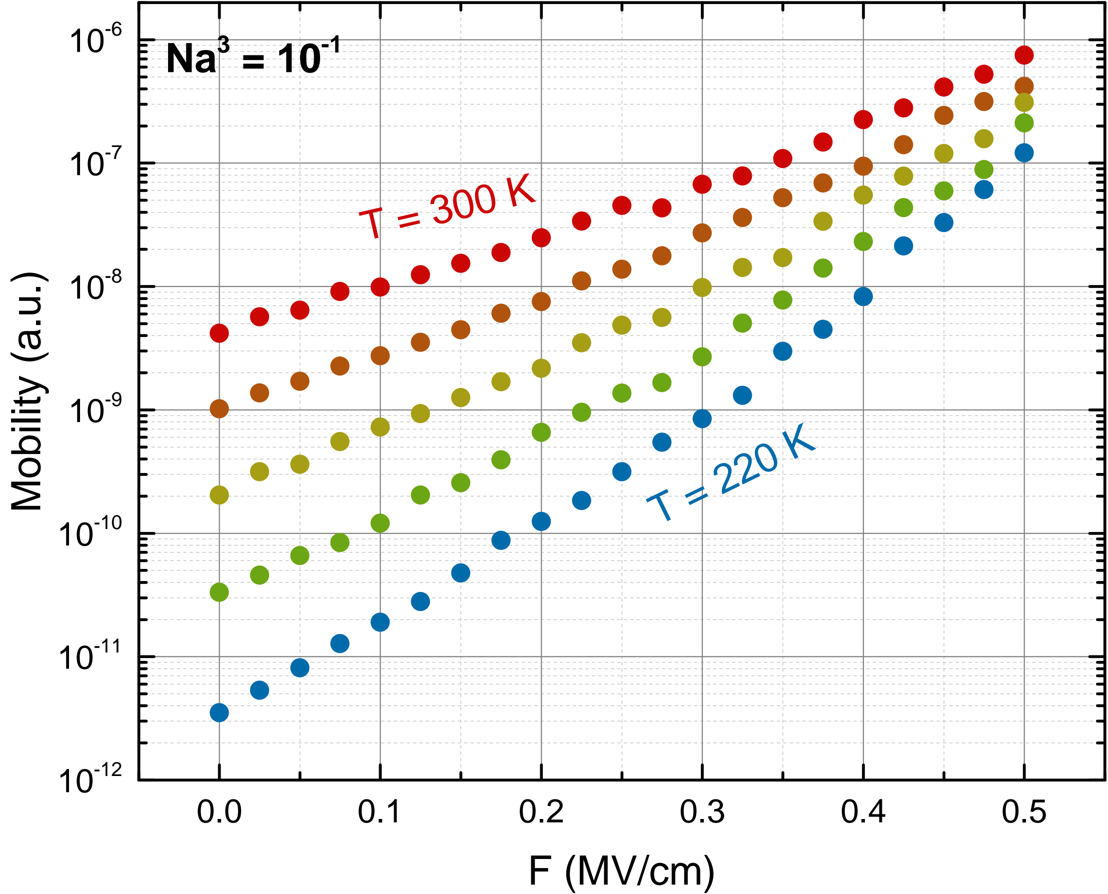

FIGURE 4.5: KMC simulation of mobility for MT transport, $\varepsilon_0 = 0.05$ eV, $\varepsilon_f = 0.5$eV, $Na^3 = 10^{-1}$.

temperature Eq. (4.1). These fits are depicted in Fig. 4.6, by blue and red dots for the cases of $Na^3 = 10^{-3}$ and $Na^3 = 10^{-1}$ correspondingly. This result shows that the concept of effective temperature is valid also for the general case of reasonably high concentration of traps. The important thing to notice here is that the value of γ in Eq. (4.1) is not a universal for all concentrations. It is actually concentration-dependent. The value of γ for the case of $Na^3 = 10^{-3}$ appears to be 0.64 , while for the case of $Na^3 = 10^{-1}$ we found γ to be 0.93. Indeed, as we know from Chapter 3, enhancement of carriers release rate at some fixed field strongly depends on the concentration of traps. The increase of γ for increasing Na^3 simply reflects the fact that the role of the electric field is higher for the higher concentration of traps. Note, that the simulation was done for the case of very low concentration of electrons, which corresponds to $\varepsilon_f = 0.5$ eV while $\varepsilon_0 = 0.05$ eV. Since the field-enhancement of carriers release decreases (i.e. the role of electric field drops) with the increase of carriers concentration (see Fig. 3.11), one should expect γ to vary in even narrower range. Thus, based on the results of simulation,

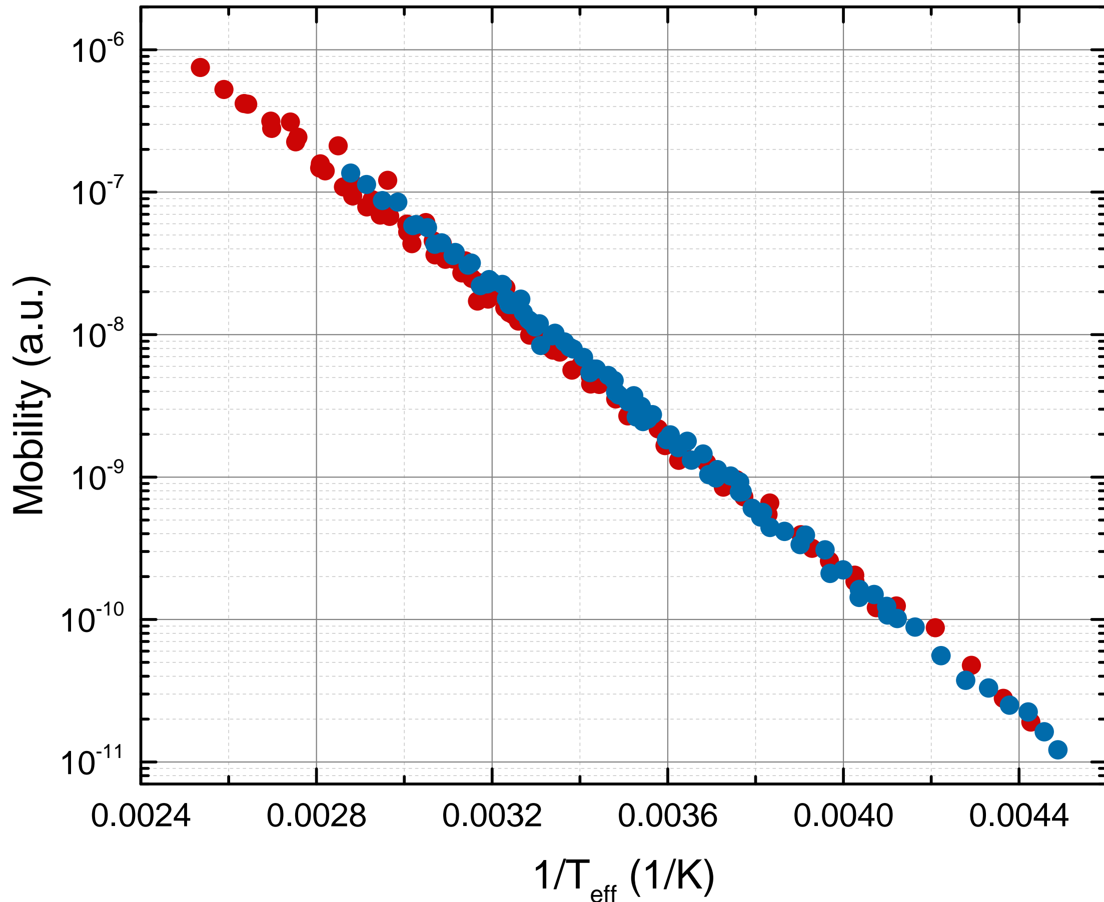

FIGURE 4.6: Effective temperature fit for simulated mobility, $\varepsilon_0 = 0.05$ eV, $\varepsilon_f = 0.5$ eV. Blue dots corresponds to $Na^3 = 10^{-3}$, red dots corresponds to $Na^3 = 10^{-1}$.

we claim that for practical cases one could consider the value of γ to be in the range $0.6 - 1$.

4.5 Conclusions

In this chapter we have shown how the concept of effective temperature can be extended to describe electron mobility in case of MT transport, which is usual for amorphous inorganic materials. The validity of the effective temperature for MT transport was shown theoretically for the case of low concentration of traps and confirmed by means of KMC simulation for the case of a reasonably high density of traps. Remarkably, the length scale in Eq. 4.1 appears to be localization radius not only for the case of hopping transport but also for MT transport. One practical consequence of this is that it is possible to estimate the value of localization radius in amorphous inorganic

materials such as a-Se and poly-PbO [9] by fitting experimentally measured $\mu(F,T)$ to the effective temperature, and assuming γ in some narrow range between 0.6 and 1. KMC simulation also reveals that the value of scaling parameter γ depends on the value of Na^3. Thus, in some cases it might be possible to estimate concentration of traps from fitting experimental data with KMC simulation.

Conclusions

Below is a short summary of the main results of current work, in accord with the sequence of chapters.

In Chapter 1 a brief description of the core theoretical concepts of carriers transport in disordered materials is given. It covers only the very basics of theory, like a density of states and hopping transitions rates, and defines the framework of implementing those concepts in Kinetic Monte Carlo simulations. Readers, who is aiming to deeper understand the modern state of theory of the carriers transport in disordered materials, are encouraged to read review articles [10, 11], which cover most of the related topics.

Chapter 2 is dedicated to the peculiarities of PL in compound semiconductor materials, particularly in Ga(NAsP). It is shown that existing theoretical approach is not capable of describing such experimental dependence as the low-temperature shrinkage of PL line with increasing excitation power [6]. Analysis of the problem by means of KMC approach, revealed that in order to explain this effect one should assume the complex shape of the DOS, which could be approximated by combination of exponential and Gaussian components. Results of this research are discussed in details in [6]. In the second part of Chapter 1 we have revised the so-called model of double-scaled disorder [7], which was earlier introduced to explain the unusual behaviour of the temperature-dependent PL features (such as the Stokes shift) in Ga(NAsP). This model contradicts the concept of complex DOS and is not capable of describing the low-temperature linewidth shrinkage effect. Therefore, we have introduced an alternative self-consistent model capable of describing both of the effects discussed above [8]. The key feature of the new model is the assumption of 2 types of localized states (due to exponential and Gaussian components of the DOS correspondingly) with strongly different temperature-dependent

non-radiative exciton lifetimes. Such an assumption allows describing all of the experimentally observed PL features.

In Chapter 3 the role of hopping transitions for carriers release in high electric fields has been discussed. Analytical description along with the KMC algorithm for the problem were provided. Our analysis shows that for deep levels the assistance of hopping to the neighbouring sites, may significantly enhance the release rate of carrier, which might have the serious impact on the phenomena that depends solely on the process of carriers detrapping, as well as on the transport properties of the disordered system.

In the final chapter (Chapter 4) we have demonstrated the validity of the effective temperature concept for description of the carrier mobility in the multiple-trapping transport mode. Which means that carrier mobility in MT transport can be described as the function of a single variable $T_{eff}(F, T)$, which takes into account the combined effect of the temperature and the electric field. Since the MT transport is widely assumed for amorphous inorganic semiconductor materials like a-Se and poly-PbO, results discussed in this chapter are important for such materials. The validity of the effective temperature for MT transport is an interesting and not trivial result from theoretical perspective, but it also provides a method for estimating the localization radius of carriers in amorphous disordered materials (for the case of MT transport) from the experimental measurements, as we have show for a-Se and poly-PbO in [9].

Through all the work a particular emphasis on using Kinetic Monte Carlo method as a powerful tool for simulating disordered materials was done.

Bibliography

[1] H. Bässler. Localized states and electronic transport in single component organic solids with diagonal disorder. *phys. stat. sol (b)*, 107, 1981.

[2] H. Bässler. Charge transport in disordered organic photoconductors. *phys. stat. sol (b)*, 175, 1993.

[3] S. D. Baranovskii, R. Eichmann, and P. Thomas. Temperature-dependent exciton luminescence in quantum wells by computer simulation. *Phys. Rev. B*, 58, 1999.

[4] H. Wang et. al. Influence of excitation power and temperature on photoluminescence in ingan/gan multiple quantum wells. *Opt. Express*, 20, 2012.

[5] Yu. I. Mazur et. al. Effects of spatial confinement and layer disorder in photoluminescence of ga(as,bi)/gaas heterostructures. *J. Phys.D: Appl. Phys.*, 46, 2013.

[6] V.V. Valkovskii, M.K. Shakfa, and K. Jandieri et al. Excitation dependence of the photoluminescence lineshape in ga(nasp)/gap multiple quantum well: experiment and monte-carlo simulation. *J. Phys. D: Appl. Phys.*, 50, 2017.

[7] C. Karcher et. al. Peculiarities of the photoluminescence of metastable ga(n,as,p)/gap quantum well structures. *Phys. Rev. B*, 82, 2010.

[8] V. V. Valkovskii et al. Rethinking the theoretical description of photoluminescence in compound semiconductors. *J. Appl. Phys.*, 123, 2018.

[9] A. V. Nenashev et al. Field-enhanced mobility in the multiple-trapping regime. *Phys. Rev. B*, 98, 2018.

[10] S. D. Baranovskii. Theoretical description of charge transport in disordered organic semiconductors. *phys. stat. sol. (b)*, 251, 2014.

[11] S. D. Baranovskii. Mott lecture: Description of charge transport in disordered organic semiconductors: Analytical theories and computer simulations. *phys. stat. sol. (a)*, 215, 2018.

[12] F. Urbach. The long-wavelength edge of photographic sensitivity and of the electronic absorption of solids. *Phys. Rev.*, 92, 1953.

[13] A. Miller and E. Abrahams. Impurity conduction at low concentrations. *Phys. Rev.*, 120, 1960.

[14] B. J. Last and D. J. Thouless. Percolation theory and electrical conductivity. *Phys. Rev. Lett.*, 27, 1971.

[15] N. F. Mott. Electrons in disordered structures. *Adv. Phys.*, 16, 1967.

[16] S. D. Baranovskii. Theoretical description of charge transport in disordered organic semiconductors. *Phys. Status Solidi B*, 251, 2014.

[17] H. Grüning et. al. Hopping relaxation of excitons in gainnas/ganas quantum wells. *Phys. Statarus Solidi C*, 1, 2004.

[18] S. D. Baranovskii et al O. Rubel, M. Galluppi. Quantitative description of disorder parameters in (ga,in)(n,as) quantum wells from the temperature-dependent photoluminescence spectroscopy. *J. Appl. Phys.*, 98, 2005.

[19] S. D. Baranovskii et al O. Rubel. Model of temperature quenching of photoluminescence in disordered semiconductors and comparison to experiment. *Phys. Rev. B*, 73, 2006.

[20] O. Rubel, W. Stolz, and S.D. Baranovskii. Spectral dependence of the photoluminescence decay in disordered semiconductors. *Appl. Phys. Lett.*, 91, 2007.

[21] P. Dawson and O. Rubel et al. Temperature-dependent optical properties of inas/-gaas quantum dots: Independent carrier versus exciton relaxation. *Phys. Rev. B*, 72, 2005.

[22] O. Rubel and P. Dawson et al. Nature and dynamics of carrier escape from inas/gaas quantum dots. *Phys. Statarus Solidi C*, 3, 2006.

[23] P. Dawson et al. Relaxation and recombination in inas quantum dots. *Phys. Statarus Solidi B*, 244, 2007.

[24] T. Niebling and O. Rubel et al. Hopping energy relaxation of localized excitons in ga(p,n)). *Phys. Statarus Solidi C*, 5, 2008.

[25] S. D. Baranovskii and A. L. Efros. *Sov. Phys. Semicond.*, 12, 1978.

[26] M. Baranovskii et al. Dynamics of localized excitons in ga(in,n,as)/gaas quantum well: Experimental studies and monte-carlo simulations. *Appl. Phys. Lett.*, 100, 2011.

[27] M. K. Shakfa and M. Wiemer et al. Thermal quenching of photoluminescence in ga(as,bi). *J. Appl. Phys.*, 117, 2015.

[28] K. Jandieri et al. Hopping relaxation of photoexcited excitons in ga(n,as,p) bulk structure. *Phys. Status Solidi C*, 8, 2010.

[29] K. Jandieri et al. Energy scaling of compositional disorder in ga(n,p,as)/gap quantum well structures. *Phys. Rev. B*, 86, 2012.

[30] J. Puustinen et al. Variation of lattice constant and cluster formation in ga(as,bi). *J. Appl. Phys*, 114, 2013.

[31] L. Keldysh. *Sov. Phys. JETP*, 7, 1958.

[32] S. D. Baranovskii et al. Thermally stimulated conductivity in disordered semiconductors at low temperatures. *Phys. Rev. B*, 55, 1997.

[33] V.I. Arkhipov et al. Hopping model of thermally stimulated photoluminescence in disordered organic materials. *Chemical Physics*, 266, 2001.

[34] V.Sugakov et al. Molecular vibrations, activation energies of trapped carriers and additional structure in thermoluminescence of organic polymers. *Synthetic Metals*, 234, 2017.

[35] B. I. Shklovskii. Hopping conduction in semiconductors subjected to a strong electric field. *Sov. Phys. Semicond*, 6, 1973.

[36] S. Marianer and B. I. Shklovskii. Effective temperature of hopping electrons in a strong electric field. *Phys. Rev. B*, 46, 1992.

[37] B. Cleve et. al. High-field hopping transport in band tails of disordered semiconductors. *Phys. Rev. B*, 51, 1995.

[38] G. Juka and K. Arlauskas. Transport of electrons in lead oxide studied by celiv technique. *phys. stat. sol. (b)*, 59, 1980.

[39] O. Semeniuk et al. Impact ionization and mobilities of charge carriers at high electric fields in amorphous selenium. *J. Phys. D*, 50, 2017.

[40] L. V. Keldysh. Concerning the theory of impact ionization in semiconductors. *Sov. Phys. JETP*, 21, 1965.

[41] M. Grünewald and B. Movaghar. Theory of photoluminescence decay and electricfield-dependent energy relaxation in disordered materials at low temperature. *J.Phys.: Condens. Matter*, 1, 1989.

[42] S. D. Baramovskii et. al. Effective temperature for electrons in band tails. *J. Non-Cryst. Solids*, 437, 1993.

[43] F. Jansson et. al. Effective temperature for hopping transport in a gaussian density of states. *Phys. Rev. B*, 77, 2008.

[44] N. F. Mott and E. A. Davis. *Electronic Processes in Non-Crystalline Materials.* Clarendon Press, Oxford, 2 edition, 1979.

[45] H. Overhof and P. Thomas. *Electronic Transport in Hydrogenated Amorphous Semiconductors.* Springer, Heidelberg, 1989.

[46] R. A. Street. *Hydrogenated Amorphous Silicon.* Cambridge Solid State Science Series. Cambridge University Press, 1991.

[47] J. Frenkel. On pre-breakdown phenomena in insulators and electronic semiconductors. *Phys. Rev.*, 54, 1938.

[48] G. Vincent, A. Chantre, and D. Bois. Electric field effect on the thermal emission of traps in semiconductor junctions. *J. Appl. Phys.*, 50, 1979.

[49] V. Karpus and V. I. Perel. Multiphoton ionization of deep centers in semiconductors in an electric field. *JETP*, 64, 1986.

[50] N. Hijazi and M. Z. Kabir. Mechanisms of temperature- and field-dependent effective drift mobilities and impact ionization coefficients in amorphous selenium. *Can. J. Phys.*, 93, 2015.

[51] K. D. Tsendin. Physical properties of doped chalcogenide glassy semiconductors which are governed by the interaction of negative-u defects and impurity states. *J. Optoelectronics and Advanced Materials*, 3, 2001.

[52] J. Singh. Effective mass of charge carriers in amorphous semiconductors and its applications. *J. Non-Cryst. Solids*, 444, 2002.

[53] A. V. Nenashev et al. Fundamental characteristic length scale for the field dependence of hopping charge transport in disordered organic semiconductors. *Phys. Rev. B*, 96, 2017.

Vitalii Valkovskii CV

After finishing high school in 2008, I have enrolled in the Faculty of Physics at the Novosibirsk State University (Novosibirsk, Russia) in 2009. During 2011 – 2015 I was employed as a student researcher in the Laboratory of Nonequilibrium Semiconductor Systems at the Rzanov Institute of Semiconductor Physics. While continuing my education in the University, I have have been working on my Bachelor's and later Master's projects under the supervision of Dr. Natalia Stepina in the Laboratory of Nonequilibrium Semiconductor Systems. My Bachelor's research was dedicated to the influence of electric field on the charge transport in the arrays of germanium quantum dots grown on a silicon substrate. Eventually, in 2013 I have defended my Bachelor's thesis named "Magnetoresistance of a two-dimensional array of quantum dots with various degrees of charge carriers localization". After getting my Bachelors degree, I have continued my education at the Novosibirsk State University as well as my research on charge transport in semiconductor systems with quantum dots under the supervision of Dr. Stepina. Finally, I have defended Master's thesis, titled "Charge transport in a one-dimensional array of quantum dots grown on a patterned substrate", in 2015. After graduating with the Master's degree, I have decided to continue my research in the field of charge transport and optical properties of disordered materials. Since October 2015 I have been working in the University of Marburg under supervision of professor Dr. Sergei Baranovskii, and this thesis reflects the results of my research made in Marburg.